The Messenger

No. 156 – June 2014

Adaptive Optics algorithms for the E-ELT
An advanced scattered moonlight model
Sub-mm galaxies with HST, VLT and ALMA
Report on the 3D Spectroscopy Workshop

The Adaptive Optics Facility Module GRAAL on its Way to Final Validation

Robin Arsenault[1]
Jérôme Paufique[1]
Johann Kolb[1]
Pierre-Yves Madec[1]
Mario Kiekebusch[1]
Javier Argomedo[1]
Andreas Jost[1]
Sébastien Tordo[1]
Rob Donaldson[1]
Marcos Suarez[1]
Ralf Conzelmann[1]
Harald Kuntschner[1]
Ralf Siebenmorgen[1]
Jean-Paul Kirchbauer[1]
Aurea-Garcia Rissmann[1]
Johannes Schimpelsberger[1]

[1] ESO

The VLT Adaptive Optics Facility (AOF) module GRAAL has been developed to provide ground layer adaptive optics correction for the HAWK-I infrared imager. This will improve the limiting magnitude and promote science cases requiring better spatial resolution. The gain in resolution is comparable to selecting a better site for the telescope. The GRAAL wavefront sensor signals are processed by a SPARTA real-time computer that drives the AOF deformable secondary mirror integrated in an upgraded secondary mirror assembly on Yepun, the VLT Unit Telescope 4. The system test phase of GRAAL has started in the integration laboratory in Garching and is described; provisional acceptance is expected to take place at the end of 2014.

The AOF project

The Adaptive Optics Facility, described in Arsenault et al. (2006), with progress reports in Arsenault et al. (2010a; 2010b; 2012; 2013), will transform the VLT's fourth Unit Telescope Yepun, (or UT4) into an adaptive telescope (Kuntschner et al., 2012). This is accomplished by replacing the conventional secondary (M2) mirror with an adaptive secondary, employing a deformable secondary mirror (DSM) described in Biasi et al. (2012), implementing the Four Laser Guide Star Facility (4LGSF; see Bonaccini Calia et al., 2011), and installing adaptive optics (AO) modules at the various foci. These AO modules consist of GRAAL (Ground Layer Adaptive optics Assisted by Lasers; described in Kissler-Patig [2005] and Paufique et al. [2012]) for HAWK-I, GALACSI (Ground Atmospheric Layer Adaptive Corrector for Spectroscopic Imaging; Stroebele et al. [2012]) for MUSE (Multi-Unit Spectroscopic Explorer), and ERIS (Enhanced Resolution Image and Spectrograph) to replace SINFONI (Spectrograph for INtegral Field Observations in the Near Infrared). The AOF components are tested on the ASSIST test bench (Adaptive Secondary Setup and Instrument Stimulator; Stuik et al. [2012]).

Project status

A GRAAL test readiness review was held in February 2013 and validated the plan to proceed with the system test phase. The GRAAL module was then integrated, with the exception of some wavefront sensor cameras needing refurbishment. It is presently mounted on the ASSIST test bench and the system test phase, using the GRAAL maintenance and commissioning mode, began in February 2014.

The ASSIST test bench itself was delivered by the Leiden Observatory and was granted Provisional Acceptance Europe (PAE) by ESO in October 2012. Shortly after, the DSM was mounted and aligned on ASSIST (see Arsenault et al., 2013). The optical tests of the DSM could then take place and lasted the best part of 2013, concluded by Technical Acceptance Europe, which was granted in December 2013.

In parallel with these activities the GRAAL module was mounted on ASSIST and aligned with the test bench; this turned out to be a complex task which took longer than expected. In January 2014 the alignment was judged to be satisfactory and several issues (such as ghost reflections and image quality) had to be solved. The infrared camera (CAMCAO) of the Multi-conjugate Adaptive Optics Demonstrator (MAD) instrument has been re-used and is installed on GRAAL in order to measure the resulting image quality after AO correction.

All the above elements were required in order to ensure a smooth and efficient transition to the conduct of the first phase of the AOF system tests with the GRAAL module.

The other AOF major systems can be developed on a parallel track for the time being. GALACSI module integration is well advanced but not completed. One of the four Laser Guide Star (LGS) optical paths has been aligned and furnished with a wavefront sensor camera (priority was granted to GRAAL). However, many of the module subsystems have been characterised and were validated during 2013. Technical templates are used to perform these tests in a consistent manner and the observing and instrument control software of GALACSI is also well developed (there was also a synergy exploited with the GRAAL software modules). The jitter loop actuator was validated as well, which allowed a complete loop with SPARTA (Standard Platform for Adaptive optics Real Time Applications), the wavefront sensor camera and the jitter actuator to be closed. The GALACSI module should be validated in standalone mode before the end of 2014 in order to take the place of GRAAL on ASSIST when the system tests with this module are complete.

The 4LGSF project is also progressing well. The first 22-watt laser unit has been delivered to Garching and PAE has been granted for this unit. The laser has been installed on the first launch telescope system and a full end-to-end test is well advanced. The second and third launch telescope system units will be integrated and aligned this summer and a subset of tests run on these units. The system test phase of the 4LGSF will start this summer with the aim for a complete system PAE in early 2015.

It is planned to ship the GRAAL module and the first LGS unit to Paranal towards the end of 2014, allowing an early installation of these systems on UT4 for the first quarter of 2015. This milestone will inaugurate the commissioning of the AOF in Paranal by combining these two systems to validate 4LGSF–GRAAL functionalities before the arrival of the DSM, planned for the fourth quarter of 2015.

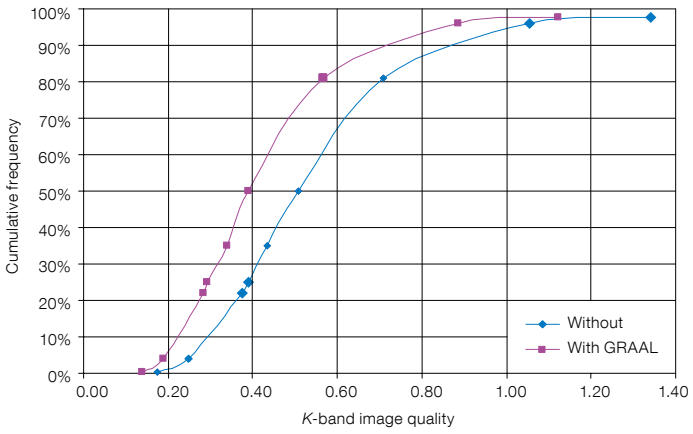

Figure 1. A plot of the cumulative frequencies of *K*-band image quality with (pink) and without (blue) the GRAAL module.

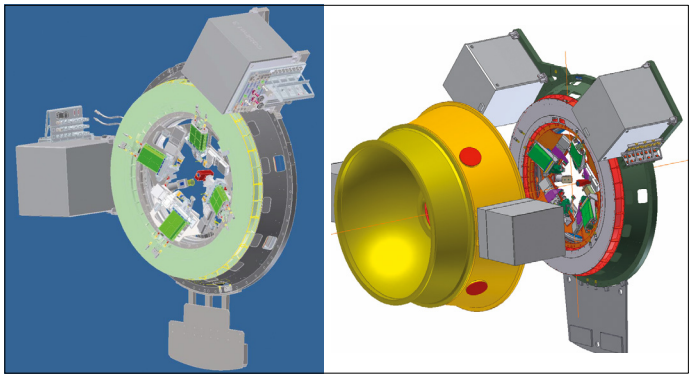

Figure 2. A schematic of the GRAAL module with the four laser guide star wavefront sensors shown in bright green (left). The HAWK-I spacer that comes over the GRAAL assembly is shown (right).

GRAAL module background

The basic idea of the GRAAL module emerged in 2005 while preparing the conceptual design review of the AOF (Arsenault et al., 2005). A basic description of the module can be found in Paufique et al. (2012). The challenge was to define how AO could serve an infrared imager with such a large field of view as 7.5 arcminutes. The proposed improvement, equivalent to moving Yepun with HAWK-I to a still better observing site, can be provided by Ground Layer Adaptive Optics (GLAO) correction (see Figure 1). Thus GRAAL allows the astronomer to perform the most challenging science cases nearly all of the time, rather than a small fraction of the time (as described in the science case document for GRAAL, Kissler-Patig [2005]).

GRAAL (see Figure 2) is designed to reduce the full width at half maximum (FWHM) for *K*-band images by 25% over the full 7.5 arcminute field of view of HAWK-I. Although it appears moderate as a goal, it represents a similar challenge to the GLAO mode of GALACSI for MUSE (the doubling of the ensquared energy per pixel over a 1-arcminute field of view at 750 nm).

GRAAL has the following features:

- The original field of view of HAWK-I is left unobstructed and a seeing-limited mode is available.
- Four laser guide star Shack–Hartman wavefront sensors (each with 40 × 40 sub-apertures) are located at 6.6 arcminutes from the field centre.
- A tip-tilt star sensor probes an annular region of 2-arcminute width, i.e., covering 13.2-arcminute inner diameter to 15.2-arcminute outer diameter.
- A natural guide star mode on-axis is provided, dubbed the maintenance and commissioning mode. The role of this mode is to ensure proper functioning of the DSM and allow a first commissioning of a basic single conjugate AO system.

The maintenance and commissioning mode will be used first on sky to evaluate the ultimate performance of the DSM in a simpler configuration. It requires a tight error budget and allows marginal failures of subsystems to be detected more easily, such as defective actuators or control issues.

In its nominal operational mode (i.e., GLAO), the four LGS wavefront sensors analyse the returned light from the four 22-watt lasers launched from the UT4 centrepiece. SPARTA determines the commands to be applied to the DSM from the four real-time video signals. The refresh rate of the command is 1 ms.

AOF synergies

GRAAL and GALACSI are the non-identical twins of the AOF; despite being different, they share similar “genetic baggage”. They of course share the 4LGSF and the DSM. In addition, their design was been also made common where possible, so as to optimise the test and operation of the systems, reduce development costs and share maintenance effort.

The SPARTA real-time computer hardware is identical for GRAAL and GALACSI (see Figure 3 left), which allowed either system to be used for development during the integration. The software is common between both, where applicable: GRAAL and GALACSI GLAO corrections are essentially identical for their real-time operation. The maintenance and commissioning mode is an additional instance of the version of SPARTA built for the SPHERE instrument.

The wavefront sensor cameras (see Figure 3 right) are also identical in GALACSI and GRAAL, which enables serial production and common management of spares. Six cameras using L3 CCD220 from e2v are used in GRAAL: one as tip-tilt sensor, one as natural guide star for the 40 × 40 Shack–Hartmann (maintenance and commissioning mode), and four as laser guide stars for the 40 × 40 Shack–Hartmann (GLAO) mode. These cameras use electron gain amplification in order to reduce the readout noise of the CCDs. Although the readout

Figure 3. The two SPARTA computers for GRAAL and GALACSI (left). They are based on identical hardware, but run different software codes adapted to the AO modules. These cabinets will be located in the *bodega* of UT4 to save room on the azimuth and Nasmyth platforms. An optical fibre pair needs to run to the wavefront sensor cameras for data transfer. A wavefront sensor camera running an e2v L3 CCD CCD220 is shown (right). The camera fulfills the expected performance of < 1 e- readout noise at 1 kHz frame rate.

noise is nominally high (70 e-) the gain amplification mechanism reduces its effective value to below one photoelectron. The gain in question can be selected from 1 to 1000 and the AOF cameras are used at a gain value of ~ 100 which reduces the readout noise to an acceptable level (1e-) to reach the system performance, while protecting the camera from quick aging (a risk at high gains). Last, but not least, this extraordinary performance is reached at 1 kHz frame rate to match the AOF closed-loop frequency.

Activities over the past year

The integration and validation of the GRAAL subsystems took place during 2012 and 2013. The co-rotator was a critical piece of equipment that necessitated careful attention during this period. Several technical templates were developed and early tests were carried out using these templates and the GRAAL observing and instrument control software.

The GRAAL main assembly concept was defined at ESO, but its final design and test was outsourced and executed by the company NTE-SENER, near Barcelona, Spain. At the heart of this concept lies the co-rotator, allowing the four LGS wavefront sensors of GRAAL to each track their artificial beacon and the pupil, while the rest of the instrument rotates with the science target field of view. The system tracks the guide stars with an accuracy on sky of better than 30 milliarcseconds, and avoids introducing any significant contribution to the laser jitter. Opto-mechanical interfaces have been verified by means of a laser tracker, both in terms of position and flexures.

The installation of GRAAL on ASSIST did not reveal any major discrepancy, thanks to the verifications performed separately on individual subsystems. Nevertheless, the large structure installed in the ESO assembly hall suffers from slow drifts due to some thermal variations, which are inherent to the design of the structure and to the laboratory environment. Vibrations related to human activities in or near the laboratory also restrict the operations with the system when delicate and long-lasting measurements are necessary. Vignetting, image quality and ghosts issues were solved in the last stages of the alignment in January 2014.

Start of system test phase: first results

The first issue of the AOF system test plan dates back to May 2009. Following the test readiness review in February 2013, a detailed test procedure document was prepared for GRAAL. A quick description is given for each test, detailing the expected duration, pre-requisites or inputs, detailed procedure and Pass/Fail criteria and the outputs. This has allowed the AOF to proceed swiftly with these tests when the GRAAL module alignment on ASSIST was completed.

The preliminary tests focused on establishing the basic characteristics of the setup:
- calibrating the wavefront sensor detectors: background versus gain, noise versus gain, etc.;
- pupil illumination on the detectors;
- measurement of slopes with various centroiding methods;
- estimation of optical aberrations;
- calibration of the flux received from the ASSIST source;
- infrared camera image quality.

Figure 4 shows some pupil images from these tests and Figure 5 shows GRAAL in its testing configuration.

Then followed the apparently simple task of measuring the pixel scale of the wavefront sensor (how many arcseconds of motion on the sky correspond to one pixel on the detector). However, it is a crucial task since it allows the good behaviour of many hardware and software components of the system to be checked, even before closing the AO loop. The measurement procedure is simple: sending small tilt offsets to the DSM hexapod and recording simultaneous images on the wavefront sensor.

Determining the interaction matrix

The next major task of the system tests concerns the generation of the AO interaction matrix (IM). It contains the response of the wavefront sensor to deformations of the DSM and allows, after inversion, the DSM commands, correcting the measured turbulence, to be applied at 1 kHz to be computed. In the case of the DSM, this matrix is composed

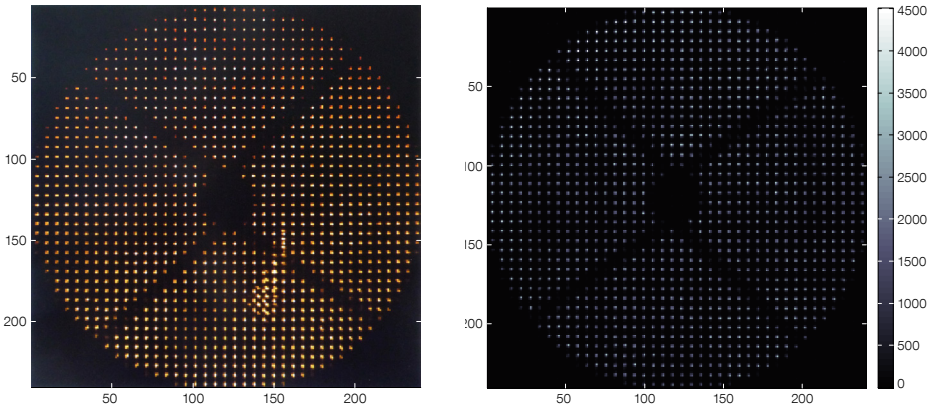

Figure 4. Pupil image on the maintenance and commissioning camera as seen on ASSIST. The spider on ASSIST is larger than the Unit Telescope design. Left: Ghost superimposed to the normal spot pattern, before correction; Right: After installation of the pupil baffle.

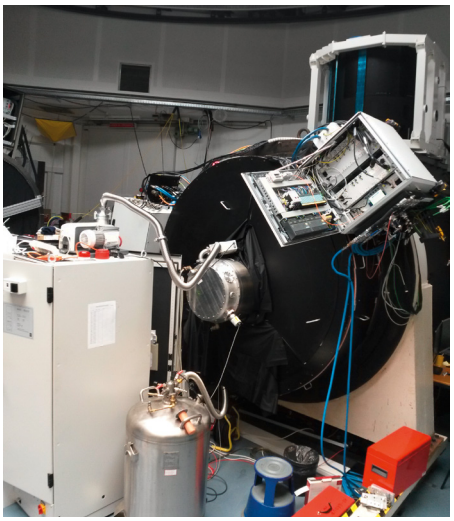

Figure 5. The AOF test configuration in the old integration laboratory in Garching. The DSM sits on top of the ASSIST bench and the GRAAL module is mounted on the Nasmyth focus simulator. In the foreground the CAMCAO silver cryostat can be seen; this camera is used to record output images corrected by the adaptive optics.

of 1156 rows (DSM valid actuators) and ~ 2480 columns (40 × 40 apertures in a circular area, each with two slopes — one in X and one in Y).

In classical post-focal AO systems like the VLT NAOS instrument, the IM can be re-measured at will by placing an artificial source at the entrance focal plane of the instrument. But this is not possible on an adaptive telescope like the VLT equipped with the AOF, as the DSM is part of the telescope optical train. Hence the baseline for the AOF is to use a pseudo-synthetic interaction matrix (PSIM), based on a computer model of the DSM and wavefront sensor, fine-tuned by matching it with measured characteristics of those same components: wavefront sensor response and DSM influence functions.

As this method is quite a novel concept to be implemented on a scientific AO instrument, it is important for it to be tested in the laboratory and ASSIST offers this possibility. The atmosphere emulated by optical turbulent phase screens can be removed, and an interaction matrix can be measured. Such matrices will be measured using several different methods and their performance will be compared with that of the PSIM. More precisely, zonal (each DSM actuator is poked individually) and modal (DSM stiffness modes or atmospheric Karhuenen–Loeve modes) IMs will be compared, either recorded with or without turbulence. For each method, several parameters, such as the amplitude and number of the cycles, can be varied to maximise the IM signal-to-noise ratio.

An AOF zonal IM is composed mostly of zeroes because the influence of one actuator is seen on a few sub-apertures only. Thus the display of such a matrix in full is pointless and is barely resolvable by a computer screen. Instead we have been using a display of the 40 largest signals along X and Y in the sub-apertures for each actuator. This reduces the matrix

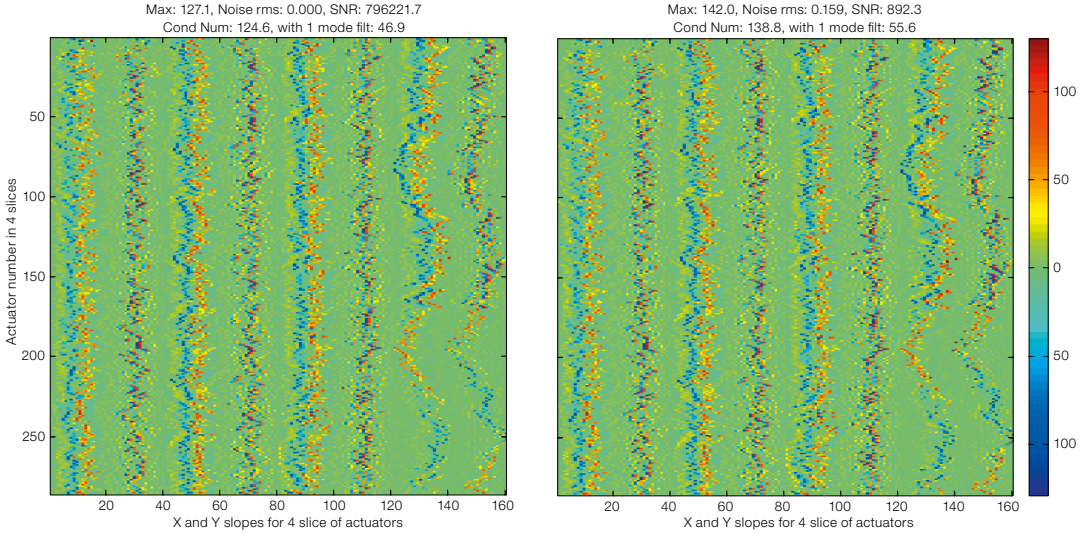

Figure 6. Pseudo-synthetic interaction matrix (left) *vs.* measured integration matrix (right) in a condensed display. The eight vertical stripes that compose them are, side-by-side, the X and Y slopes for the actuators 1–289, 290–578, 579–867 and 868–1156. The two matrices seem to differ only in their signal to noise ratio (SNR): ~ 900 for the measured integration matrix against almost infinite for the pseudo-synthetic integration matrix.

to 80 × 1156 elements, which we have then folded four times to produce a squarer and easier to display matrix of 289 × 320 elements (Figure 6).

Some parameters of the PSIM have to be tuned in order to match the real IM of the system. Those parameters, which describe the pupil mismatch between the DSM and the wavefront sensor, are the X and Y shifts, the rotation and the X and Y magnification. A method developed at ESO (Bechet et al., 2012) allows those parameters to be identified after iterative comparison of the PSIM with a measured one — hence the importance of being able to measure an IM even on-sky. This method has been applied and a PSIM could be generated that is very close to the measured one (see Figure 6). It has even been used to close the AO loop and, on a limited number of tests, managed to deliver the same performance as the measured one.

Closing the AO loop at 1 kHz between the wavefront sensor and the DSM via SPARTA revealed no major issues. This was tested at first on the calibration fibre, correcting only the local turbulence in the laboratory with an increasing number of modes. When few modes are truncated, the print-through of the spiders is visible, indicating that the sub-apertures behind them have to be handled carefully to avoid the "island effect" inherent to systems with a segmented pupil. In addition to a differential piston in the four islands, another problem to consider in the case of a force-controlled DSM is that the sharp discontinuities in the DSM shape behind the spiders require more force to control and thus limit the available range of correction. These issues will be fixed in the coming months during AOF system tests.

Finally, the optical phase screens that emulate turbulence with seeing of 0.65 arcseconds were introduced and rotated to reproduce the characteristic Paranal wind profile. The AO loop could be closed with an integral gain of 0.4 and three different sets of modes: 150, 550 and 950 (see Figure 7). It can be noticed that the major part of the turbulence is corrected and the GRAAL maintenance and commissioning mode delivers very sharp images, close to the one recorded on the calibration source (rightmost image on Figure 7). Preliminary results provide a reference Strehl ratio measured on the calibration fibre of 76% and on the closed loop images of 65%, i.e., a relative correction of 85% at 1.65 µm.

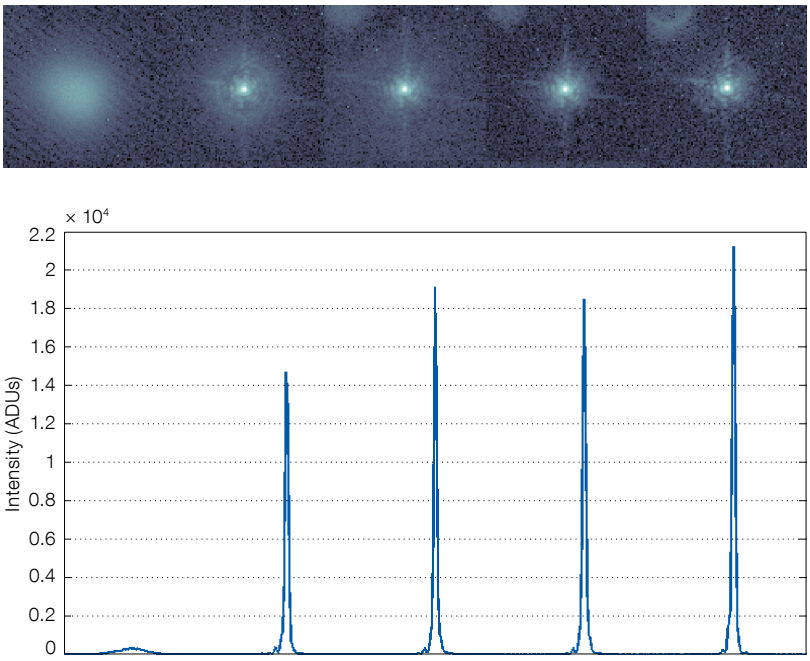

Figure 7. Long-exposure *H*-band images (top) and their horizontal cuts (bottom) recorded (from left to right): in open loop turbulence, in closed loop on turbulence with 150, 550 and 950 modes controlled, and in closed loop on the calibration fibre (rightmost image).

Prospects

With the completion of the integration of its AO module, GRAAL, the AOF project has entered the system test phase. With the maintenance and commissioning mode and a natural guide star wavefront sensor of 40 × 40 sub-apertures, combined with the SPARTA computer and the DSM, the AOF team has started obtaining data that validate the strategy developed and are already showing spectacular results.

The system test phase will continue with the GRAAL ground layer AO mode until the end of 2014. Then the GALACSI module will take the place of GRAAL on the ASSIST bench and this module will undergo similar tests until mid-2015.

The first commissioning activities in Paranal are planned to take place in early 2015 after the shipment of the GRAAL module and the first LGS unit. The DSM with GALACSI will be delivered toward the end of 2015.

Acknowledgements

It is becoming more and more difficult to select a list of authors for articles concerning the AOF project because it has been going on for a long time and so many ESO staff have been involved in one way or another. The first author wishes to thank the collaborative and pro-active attitude not only of all the project team members, but also of all ESO staff who have contributed and are always willing to help.

References

Arsenault, R. et al. 2006, The Messenger, 123, 11
Arsenault, R. et al. 2010, The Messenger, 142, 12
Arsenault, R. et al. 2010, Proc. SPIE, 7736, 20
Arsenault, R. et al. 2012, Proc. SPIE, 8447, 0J
Arsenault, R. et al. 2013, The Messenger, 151, 14
Bechet, C. 2012, VLT-TRE-ESO-22000-5810, Iss.1
Biasi, R. et al. 2012, Proc. SPIE, 8447, 88
Bonaccini Calia, D. et al. 2011, Second Int. Conf. on AO for ELTs. Online proceedings, id.P39
Kasper, M. et al. 2004, JOSA, 21, 1004
Kissler-Patig, M. 2005, VLT-SPE-ESO-14850-3744, Iss.1
Kuntschner, H. et al. 2012, Proc. SPIE, 8448, 07
Paufique, J. et al. 2012, Proc. SPIE, 8447, 116
Ströbele, S. et al. 2012, Proc. SPIE, 8447, 115
Stuik, R. et al. 2012, Proc. SPIE, 8447, 118

CRIRES+: Exploring the Cold Universe at High Spectral Resolution

Reinhold J. Dorn[1]
Guillem Anglada-Escude[2]
Dietrich Baade[1]
Paul Bristow[1]
Roman Follert[3]
Domingo Gojak[1]
Jason Grunhut[1]
Artie Hatzes[3]
Ulrike Heiter[4]
Michael Hilker[1]
Derek J. Ives[1]
Yves Jung[1]
Hans-Ulrich Käufl[1]
Florian Kerber[1]
Barbara Klein[1]
Jean-Louis Lizon[1]
Matthew Lockhart[4]
Tom Löwinger[3]
Thomas Marquart[4]
Ernesto Oliva[5]
Livia Origlia[6]
Luca Pasquini[1]
Jérôme Paufique[1]
Nikolai Piskunov[4]
Eszter Pozna[1]
Ansgar Reiners[2]
Alain Smette[1]
Jonathan Smoker[1]
Ulf Seemann[2]
Eric Stempels[4]
Elena Valenti[1]

[1] ESO
[2] Institut für Astrophysik, Georg-August Universität Göttingen, Germany
[3] Thüringer Landessternwarte, Tautenburg, Germany
[4] Department for Physics and Astronomy, University of Uppsala, Sweden
[5] Osservatorio di Arcetri (INAF), Firenze, Italy
[6] Osservatorio di Bologna (INAF), Italy

The CRIRES upgrade project, CRIRES+, transforms this VLT instrument into a cross-dispersed spectrograph to increase the wavelength range that is covered simultaneously by a factor of ten. In addition, a new detector focal plane array of three Hawaii 2RG detectors with a 5.3 µm cut-off wavelength will replace the existing detectors. For advanced wavelength calibration, custom-made absorption gas cells will be added. A spectropolarimetric unit will allow circularly polarised spectra to be recorded. These upgraded capabilities will be all supported by dedicated data reduction software which will allow the community to take full advantage of the new capabilities offered by CRIRES+.

Introduction

High-resolution infrared spectroscopy plays an important role in astrophysics, from the search for exoplanets to cosmology. The majority of currently existing infrared spectrographs are limited by their small simultaneous wavelength coverage. The scientific community has recognised the need for large wavelength range, high-resolution infrared spectrographs, and several are currently either in the design or integration phase. Examples are: the Immersion Grating Echelle Spectrograph (ISHELL; Rayner et al., 2013) at the NASA Infrared Telescope Facility; SPIROU (Delfosse et al., 2013) for the Canada France Hawaii Telescope (CFHT); and the Calar Alto high-Resolution search for M dwarfs with Exoearths with Near-infrared and optical Échelle Spectrographs (CARMENES; Quirrenbach et al., 2012) for the Calar Alto Observatory.

The adaptive optics (AO)-assisted CRIRES instrument, installed at the Very Large Telescope (VLT), is an infrared (0.92–5.2 µm) high-resolution spectrograph which has been in operation since 2006. CRIRES is a unique instrument, accessing a parameter space (wavelength range and spectral resolution) which up to now was largely uncharted, as described in Käufl et al. (2004). In its current setup, it consists of a single-order spectrograph providing long-slit (40-arcsecond) spectroscopy with a resolving power up to R = 100 000. However the setup is limited to a narrow, single-shot, spectral range of about 1/70 of the central wavelength, resulting in low observing efficiency for many modern scientific programmes requiring a broad spectral coverage.

By introducing cross-dispersing elements and larger detectors, the simultaneous wavelength range can be increased by at least a factor of ten with respect to the present configuration, while the total operational wavelength range can be preserved (see Figure 1).

Science drivers

A search for super-Earths in the habitable zone of low-mass stars

A large fraction of all exoplanets has been discovered primarily through radial velocity measurements. However, only 5 % of the planets detected so far orbit stars with stellar masses less than about 0.5 $M_{\odot}$. Thus, we lack key knowledge about the process of planet formation around the most numerous stars in our galaxy — M dwarfs. Low-mass stars are especially interesting because these objects are cool and the habitable zones are quite close to the star. The reflex motion of an M star (0.15 $M_{\odot}$) with a 1 $M_{\oplus}$ planet in its habitable zone is about 1 m s^{-1}. Since M dwarfs and brown dwarfs have low effective temperatures, radiating most of their energy in the infrared (1.0–2.5 µm), a high-resolution infrared spectrograph is therefore ideal for searching for low-mass planets around these objects.

A new gas absorption cell to provide a stable wavelength reference as well as the increase in wavelength coverage by about a factor of ten should result in an attainable radial velocity precision for CRIRES+ of 2–3 m s^{-1}. This would enable the detection of superEarth-mass planets in the habitable zone of an M-dwarf star in the Solar Neighbourhood (see Figure 2).

Atmospheric characterisation of transiting planets

In-transit spectroscopy of exoplanets currently provides us with the only means of studying exoplanetary atmospheres. Transiting planets are almost always close-in planets that are hot and radiate most of their light in the infrared. Furthermore the infrared is a spectral region where lines of molecular gases like CO, NH_3, CH_4, etc. are expected from the exoplanetary atmosphere. This important wavelength region is covered by CRIRES+, which will also allow multiple absorption lines to be tracked simultaneously.

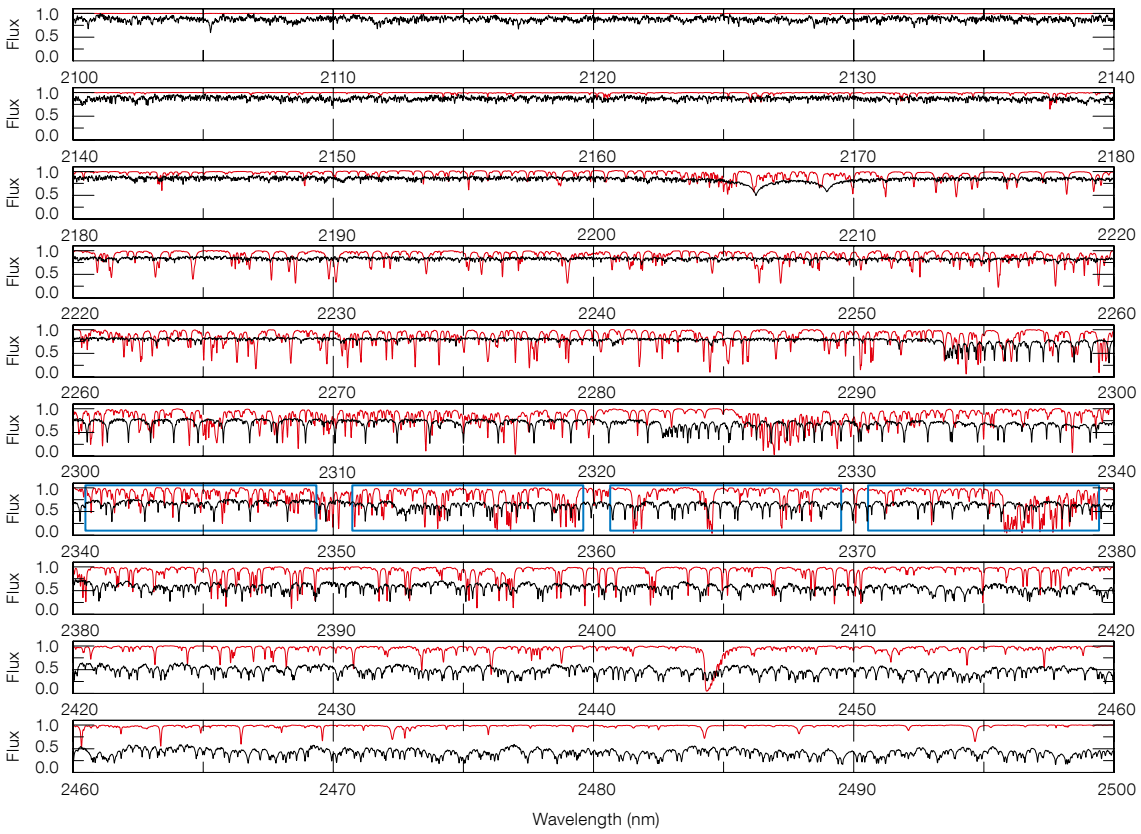

Figure 1. The wavelength coverage of the current CRIRES (blue boxes correspond to the four Aladdin detectors currently installed) in the *K*-band compared to the expected coverage of a single exposure from CRIRES+. The black line shows the spectrum of an M4 dwarf star (~ 0.15 $M_{\odot}$) and the light brown line is a laboratory spectrum of the first gas cell prototype being developed at the University of Göttingen.

Origin and evolution of stellar magnetic fields

Magnetic fields play a fundamental role in the life of all stars: they govern the emergence of stars from proto-stellar clouds, control the in-fall of gas onto the surfaces of young stars and aid the formation of planetary systems. Measurements of magnetic fields have mostly been confined to A- and B-type stars, so our knowledge of magnetic fields in Sun-like stars, and the low end of the main sequence, is still poor. CRIRES+ will make it possible to measure with greater accuracy magnetic fields in M dwarfs and brown dwarfs for several reasons:

1) The Zeeman splitting of a spectral line is proportional to λ^2, so there is a huge leverage in going to the infrared.
2) For cool objects most of the flux is in the infrared so there is also a gain due to the increased signal-to-noise ratio.
3) In order to disentangle Zeeman broadening from other broadening effects, one must compare the broadening of Zeeman sensitive lines to magnetically insensitive lines. The large wavelength coverage of CRIRES+ will include many more lines of different magnetic sensitivities needed for an accurate determination of the field strength.
4) The capability of CRIRES+ to take circularly polarised spectra will support these measurements.

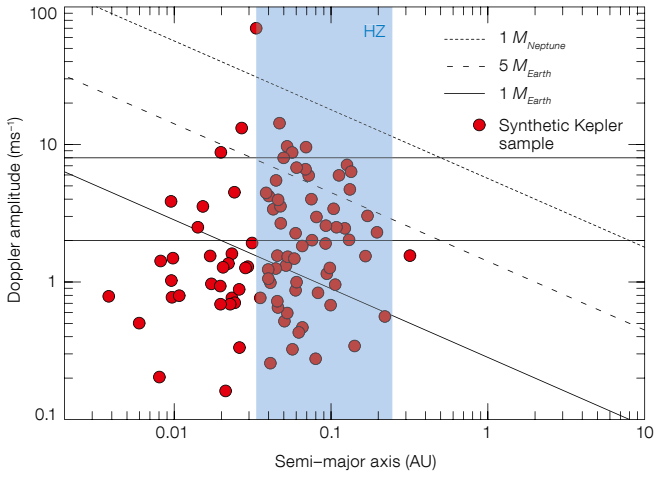

Figure 2. The expected Doppler amplitudes for different planet masses, depicted as diagonal lines, for a 0.1 $M_{\odot}$ star are shown. The top horizontal line is the current radial velocity precision of CRIRES; the lower is a conservative predicted value for CRIRES+. These horizontal lines also display the estimate of the detection thresholds after obtaining 25 epochs. The red dots correspond to the expected planets based on Kepler results (Dressing & Charbonneau, 2013). The blue shaded zone is the approximate extent of the habitable zone for low-mass stars.

The "+" for CRIRES

Many astrophysical applications will benefit significantly from the increase in wavelength coverage introduced by turning CRIRES into a cross-dispersed echelle spectrograph. The CRIRES upgrade project attempts to improve the

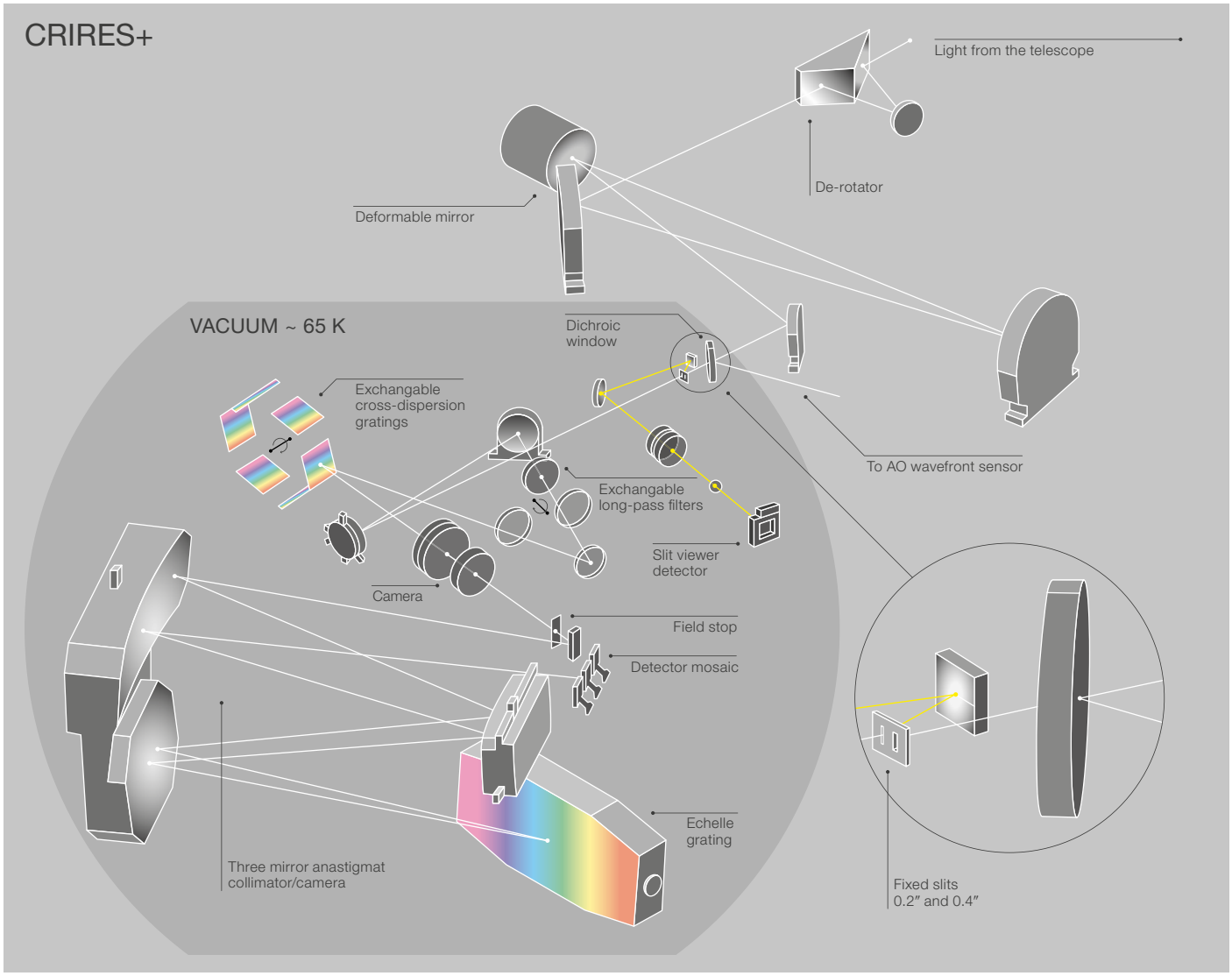

Figure 3. The optical design of the new cross-dispersion pre-optics for CRIRES+ is shown.

instrument by either refurbishing or replacing subsystems. Furthermore, there are plans to add subsystems that will provide additional observing modes. The project identified the following upgrades as significantly impacting the scientific capabilities of CRIRES.

Transform CRIRES into an echelle spectrograph

To assess how cross dispersion could be introduced into CRIRES, an analysis of the current and future scientific requirements and science cases was made. To cover the additional orders, the spatial extent of the main slit was reduced from 40 to 10 arcseconds, providing a balanced compromise between cross-dispersion implementation and catering for the current CRIRES long-slit usage. The cross dispersion of the spectrum will be carried out by reflection gratings. The optical layout of the new design is shown in Figure 3. Six gratings are foreseen, mounted on a cryogenic wheel. Each of them is optimised for operation in a single wavelength band (*Y, J, H, K, L* and *M*). Another wheel will carry the order sorting filters to eliminate contamination by second- and higher-order spectra of the gratings. The re-imaging of the slit is then performed by a fixed-lens camera, designed for the full wavelength coverage and used for all observing modes. In this configuration, the observing modes will require only one exposure to cover the full *Y*-band, two exposures, with different echelle angles, for the *J*- and *H*-bands, three exposures for the *K*-band, four for the *L*-band and five exposures are needed to cover the *M*-band. A new optical design for the slit viewer will complement the new pre-optics unit.

Overall the new design will maintain the current throughput of CRIRES (with

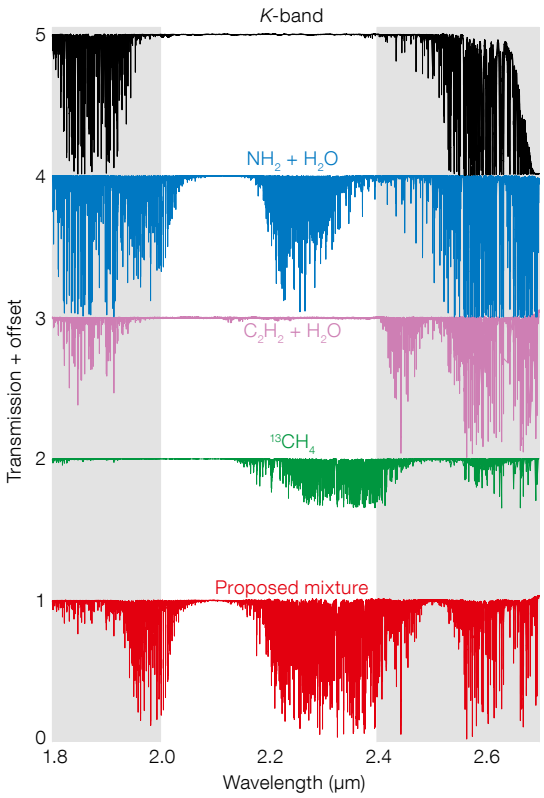

Figure 4. Transmission spectra of the gases for the CRIRES+ gas cell in the *K*-band are shown. The top panel plots the telluric (water) contribution, while the second to fourth panels show measurements of the individual species. The bottom spectrum presents the measured compound gas cell, which is a mixture of the above.

the goal of increasing it) and the spectral resolution of 50 000 and 100 000, as before. The slit length (10 arcseconds) will not limit observations of moderately extended sources and will allow nodding for precise background subtraction.

Gas cells for a new level of wavelength calibration

The CRIRES+ science cases also demand specialised, highly accurate wavelength calibration techniques. Therefore, another part of the proposed upgrade is concerned with the installation of novel infrared absorption gas cells with multi-species gas fillings (NH_3, $^{13}CH_4$, C_2H_2). These gases will provide a set of densely distributed absorption lines imprinted on the stellar spectra in the *H*- and *K*-bands (see Figure 4). In addition it is intended to replace the existing thorium argon hollow cathode lamps with similar uranium–neon lamps that produce a richer wavelength calibration spectrum.

New state-of-the-art detectors

The third major part of the upgrade project is to increase the coverage of the focal plane by introducing a set of new detectors. The current CRIRES scientific detector system uses four Raytheon 1024 × 1024 pixel InSb Aladdin arrays as described in Dorn et al. (2006). Another Aladdin detector is used for the slit-viewer camera. Owing to the planned cross dispersion, a larger field is required to cover the ten orders per band with a slit length of 10 arcseconds. Therefore a new and current state-of-the-art detector mosaic is foreseen. Figure 5 presents a comparison between the current CRIRES focal plane array area and the future array of CRIRES+. The future detector array, composed of three Hawaii 2RG detectors (a single H2RG detector is shown in Figure 6), will span 6144 × 2048 pixels (111 mm × 37 mm) at a pixel size of 18 μm. For comparison, the current mosaic spans only 4096 × 512 pixels (111 mm × 14 mm) with a pixel size of 27 μm.

The new detector mosaic will not only provide a larger area but also lower noise, higher quantum efficiency, better cosmetic quality and much lower dark current. Also the gaps between the detectors in the mosaic will be smaller. The detectors will be operated at 40 K with cryogenic preamplifiers located next to the focal plane. In addition all detector systems, including the slit-viewer camera, will be upgraded to the current ESO standard New General Detector Controller (NGC; Baade et al., 2009).

This detector upgrade will not only significantly increase the coverage of the focal plane, but the increased spatial homogeneity of the pixel response will result in improved data quality.

Spectropolarimetry with CRIRES+

The new polarimetry module planned for CRIRES+ uses two polarising gratings to split the incoming converging beam into left and right circularly polarised beams that continue along parallel optical axes. The choice of polarising gratings as polarising elements is motivated by their different behaviour at short and long wavelengths, their thinness, the possibility of producing large and homogeneous samples, and their modest price. The geometry of the periodic pattern that makes up the polarising gratings is chosen such that infrared light (with wavelength longer than 1 μm) is deviated, while optical light is transmitted essentially unaltered. Thus the polarising grating will act as a polarising beam splitter for circular polarisation without disturbing the operation of the AO system.

The polarisation module consists of a rotating stage with the two polarising gratings. The rotation axis is parallel to the axis of the incoming beam. It allows the positions of the two output beams to be switched to allow calibration of the difference in throughput for the two beams. Laboratory tests were already performed on a prototype system. The measured polarisation extinction, throughput and scattering, as a function of wavelength, show that the proposed device fits the requirements for spec-

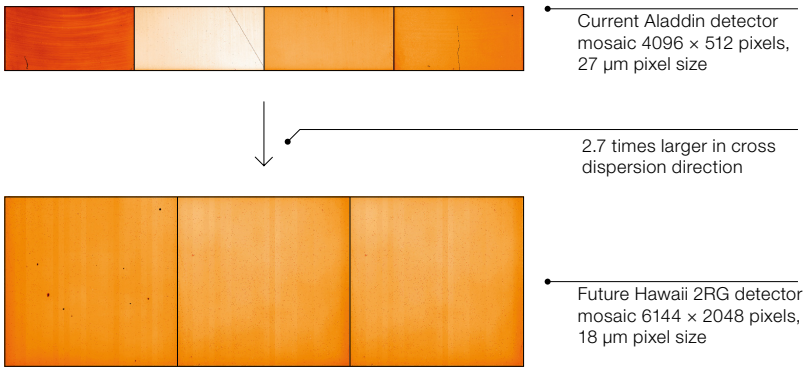

Figure 5. The present CRIRES detector mosaic focal plane array area compared to the new detectors with an increase of a factor of 2.7 in the cross dispersion direction.

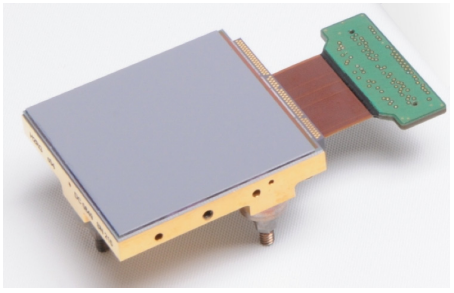

Figure 6. A ground-based astronomy HgCdTe H2RG is shown: Teledyne's H2RG package allows 32-output operation to be used for CRIRES+.

tropolarimetric measurements with CRIRES+ in the 1–2.7 µm wavelength range. The polarimetric unit will be compact and can be installed on the current CRIRES calibration slide.

MACAO refurbishment

The foreseen lifetime for the upgraded CRIRES+ is at least ten years. CRIRES is operated in conjunction with a 60-element curvature adaptive optics system, Multi-Application Curvature Adaptive Optics (MACAO), described by Paufique et al. (2004), and will require interventions to prevent its obsolescence. This is already planned for the MACAO Very Large Telescope Interferometer (VLTI) systems, installed in the coudé laboratory of the VLT Unit Telescopes (UTs). Accordingly, the CRIRES MACAO system will be refurbished in a similar manner to the VLTI systems by replacing and upgrading obsolete electronic boards. In addition there are plans to exchange the membrane mirror, re-coat additional mirrors, realign the optics and re-commission the full AO system.

The CRIRES+ metrology concept

In order to obtain deep enough datasets to explore exoplanetary atmospheres, CRIRES+ will need to be able to take stable exposures with high repeatability. The original CRIRES was limited by a spectral format reproducibility of about one pixel due to imperfect positioning of the pre-disperser and echelle grating mechanisms. However, a system of metrology was developed that facilitated the fine-tuning of the positioning of these mechanisms such that a 0.1 pixel reproducibility was achieved. Since CRIRES+ retains the original echelle grating mechanism, an adapted version of the metrology system will be required. This will comprise a fibre feed with an arc lamp spectrum that illuminates the echelle grating, automated detection and identification of reference lines, computation of correctional adjustment, and feedback to the grating mechanism and to a piezo actuator for fine tuning.

New data reduction software

The CRIRES+ project will also provide the community with a new data reduction software (DRS) package. The CRIRES+ DRS will support all of the offered observing modes and it is planned to provide the user with both science and publication-ready data products.

Project organisation and schedule

The project is being developed by ESO in collaboration with a consortium led by the Principal Investigator (PI) Artie Hatzes from the Thüringer Landessternwarte. Co-PIs are Ansgar Reiners (Göttingen) and Nikolai Piskunov (Uppsala). The partner institutes are:

- Thüringer Landessternwarte, Tautenburg (Germany)
- Georg-August-Universität Göttingen, Institut für Astrophysik (Germany)
- Istituto Nazionale di Astrofisica, Osservatorio di Arcetri and di Bologna (Italy)
- Uppsala University, Department of Physics & Astronomy (Sweden).

The reinstallation of NACO at the CRIRES focus of UT1 requires the removal of CRIRES in mid-2014, one year earlier than the original CRIRES+ schedule. For the upgrade, the instrument will be shipped back to ESO in Garching. Currently the project is in its preliminary design phase and the commissioning of the upgraded instrument is foreseen in 2017.

References

Baade, D. et al. 2009, The Messenger, 136, 20
Delfosse, X. et al. 2013, SF2A-2013: Proc. Annual meeting of the French Society of Astronomy and Astrophysics, ed. Cambresy, L., Martins, F., Nuss, E., Palacios, A., 497
Dorn, R. J. et al. 2006, SPIE, 5499, 510
Dressing, C. D. & Charbonneau, D. 2013, ApJ, 767, 95
Käufl, H. U. et al. 2004, SPIE, 5492, 1218
Paufique, J. et al. 2004, SPIE, 5490, 216
Quirrenbach, A. et al. 2012, SPIE, 8446, 84460R
Rayner, J. et al. 2012, SPIE, 8446, 84462C-12

NAOMI — A New Adaptive Optics Module for Interferometry

Reinhold J. Dorn[1]
Emmanuel Aller-Carpentier[1]
Luigi Andolfato[1]
Jean-Philippe Berger[1]
Françoise Delplancke-Ströbele[1]
Christophe Dupuy[1]
Enrico Fedrigo[1]
Philippe Gitton[1]
Norbert Hubin[1]
Miska Le Louarn[1]
Paul Lilley[1]
Paul Jolley[1]
Enrico Marchetti[1]
Steward Mclay[1]
Jérôme Paufique[1]
Luca Pasquini[1]
Jutta Quentin[1]
Andrew Rakich[1]
Robert Ridings[1]
Javier Reyes[1]
Christian Schmid[1]
Marcos Suarez[1]
Duc Thanh Phan[1]
Julien Woillez[1]

[1] ESO

The future adaptive optics system for the Auxiliary Telescopes of the Very Large Telescope Interferometer (VLTI), NAOMI, is presented. The NAOMI project will equip the telescopes with a low-order Shack–Hartmann system for the VLTI dual-feed light beams. The key benefits to current and future VLTI instruments and the preliminary design concept are described.

Introduction

The New Adaptive Optics Module for Interferometry (NAOMI) will be developed for and installed at the 1.8-metre Auxiliary Telescopes (ATs). The four ATs (Koehler et al., 2000) are designed for interferometry applications. Currently the ATs are equipped with a visible tip/tilt sensor called STRAP (System for Tip/tilt Removal with Avalanche Photodiodes; Bonaccini et al., 1997) and the corrections are applied with a fast steering mirror. Under good seeing conditions this provides a reasonable correction of the atmospheric turbulence in the *K*- and *N*-bands, but as soon as the seeing degrades below 1 arcsecond, the instantaneous Strehl ratio delivered by the telescopes degrades significantly.

The goal of the project is to equip all four ATs with a low-order Shack–Hartmann adaptive optics system operating in the visible, in place of the current STRAP, in order to overcome the current limitations.

Motivation

Similar to high angular resolution instruments on single telescopes, the Very Large Telescope Interferometer is impacted by the residual wavefront errors from each of the telescopes in the array. These errors either degrade the fringe contrast directly or lower the flux coupled into a single mode fibre instrument. Whatever the exact mechanism, the sensitivity of the array is affected. With just the tip/tilt correction provided by STRAP, the quality of the wavefront delivered by the ATs depends heavily on the turbulent conditions. Nights with poor seeing, either in the free atmosphere or in the turbulent ground layer when there is almost no wind, are an impediment to the successful execution of demanding scientific observations.

By improving the wavefront quality delivered by the ATs for guide stars brighter than R = 13 mag, NAOMI will make the existing interferometer performance less dependent on the seeing conditions. The quality of interferometric data will therefore improve as a result. Fed with better and more stable image quality, the fringe trackers will achieve the fringe stability necessary to reach the full performance of the second generation instruments GRAVITY (Eisenhauer et al., 2011) and MATISSE.

Expected performance

Simulations based on the top-level requirements have been carried out to predict NAOMI's performance in various configurations and for different concepts. A trade-off analysis selected a 4 × 4 sub-aperture system operating at up to 500 Hz frame rate. On account of the limited size of the ATs (1.8-metre diameter primary mirror), a low-order system is sufficient to meet the required performance. Other drivers for this choice were simplicity and low-flux performance. The most stringent top-level requirement, that for a natural guide star of magnitude R = 15.5, NAOMI will be able to close the tip/tilt loop with a root mean square (RMS) of 0.14 arcseconds (measured at 500 Hz) on the sky over a period of typically 1 minute, is met with this configuration. Figure 1 shows the expected NAOMI Strehl ratio as a function of guide star magnitude. One can see that more sub-apertures bring a higher on-axis performance, but suffer somewhat at the faint end. All the presented configurations

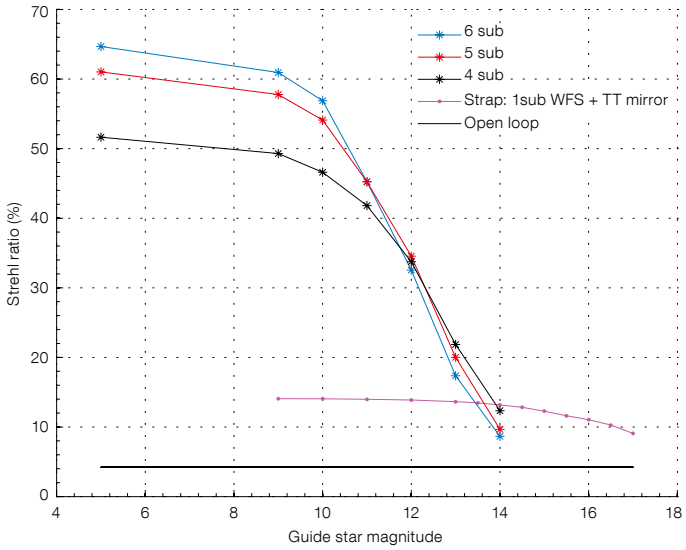

Figure 1. NAOMI performance simulation results showing the Strehl ratio as a function of guide star magnitude for three simulated sub-aperture configurations, 4 × 4, 5 × 5 and 6 × 6. The Strehl ratio was obtained on-axis in the *H*-band with a 6 × 6 pixel sub-aperture, 1-arcsecond seeing, overall delay of the wavefront sensor data by 2 ms and simulated at a frame rate of 500 Hz. Additionally the theoretical Strehl ratio curve for a tip/tilt correction with one sub-aperture (roughly corresponding to the current STRAP system) is shown, as well as the open-loop performance caused by the seeing.

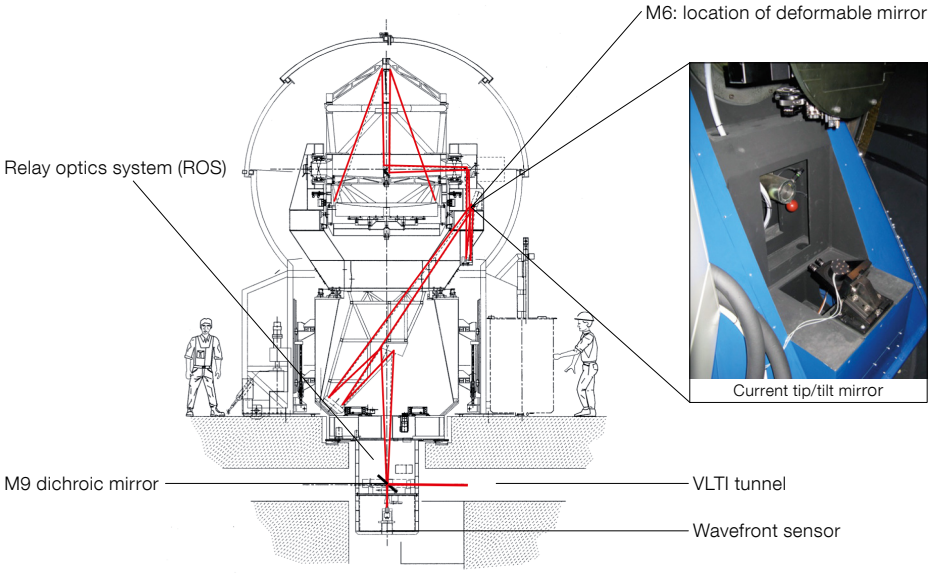

Figure 2. Schematic of an Auxiliary Telescope showing the optical train and the positions of the new modules for NAOMI: corrective optics (upper right) and wavefront sensor (below VLTI tunnel).

Figure 3. An Auxiliary Telescope with lifted ROS module ready to be moved to a different baseline position.

are within the specifications for high flux and about half of the performance is reached for guide stars of magnitude ~ 13.

NAOMI preliminary design

NAOMI will serve several VLTI modes and instruments operating from *H*- to *N*-band (i.e., PIONIER, AMBER, MATISSE and GRAVITY). The NAOMI operating mode will depend on the observing wavelength and the magnitude of the guide star and will be optimised accordingly. NAOMI will correct for active turbulence, tip/tilt and focus errors (also introduced by the telescope). In addition a chopping capability up to 5 Hz will be provided to be used for MATISSE to subtract the thermal background and to suppress low frequency detector noise.

Figure 2 shows the opto-mechanical layout of an AT and the lightpath through the telescope to the VLTI tunnel. The Coudé train re-images the pupil at an intermediate location (M6) where the actual fast steering tip/tilt mirror is installed. The dichroic (M9) splits the visible and infrared photons between the wavefront sensor in transmission and the interferometer in reflection. The infrared photons are reflected and sent via a field mirror and collimator to the delay line tunnel. For each telescope there is a dedicated relay optics system (ROS) located under the telescope. This relay optics system contains the Coudé optics, the star separators and the adaptive optics system wavefront sensor. If the telescope needs to be relocated to a different baseline position, the ROS is disconnected, lifted up and moved together with the telescope to the new location. Figure 3 shows an AT with a raised ROS module.

Corrective optics concept

NAOMI will replace the current tip/tilt mirror in the intermediate pupil plane with a corrective optics unit. M6 is located in the Coudé train facing down 20 degrees from the vertical in a diverging beam. This corrective optics module will be able to correct for the atmospheric turbulence, including tip/tilt, telescope static and dynamic errors, and should provide a chopping capability. ESO has launched a call for proposals for a competitive process to several institutes. The selected institute is expected to work with ESO on the preliminary and final design, prototyping, pre-production unit, manufacturing, assembly, integration and testing of the five to six corrective optics units according to the technical specification.

In order to reduce the cost and complexity of the corrective optics design we are exploring in parallel the use of other devices in the optical train to meet the chopping needs. One option under investigation is the use of the chopping capabilities of the star separator module. The star separator provides four major functions: pointing, chopping, tip/tilt control and pupil alignment. The mirror used for pointing can also be used for chopping because it coincides with the pupil plane. We are testing this function to compare the performance with the currently used tip/tilt mirror M6.

Wavefront sensor module

The NAOMI wavefront sensor will sense the visible light transmitted by the dichroic. The wavefront sensor (WFS) will use 16 × 16 pixels per sub-aperture, providing a large field of view to be used for star acquisition and open loop operations. Once the loop is closed, a window of 6 × 6 pixels will be sufficient to sense the wavefront distortions. This robust setup provides relative simplicity and is

compatible with the ESO Standard Platform for Adaptive optics Real Time Applications (SPARTA) baseline.

The main drivers for the choice of wavefront sensor are detector read noise (< 1 electron RMS) and high frame rate capability. The camera selected for NAOMI can be bought as a standard product from various companies and will be placed in the coudé focus fixed to the relay optics system ground plate on a movable *xy*-translation stage working as a field selector. As an example, Andor provides a detector with 128 × 128 pixels and 24 µm pixel size. This camera has already been used for some prototyping work. Andor's iXon3 860 (Figure 4) is a back-illuminated EMCCD (E2V CCD-60) and is designed for very rapid imaging of low-light events, combining > 500 frames/s with single photon detection capability and > 90 % quantum efficiency. Thermoelectric cooling down to –100° C minimises electron multiplication amplified dark current.

The raw image data of such cameras can be extracted for adaptive optics purposes by introducing a cable splitter box into the cable link between the camera head and a peripheral component interconnect express card from which the camera is controlled. The pixel stream from the camera is received via an in-house developed field programmable gate array card based on the AO new generation detector controller developed by the ESO Detector Department (Reyes et al., 2012). This card picks up the data via a low voltage differential signalling interface and sends it out as a serial front panel data port pixel stream compatible with SPARTA-Light.

Figure 4. View of the package for Andor iXon3 860: a possible wavefront sensor camera for NAOMI.

Software de-rotation

The deformable mirror (DM) for NAOMI rotates with the AT azimuth axis, whereas the wavefront sensor, which provides the control signals for the DM, has a fixed position in the telescope basement and does not co-rotate with the DM. The result is that the projection of the actuator pattern is rotating with respect to the wavefront sensor when the telescope is tracking an object on the sky. In order to avoid the use of an optical de-rotator, we have developed an algorithm to de-rotate the commands to the DM. NAOMI employs an algorithm based on the projection of the slope measurements into a modal base in order to recover the projected coefficients. A rotation matrix is then applied to the coefficients to recover the correct values for the DM orientation. The calculated and de-rotated coefficients are then projected into the DM space to recover the DM commands. The de-rotation matrix can be easily computed using the Zernike modal base due to its symmetric properties over a full rotation. The performance of this concept has been verified with end-to-end simulations. Figure 5 shows the software de-rotation performance expressed as Strehl ratio values as a function of rotation angle for the three DM configurations.

Real-time computing

For real-time computing, the ESO standard platform for Adaptive Optics Real Time Control (AO-RTC) applications, in its simplified version SPARTA-Light, will be used (Suarez Valles et al., 2012). It is the standard platform for building small/medium AO-RTC and is used also for GRAVITY's infrared wavefront sensors. SPARTA-Light is well suited for a loop rate of > 500 frames/s and an RTC latency of ≤ 1 ms, as required for NAOMI. Furthermore SPARTA will include the possibility of implementing the software de-rotation concept and can host a piston removal algorithm and chopping control.

Figure 5. The software de-rotation performance as a function of rotation angle for the three DM configurations controlling 15 Zernike modes (pure Zernike, 5 × 5 and 9 × 9 actuators for the deformable mirror) is plotted. The simulations have been obtained in *H*-band with 6 × 6 pixels per sub-aperture at 1 arcsecond seeing conditions with a wavefront sensor data delay of 3 ms. The Strehl ratio varies between 51.4 % and 50.2 %. This is less than 2 % (relative) and hence the result shows no significant loss in performance due to the rotated pupil images.

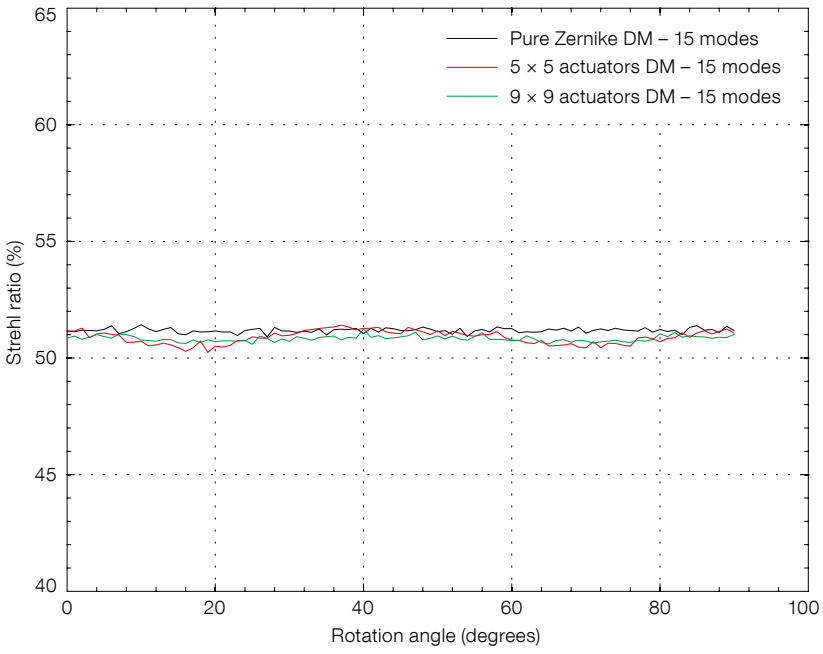

Software architecture

The NAOMI-related software architecture can be split into different layers or modules: the RTC software, the NAOMI control software, the telescope control software and the VLTI interferometer supervisor software (ISS). The NAOMI software is a subsystem of the auxiliary telescope control software (ATCS) as depicted in Figure 6. It includes a high-level control component responsible for driving the AO software and all additional hardware devices like the filter wheel and the pupil alignment function. The AO software is based on the SPARTA software, providing the coordination components running on the NAOMI workstation and a real-time part executed by the RTC. The RTC software processes the data coming from the WFS camera and calculates the commands to be applied to the corrective optics. The auxiliary telescope control software will be updated to support the new calibration and alignment procedures required by NAOMI. The selected architecture minimises the changes to the interface between the interferometer supervisor software and the auxiliary telescope control software.

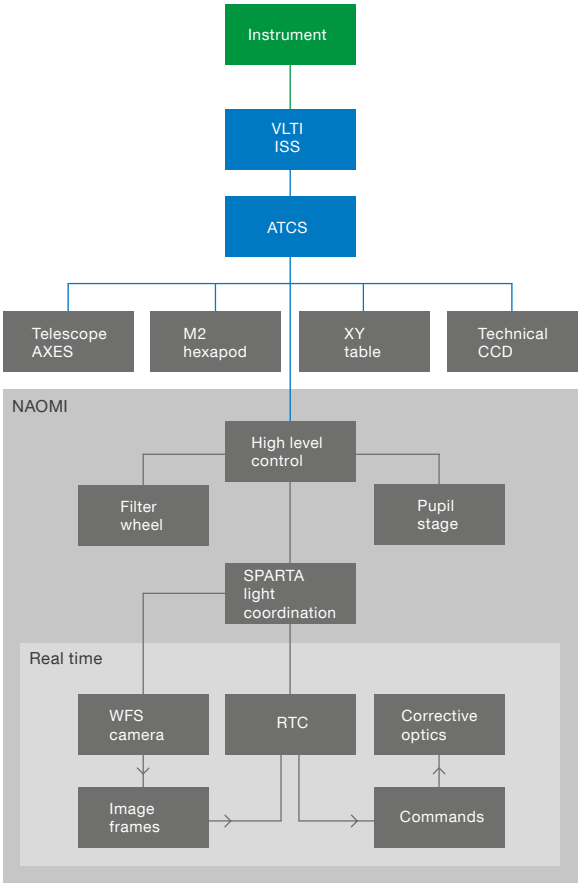

Figure 6. Flowchart of the NAOMI software design within the VLTI software architecture.

Project schedule

NAOMI was originally proposed in 2008. The project held a design review in March 2011 presenting a conceptual design and its scientific and technical rationale. NAOMI is now being promoted due to the upcoming second generation VLTI instruments. The current timeline foresees the preliminary design review by the end of this year, the shipment of a first system to Paranal in 2016 with the installation of the remaining three systems by the end of 2017.

References

Bonaccini, D. et al. 1997, Proc. SPIE, 3126, 3126–77
Eisenhauer, F. et al. 2011, The Messenger, 143, 16
Koehler, B. et al. 2000, Proc. SPIE, 4006, 13
Reyes Moreno, J. 2012, Proc. SPIE, 8447, 8447A
Suárez Valles, M. et al. 2012, Proc. SPIE, 8447, 84472Q

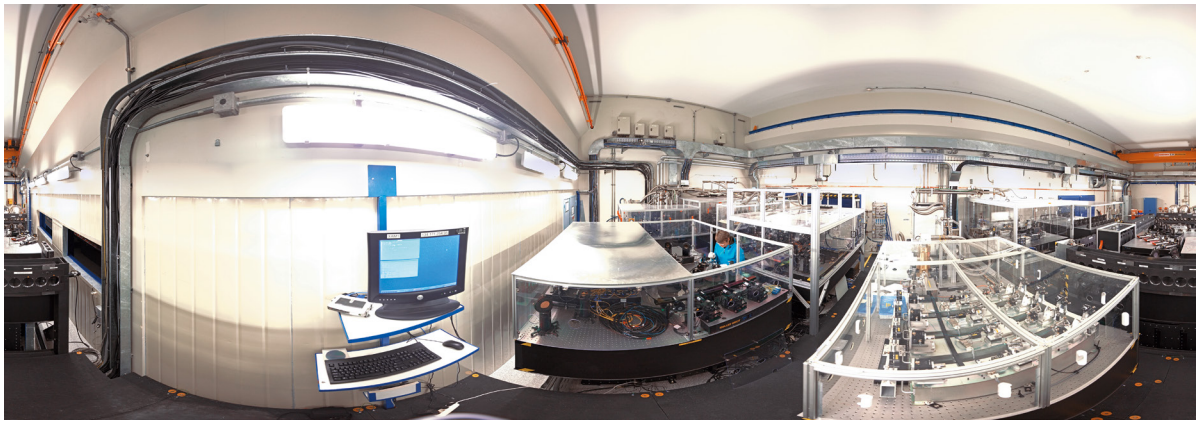

360-degree panorama image of the Very Large Telescope Interferometer (VLTI) underground laboratory.

Mathematical Algorithms and Software for ELT Adaptive Optics — The Austrian In-kind Contributions for Adaptive Optics

Andreas Obereder[1]
Ronny Ramlau[2]
Enrico Fedrigo[3]

[1] MathConsult GmbH, Linz, Austria
[2] Industrial Mathematics Institute, Johannes Kepler University Linz, Austria
[3] ESO

The four-year Austrian in-kind project to provide improved algorithms and software for the correction of atmospheric turbulence in adaptive optics (AO) imaging, part of Austria's contribution to accession to ESO, has just concluded. The project work of the Austrian Adaptive Optics (AAO) team is summarised. Very fast algorithms, which are substantially quicker than previous implementations, have been developed in the fields of single conjugate, multi-conjugate, multi-object and extreme AO. As a result of this project, control of AO systems to achieve the necessary level of correction on extremely large telescopes can become managable with computers of reasonable size and cost.

On 22 October 2013, the final review of a four-year project, Mathematical Algorithms and Software for ELT Adaptive Optics, came to its conclusion. This project, part of Austria's in-kind contributions on its accession to ESO, was approved by the ESO Council in June 2008 and started officially in October 2009. The aim was the development of algorithms and software for the correction of images, degraded by atmospheric turbulence, using adaptive optics (AO), and faster than the traditional approach taken until now. This correction process is based on the reconstruction of the refractive index of the atmosphere from noisy measurements of the incoming wavefront; up until now, these corrections have been implemented with a matrix-vector multiplication. The challenging goal of this project was to invent a new and different approach to this problem while, at the same time, reducing the load on the computer that performs the computation.

The algorithms developed are very fast, of excellent quality and can provide enormous savings in the computing power required to reconstruct the wavefront on future AO systems for the European Extremely Large Telescope (E-ELT). But probably the most significant achievement of this study is to make the control of those AO systems manageable with computers of reasonable size and cost, and, in the case of eXtreme Adaptive Optics (XAO), to bring such a complex system into the domain of feasible implementations.

The team

Three institutes, all based in Linz, have contributed to this project: the Industrial Mathematics Institute of the Johannes Kepler University (JKU) Linz, with around ten applied mathematicians who specialise in inverse problems, regularisation theory and signal processing, among others; the Johann Radon Institute for Computational and Applied Mathematics (RICAM), a mathematical research institute belonging to the Austrian Academy of Sciences, with approximately 50 mathematicians; and MathConsult GmbH, a company that provides mathematical methods and software in industry and finance and consists of mathematicians, physicists and computer scientists. Thus, several applied mathematicians and physicists — from Masters and PhD students, to postdocs and professors — were combined in the Austrian Adaptive Optics (AAO) team[1]; part of the team is pictured in Figure 1.

Why adaptive optics?

Images from ground-based telescopes suffer from turbulence in the atmosphere, which lead to serious image degradation. AO is a technique for the correction of the phase of the incoming light which aims to compensate, in real time, for rapidly changing optical distortions in the atmosphere by deforming a mirror. The correction is based on the reconstruction of the turbulence in the atmosphere from measurements in the direction of one or several guide stars. A guide star is any star in the sky bright enough to be used as a sensor (natural guide star [NGS]) or an artificially generated light source using a laser (laser guide star [LGS]).

For each AO correction step, several subproblems have to be solved, where the most important is the severely ill-posed atmospheric tomography. This subproblem resembles limited angle tomography, as the approach to the solution requires the reconstruction of the atmospheric turbulence layers from data measured by wavefront sensors in several guide star directions, separated only by a fraction of a degree.

Many of these systems, such as multi-conjugate adaptive optics (MCAO), laser tomography adaptive optics (LTAO) and multi-object adaptive optics (MOAO) depend on a sufficient reconstruction of the turbulence profiles in order to obtain a good correction. Due to the steady

Figure 1. The Austrian Adaptive Optics (AAO) team photographed in the hallway at ESO Headquarters during the final project review. Back row, left to right: Roland Wagner, Andreas Binder, Daniela Saxenhuber, Ronny Ramlau, Iuliia Shatokhina; front row, left to right: Andreas Obereder, Mischa Yudytskiy, Günter Auzinger. Other team members not pictured: Tapio Helin, Sergiy Pereverzyev jun., Matthias Rosensteiner, Masha Zhariy.

growth in telescope size, there is a strong increase in the computational load for atmospheric reconstruction with current methods, in particular using the standard brute-force technique of matrix-vector multiplication (MVM).

The specialist team from Linz had the challenging goal of inventing new approaches to this problem that delivered the same quality of correction as current techniques, while, at the same time, greatly reducing the computing load. This four-year project has recently successfully completed its final review. In order to test and compare the different methods in terms of reconstruction quality, as well as computational speed, the ESO end-to-end simulation tool OCTOPUS was used. For all the subprojects, the team provided technical reports on the algorithms that had been developed and the computational architecture in terms of conceptual design, performance verification and prototypes of the algorithms, including user and installation manuals. There were separate mid-term and final reviews for each subproject in order to verify the compatibility of the first deliverables with the technical specification.

Project organisation

The AAO project was divided into four subprojects. Within the first subproject, AO1, the team acquired the necessary knowledge in the field of AO. This phase lasted for nine months and ensured a mutual understanding of the requirements fixed by the technical specifications. In the introductory study to AO1, the Austrian team reviewed existing AO algorithms, methods and techniques and became acquainted with the state of the art in the field. The modelling of the influence of the turbulent atmosphere on wavefront sensor measurements also included a study of the physics of different sensors and the derivation of forward operators that describe this connection mathematically.

The subprojects AO2 and AO4 comprised the work on MCAO, single-conjugate adaptive optics (SCAO) and XAO and both began at the end of AO1, i.e., in July 2010. Through the next 27 months, the team worked on the development of algorithms and software prototypes. The last subproject — AO3 — began in October 2010 and finished in October 2013. Within the subproject AO3, the research was focused on ground layer adaptive optics (GLAO), MOAO and LTAO systems as a pre-study for the latter.

SCAO and XAO

The subproject AO4 was concerned with the development of reconstruction methods for SCAO. An SCAO system uses the measurements of the wavefront of an NGS in order to obtain the optimal shape for a deformable mirror, such that, after the wavefront conjugation, a sharp image of the science target is obtained. The main computational task for SCAO is the reconstruction of the incoming wavefront of the guide star from measurements of a wavefront sensor. As the sensors usually do not measure the wavefront directly, the reconstruction of the wavefront requires the solution of an inverse problem. For SCAO, different types of wavefront sensors are used. We considered systems that use a Shack–Hartmann sensor, which measures averages of the gradient of the incoming wavefront, and systems that use pyramid-type wavefront sensors. Pyramid wavefront sensors allow for a higher contrast of the corrected images as well as a higher resolution of the wavefronts and are therefore used for XAO systems.

For the reconstruction of the incoming phase from Shack–Hartmann wavefront sensor data, the cumulative reconstruction algorithm (CuRe) was developed (Zhariy et al., 2011). CuRe is based on one-dimensional line integration and a subsequent coupling of those lines in the orthonormal direction to obtain the full two-dimensional reconstruction. CuRe has been further improved in terms of noise propagation by the application of domain decomposition leading to the CuReD algorithm (CuRe with domain decomposition; Rosensteiner, 2011). Simulated results obtained with CuReD are shown in Figure 2.

CuReD has been tested on ESO's optical high order test bench (HOT) as well as on-sky (by Durham University on the William Herschel Telescope, La Palma). The CuReD algorithm performs with a computational complexity of O(n), that is, it scales linearly with the number of degrees of freedom and not quadratically (as in the standard matrix-vector multiplication), it can be parallelised in all guide star directions and is pipelineable. The algorithm fulfills the requirements of the project both with respect to quality and

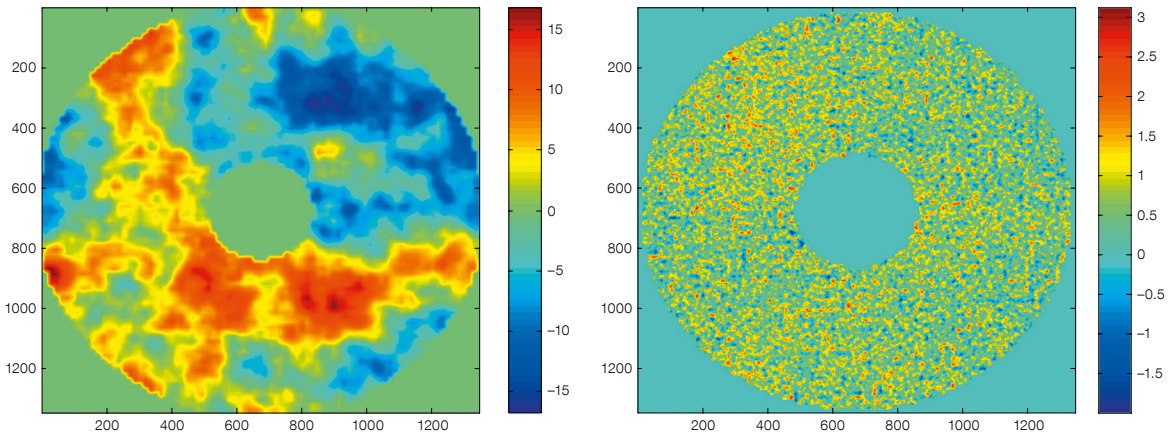

Figure 2. Reconstructions with CuReD for a 42-metre telescope with an 84 × 84 sensor are shown. Left: the wavefront as reconstructed with CuReD. Right: the residual between the reconstructed wavefront and the simulated one. Colour bars show units in radians.

speed. The speed-up factor reached, for example, for XAO was 1100 (see Table 1 for a summary of the results obtained). In combination with a data-preprocessing step, CuReD is also well suited for the XAO system with a modulated pyramid wavefront sensor (Shatokhina et al., 2013).

Besides giving the required quality, both methods (CuRe and CuReD) provide a significant increase in the reconstruction speed compared to the MVM method. More methods for wavefront reconstruction from Shack–Hartmann data have been developed, such as the wavelet method or an algorithm based on singular value decomposition. Further methods for the pyramid sensor were developed: the CLIF (convolution with linearized inverse filter) and the CGNE (conjugate gradient for the normal equation) for the modulated and the HTMR (Hilbert transform with mean restoration) for the non-modulated sensor. See Table 1 for their performance figures.

MCAO

The subproject AO2 was concerned with the development of reconstruction methods for MCAO, with the aim of achieving a uniform image quality over a larger field of view, and, thus, allowing the observation of different astronomical objects at the same time. To this end, many MCAO systems use a combination of laser and natural guide stars. A wavefront sensor is assigned to each guide star and several deformable mirrors, optically conjugated to different altitudes, are used for image correction. The shape of the deformable mirrors is computed based on measurements from the wavefront sensors.

Owing to the rapidly changing atmosphere, the mirror shapes of the telescope have to be updated with a frequency of 500 Hz, i.e., each reconstruction has to be performed within a millisecond. The algorithms developed were the finite element–wavelet hybrid algorithm (FEWHA), see (Yudytskiy et al., 2014), and three-step approach methods that solve the atmospheric tomography problem using the Kaczmarz iteration (Rosensteiner & Ramlau, 2013), the gradient-based method or the conjugate gradient (CG) algorithm.

Algorithm	Applicable System	Speed-up
Cure (CuReD, Cure w/ preprocessing)	SCAO/XAO	100–1000
CLIF for pyramid sensor	XAO	200
Multi-Cure for GLAO	GLAO	100–1000
Kaczmarz, Gradient-based, CG	MCAO/LTAO/MOAO	10–200
Wavelets (FEWHA) with PCG	MCAO/LTAO/MOAO	10–200

Table 1. Portfolio of algorithms developed by the Austrian team for in-kind contributions for AO and the speed-up with respect to the reference case (ESO MVM implementation).

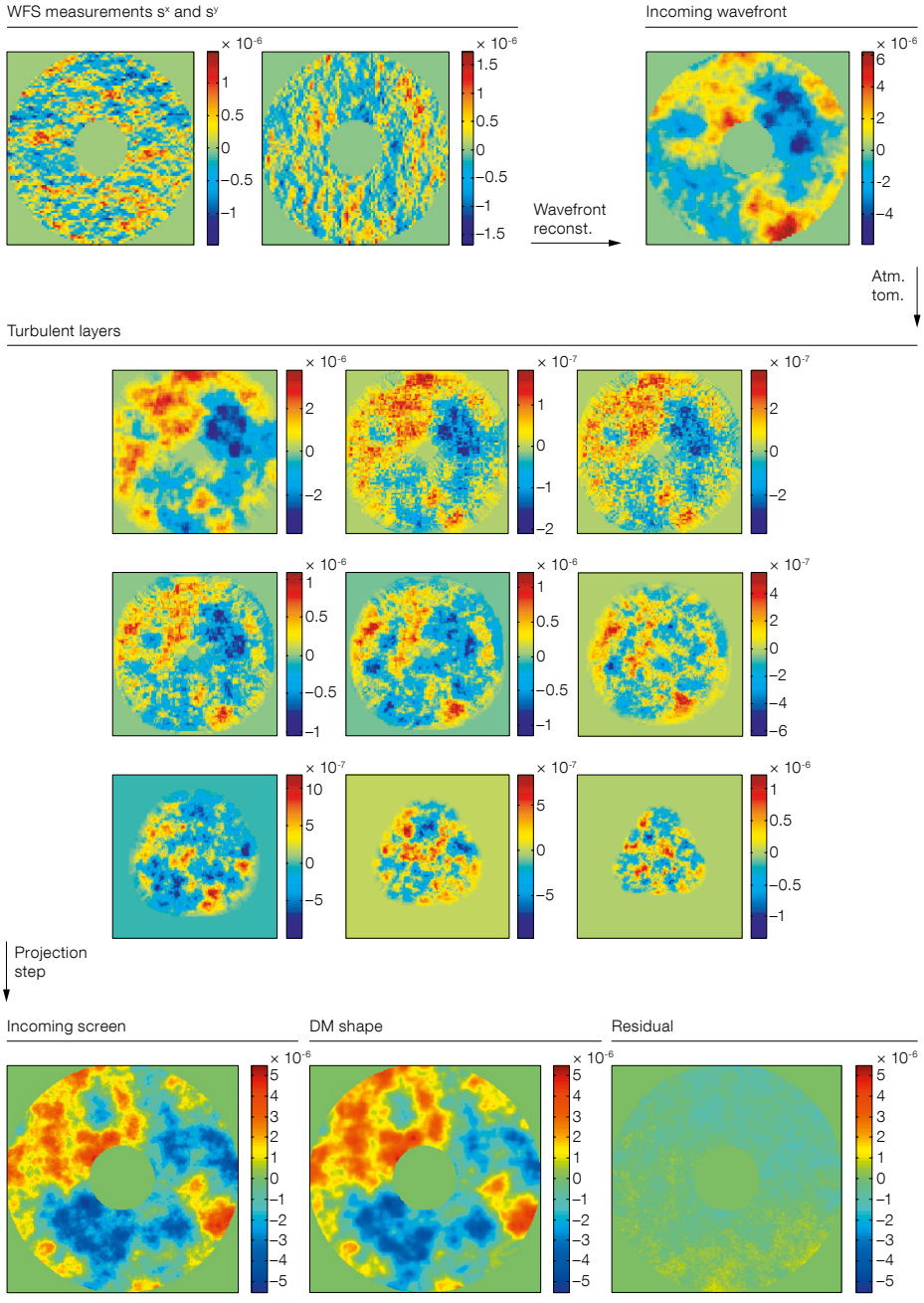

Figure 3. A visualisation of the three-step approach. From the wavefront sensor measurements, the wavefront is reconstructed using CuReD (step 1, upper). This is performed in parallel on all wavefront sensors. The reconstructed wavefronts are used in the second step to perform the atmospheric tomography using, for instance, the Kaczmarz algorithm (step 2, middle). Finally the reconstructed layers that have been computed in step 2 are used in the projection step to compute the best configuration of the available deformable mirrors (step 3, lower). All colour bars show optical path difference in metres.

FEWHA is a two-step method, i.e., it reconstructs turbulent layers from Shack–Hartmann data and then performs a projection step. It tackles the problem of atmospheric tomography reconstruction by computing the Bayesian maximum *a posteriori* estimate with a preconditioned conjugated gradient algorithm coupled with a multi-scale strategy. In the hybrid algorithm, the turbulence layers of the atmosphere are made discrete using a finite element and a wavelet basis simultaneously. A wavelet representation of layers has several advantages. First, wavelets have useful properties in the frequency domain, which allow turbulence statistics to be represented efficiently. Secondly, the operation of transforming the coefficients between the bilinear finite element basis and the wavelet basis, called the discrete wavelet transform (DWT), has a linear complexity and can be parallelised. Finally, wavelets have a good property of approximation, which means a turbulence layer can be well approximated using only a few wavelet coefficients. In contrast, the finite element representation of layers allows the atmospheric tomography operator to be represented very efficiently. Due to these properties, the resulting finite element–wavelet hybrid algorithm delivers good qualitative performance, requires only a few iterations, and is computationally cheap compared to MVM, due to FEWHA's linear complexity and high level of parallelisation.

The three-step approach, shown in Figure 3, decouples the problem into the reconstruction of the incoming wavefronts from the wavefront sensor data, the reconstruction of the turbulent layers (atmospheric tomography) from the reconstructed incoming wavefronts and the computation of the optimal mirror shape (fitting step) from the reconstructed atmosphere. The first step has been very efficiently solved by the CuReD algorithm, developed within the subproject AO4. For the atmospheric tomography problem, the Kaczmarz algorithm, the gradient-based method and the CG method have been used. All three perform with linear complexity and parallelise well. An efficient preprocessing step has been developed to counter noise due to spot elongation. The three-step approach allows each of the three subproblems to be solved independently and, thus, guarantees a fast and flexible reconstruction. Moreover, it can be easily used with the wavelet wavefront reconstructor, instead of CuReD, and also for the pyramid wavefront sensor with the CuReD algorithm with preprocessing (P-CuReD).

Both methods, FEWHA and the three-step approach, fit the atmosphere onto the deformable mirrors as the final step. Atmospheric reconstruction can be performed, either on artificial layers at the altitudes to which the deformable mirrors are conjugated or on more layers. Then, by means of the Kaczmarz iteration or the conjugate gradient method, the mirror shapes can be optimised in multiple directions. See Table 1 for the respective performance figures.

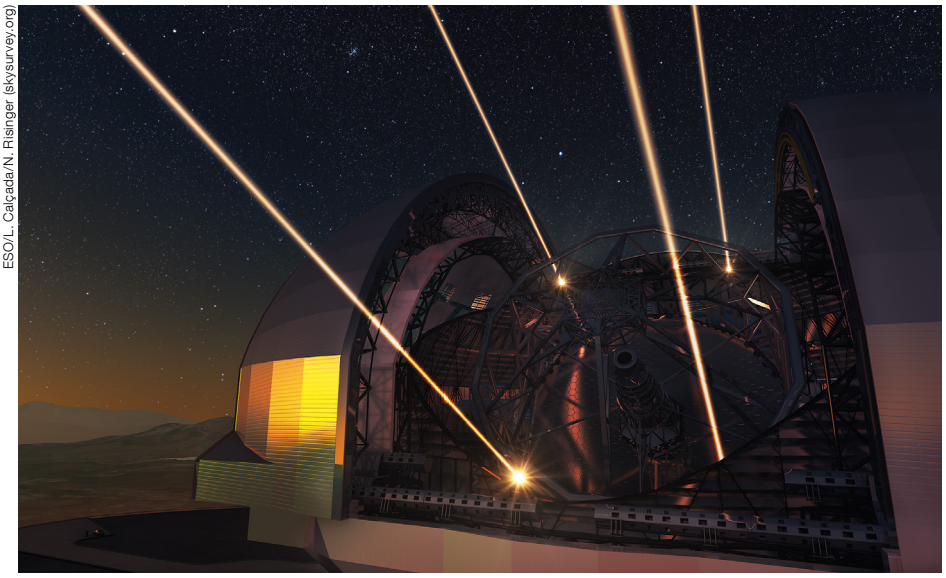

ESO/L. Calçada/N. Risinger (skysurvey.org)

Figure 4. An artist's impression of a laser guide star system in action on the E-ELT, showing how the laser-based MCAO, LTAO or MOAO systems studied in the course of this project could be operated.

GLAO, LTAO and MOAO

For GLAO, the CuReD algorithm was used to reconstruct each of the incoming wavefronts from the guide stars separately. Then the wavefronts were averaged to make an estimate of the ground layers. LTAO and MOAO systems — similar to MCAO — require fast and efficient algorithms for the atmospheric tomography subproblem. However, in an MOAO system, several deformable mirrors are used for wavefront correction in the directions of each of the multiple objects of interest. A sufficiently accurate reconstruction of atmospheric turbulence over a wider field of view is vital to obtain a good wavefront correction for these systems.

FEWHA was the method of choice for the LTAO and MOAO parts of subproject AO3. This algorithm was able to overcome the new challenge of a wide field of view (7.5 arcminutes) combined with the problem of spot elongation introduced by the LGS. FEWHA was compared to the ESO version of the state-of-the-art algorithm and has been shown to surpass the reference provided in almost all test cases. In terms of speed, a real-time computing (RTC) prototype of the algorithms showed that the method performs well on off-the-shelf hardware and has the potential to achieve the required reconstruction time of 1 millisecond on a dedicated RTC system. FEWHA outperforms ESO's MVM method, which serves as a benchmark in terms of speed, by a significant margin and is significantly more compact in terms of the required RTC hardware configuration for MOAO.

All algorithms can tackle the problem of tip/tilt indetermination and the cone effect efficiently. All the developed methods are formulated matrix-free, i.e., operate in a purely functional setting, which reduces computational complexity considerably. Furthermore, they scale linearly and yield

a speed-up factor for MCAO/LTAO/MOAO of between 10 and 200, as shown in Table 1.

Future work

The next steps following on from this work are the analysis and inclusion of real-world effects such as spiders, dead actuators, mis-registration, different NGS asterisms or sodium layer variability for LGS, among others. The AAO team also would appreciate being able to test the developed reconstructors on more simulation systems, optical benches and on sky.

Project completion

Throughout the whole project, the AAO team analysed six AO-system types and published more than 17 scientific papers and attended several AO-related conferences and workshops. Four to eight mathematical reconstruction algorithms were analysed extensively for each of the considered systems, for a total of ~ 30 algorithms or customisations of an algorithm to a particular case, and the AAO project produced about 50 mathematically dense technical reports.

The benefits of the project are many-sided: easy implementable algorithms have been developed, which reduce parameter tuning considerably and do not require time-consuming pre-computations. Major speed-up factors were achieved, which could substantially reduce hardware costs. These new adaptive optics algorithms are very fast, as shown in Table 1, and provide excellent performance results. This leads to enormous savings in the computing power required to handle AO data from a telescope like the E-ELT. The most significant achievement of this study was to make the control of those systems manageable with computers of reasonable size and cost and, in the case of more extreme kinds of adaptive optics, to bring such a complex system into the realm of feasible implementation.

Acknowledgements

The successful work of the Austrian Adaptive Optics team would not have been possible without the help of the staff involved at ESO. We would like to thank in particular Enrico Fedrigo and Miska Le Louarn for their constant support. Valuable input also came from Richard Clare, Clementine Béchet, Curtis Vogel and Kirk Soodhalter.

References

Rosensteiner, M. 2011, *Wavefront reconstruction for extremely large telescopes via CuRe with domain decomposition*, J. Opt. Soc. Am. A, 28, 2132

Rosensteiner, M. & Ramlau, R. 2013, *The Kaczmarz algorithm for multi-conjugate adaptive optics with laser guide stars*, J. Opt. Soc. Am. A, 30, 1680

Shatokhina, I. et al. 2013, *Preprocessed cumulative reconstructor with domain decomposition: a fast wavefront reconstruction method for pyramid wavefront sensor*, AO, 52, 2640

Yudytskiy, M., Helin, T. & Ramlau, R. 2014, *A finite element-wavelet hybrid algorithm for atmospheric tomography*, J. Opt. Soc. Am. A, 31, 550

Zhariy, M. et al. 2011, *Cumulative wavefront reconstruction for the Shack–Hartmann sensor*, Inv. Prob. Imag. 5, 893

Links

[1] Austrian Adaptive Optics Team webpage: http://eso-ao.indmath.uni-linz.ac.at/

ESO/J. Girard

Time-lapse view of the Paranal Observatory when the Laser guide star was tracking a target for 30 minutes. See Picture of the Week 1234 for more details.

The X-shooter Imaging Mode

Christophe Martayan[1]
Andrea Mehner[1]
Giacomo Beccari[1]
Eduardo Peña[1]
Wolfgang Hummel[1]
Alain Smette[1]
Andrea Modigliani[1]
Joel Vernet[1]
Hans Dekker[1]
Nadine Neumayer[1]
Vincenzo Mainieri[1]
Sabine Moehler[1]
Roberto Castillo[1]
Miguel Riquelme[1]

[1] ESO

X-shooter is a three-arm multi-wavelength (~ 300–2500 nm) medium resolution spectrograph installed on the VLT's Unit Telescope 3. From April 2014, a complementary imaging mode is offered to the astronomical community. This new observing mode uses the acquisition and guiding camera facility equipped with a set of Johnson and SDSS filters and gives the option of complementing the spectroscopic data with multi-band images and photometry. The main characteristics of the X-shooter imaging mode, an outline of its calibration and a few examples of scientific applications are presented.

Motivation for a limited imaging mode

Right from the design phase, there has been the intention to offer a complementary imaging mode for X-shooter, utilising its acquisition and guiding camera (AGCCD, see Sørensen et al. [2004]), in addition to its spectroscopic capabilities. Since X-shooter remains primarily a set of spectrographs (see Vernet et al., 2011), the imaging mode of X-shooter was not developed, commissioned or offered to the community until Period 93 (P93). Nevertheless, the AGCCD is provided with a set of Johnson and Sloan Digital Sky Survey (SDSS) filters. The images taken with the AGCCD are often used by the community to complement spectroscopic data with multi-band photometry. Typical uses of the AGCCD images are the flux calibration of spectra or the study of variability in transient objects such as gamma-ray bursts, exoplanets or variable stars. Following the growing interest by the community, it was decided to offer an imaging mode for X-shooter starting from Period 93 (April 2014).

Main characteristics, calibration plan and stability

The detector of the AGCCD is an E2V CCD with a peak sensitivity at 580 nm. The field of view is about 1.5 by 1.5 arcminutes and the pixel scale is about 0.17 arcseconds. Only the fast unbinned readout mode is offered in order to minimise overheads. However, the data quality is preserved by using a new gain that allows a relatively low readout noise and noise structure. This gain will help to avoid saturation of bright objects as well, while the bias value also becomes lower than in previous periods. Finally, the non-linearity is lower than 1 % over most of the dynamic range. Details (gain, readout noise [RON], dark and bias levels, etc) of the AGCCD are summarised in the Table 1. In Table 2, the list of filters and their fringing amplitudes are presented. The zero points at Unit Telescope 2 (UT2), where X-shooter was previously placed, and later on at UT3, its current location, are provided in Table 2. Their small variation corresponds to differences in the optical quality of the two telescopes.

Stability and accuracy

A study of the detector stability and performance was performed using daytime calibrations and photometric standard star observations. In Figure 1 we show the variability of the AGCCD bias and readout noise levels over a period of 52 days. The root mean square (RMS) of the bias level variability is 0.33 % while for the RON it is 0.56 %.

The short-term photometric stability was monitored over 1 hour using the spectrophotometric standard star GD71. The 1σ standard deviations in the *B*- and *V*-bands are 0.006 mag for both bands. Archival data of the standard star EG274 were used to check the long-term stability of the *V* magnitude over 500 days. In Figure 2, we show the variability of the *V* magnitude of EG274 with time (blue points). Only images obtained with photometric transparency (as determined by other Paranal instruments), with a seeing better than 1.3 arcseconds and not too early in twilight, when the sky background varies quickly, were employed for these monitoring observations. However, about 95 % of the observations were performed in twilight, with an unavoidable negative impact on the stability of the magnitudes. We performed aperture photometry on the images with an aperture radius of about 1.5 arcseconds using Sextractor (Bertin & Arnouts, 1996).

Table 1. Main AGCCD detector characteristics.

Detector type	E2V CCD57-10IE	Quantum efficiency	82 % at 580 nm, 50 % at 380 and 820 nm
Pixel scale (arcsecond/pixel) since P92 at UT3	0.1744 ± 0.0016	Field of view (arcminutes)	1.5 × 1.5
Gain (e-/ Analogue-to-Digital Unit [ADU])	1.29 ± 0.02	Readout noise (RMS in e-)	4.14 ± 0.08
Saturation (ADU)	65 535	Readout mode, binning, and overheads	Fast, binning 1 × 1, total time = 1.12 s
Dark current level (e-/pixel/s)	0.97	Bias level (ADU)	1688 ± 5.5
Non-linearity (ADU)	< 1 % at 10 000 and 50 000		

Table 2. Filters and zeropoints.

List of filters	*U,B,V,R,I, u',g',r',i',z'*	Position angles	9999 = parallactic (default) or other
Fringing amplitude (peak to peak)	Filter-dependent, 3 % in *I, z'*		
Zeropoints U/B/V/R/I ± 0.10 mag at UT3 (P92 onward)	24.83 / 27.91 / 27.83 / 27.74 / 27.36	Old zeropoints U/B/V/R/I ± 0.10 mag at UT2 (until P91)	24.95 / 27.74 / 27.63 / 27.83 / 27.49

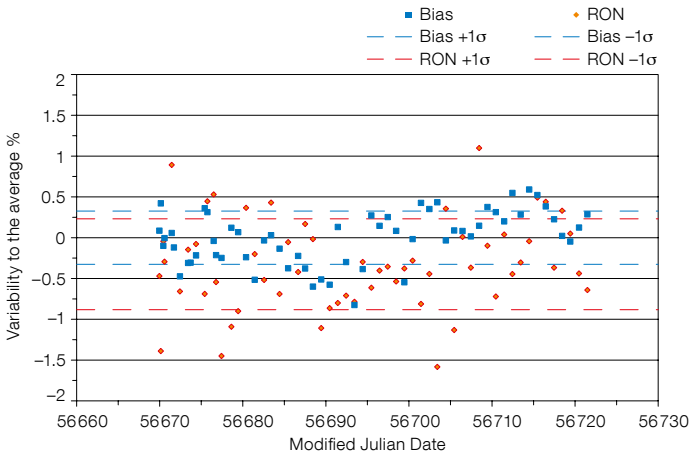

Figure 1. X-shooter AGCCD variability (or relative difference) in the bias level (blue squares) and RON level (orange diamonds) in % from the average with time are plotted. For each of the curves the ± 1σ spread is shown.

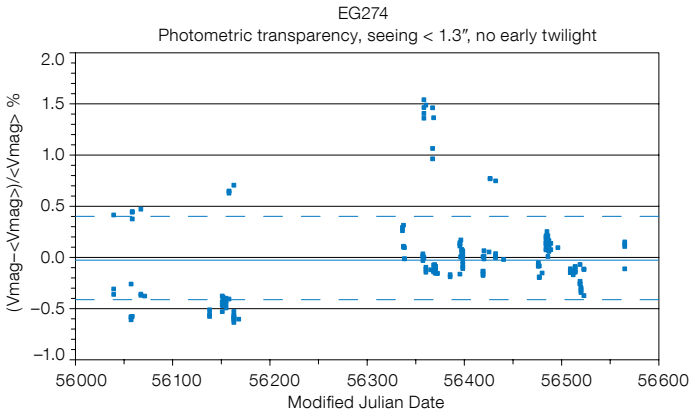

Figure 2. AGCCD photometric variability (%) for the *V* magnitude of the star EG274. Only points observed under photometric transparency, seeing < 1.3 arcseconds and with maximum Sun altitude of −10° were retained. The average and 1σ limits are shown.

Despite the non-ideal observing conditions, the average deviation appears to be stable (RMS of 0.42 % over 1.4 years).

Astrometric measurements show a standard deviation of 0.1 arcseconds. Distortion maps are also available. The astrometric system of X-shooter was calibrated using Two Micron All Sky Survey (2MASS) coordinates for standard star fields.

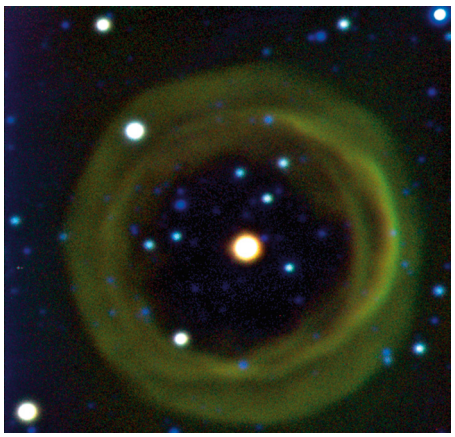

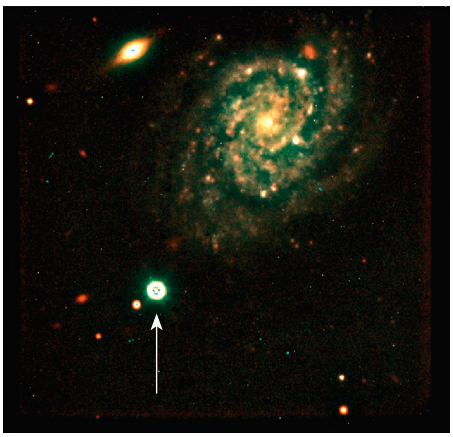

Figure 3. Examples of complementary scientific observations with the X-shooter AGCCD.
Left: The planetary nebula Shapley 1 from *BVI* filter images, taken with GenericOffsets and exposure times of 60, 45 and 30 s respectively.

Right: The galaxy NGC 7259 with SN2009ip indicated. For this image, *VRI* filter observations with 60-second stare observations were combined.

Calibration plan and templates

Several calibration and science templates were created to perform biases (ten are taken daily), darks (3 × 10 s monthly, or on request), detector linearity measurements (taken on a monthly basis), twilight flat-fields and optical distortion measurements. Twilight flat-fields (ten per filter, taken monthly) are preferred because the optical configuration of the instrument, optimised for the spectrographs, leads to only partial light coverage of the AGCCD and therefore to non-uniform illumination of the detector.

For science observations, the user has the choice between stare (XSHOOTER_img) and generic offset (XSHOOTER_img_GenericOffset) templates. The latter allows the telescope to be offset to map a field. There is also a pure imaging acquisition template (XSHOOTER_img_acq) that does not perform any flexure correction or setups of the spectrographs. In most cases we recommend the use of the generic offset template instead of the stare template to achieve better image quality. X-shooter, however, remains foremost a set of spectrographs and imaging-mode-only observation blocks (OBs) are not offered in service mode (SM) except for standard OBs of zeropoints/astrometric references, which will be charged to the users. Visitor mode (VM) users are not affected by this restriction.

In the imaging user manual[1], the allowed combinations of templates in SM and VM and other technical details such as the distortion maps, filters curves, etc., are reported. In addition, because there is no exposure time calculator support, the manual provides some clues about the expected signal-to-noise ratio (SNR) and exposure times. The health of the AGCDD is monitored every day and some plots are publicly available[2].

Science examples and basic data reduction

In Figure 3, two examples of science observations with the X-shooter imaging

mode are shown. The planetary nebula, Shapley 1 (PN G329.0 +01.9) was also observed in *BVI*-bands in generic offsets mode and a three-colour image (created with stiff [Bertin, 2011]) is shown in Figure 3 (left). The structures of the nebula are clearly visible. Observations of the galaxy NGC 7259 with the supernova SN2009ip were performed in stare mode and are shown in Figure 3 (right). This object was a luminous blue variable (LBV) star which underwent two strong LBV outbursts in 2009 and 2010, before finally exploding as a SN IIn in 2012 (Mauerhan et al., 2013).

The binary star AA Dor was monitored during several nights (mostly in twilight) using the stare mode and the resulting light curve is shown in Figure 4a. Only the primary transit was observed, but the resulting lightcurve already gives a good indication of what can be done concerning binary objects. A colour–magnitude diagram of the globular cluster 47 Tucanae obtained from multi-band observations is shown in Figure 4b. With 2 s exposure time in *V*-band and 40 s in the *B* and *U* filters, we are able to sample the cluster stars from the tip of the red giant branch (RGB) down to ~ 1.5 mag below the main sequence turn-off (MS–TO).

No pipeline support will be provided. The standard data-reduction tools already available can be used to efficiently pre-reduce and calibrate the data. As an example, to perform the tests shown in this article, we used the *IRAF* tasks imcombine, imarith, ccdproc (for the masterbias, masterdark, mastertwilight flat-fields, and to correct the science frames of the latter). To stack the calibrated science images using the world coordinate system, we suggest using the swarp software (Bertin, 2010). The ESO detmon recipes[3] can be used to analyse the linearity of the images.

To conclude, the X-shooter imaging mode is a tool that complements its spectroscopy. It helps to improve the flux calibration of the spectra and provides photometry for the study of transient objects like gamma-ray bursts, exoplanets or variable stars. In addition, its stability allows time monitoring of these objects to be carried out.

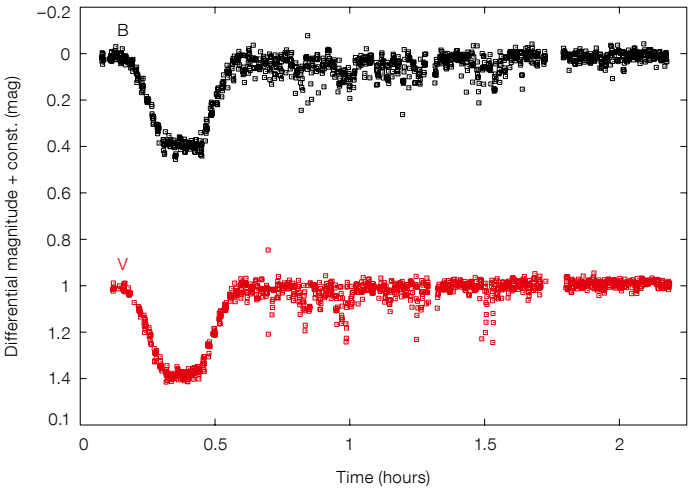

Figure 4a. Photometry of AA Dor: *B* and *V* light-curves displaying the primary eclipse are plotted. The secondary eclipse has not been observed. The dispersion of some points is possibly related to the sky background variability in twilight. Observations were made in stare mode and the photometry is relative.

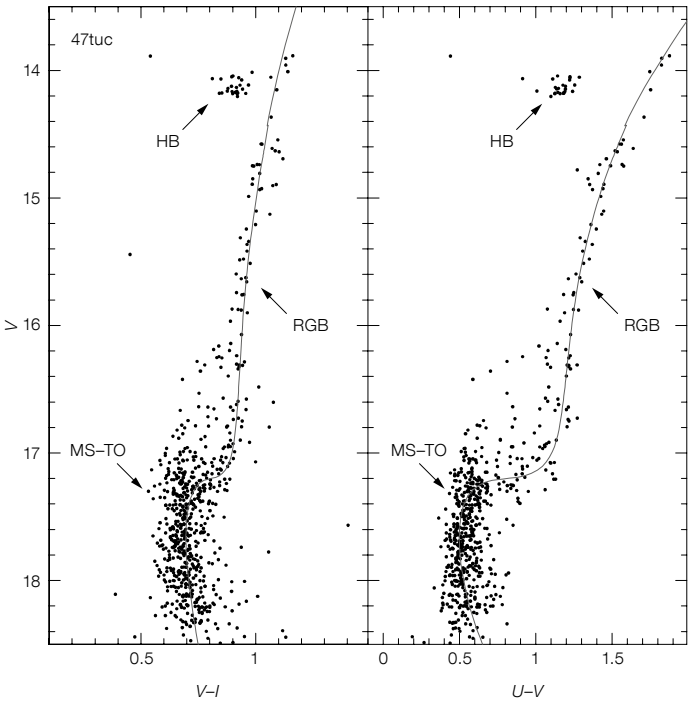

Figure 4b. Colour–magnitude diagrams of the globular cluster 47Tuc: *V v. V-I* is shown left and *V v. U-V* at right. The positions of the main-sequence turn-off (MS-TO), the red giant branch (RGB) and the horizontal branch (HB) are indicated. The isochrone is taken from Dotter et al. (2008) for a metallicity [Fe/H] = −0.7 and age 12 Gyr for the distance of 47Tuc. Observations were performed in stare mode under photometric transparency.

References

Bertin, E. & Arnouts, S. 1996, A&AS, 117, 393
Bertin, E. 2010, Astrophysics Source Code Library, ascl:1010.068
Bertin, E. 2011, Astrophysics Source Code Library, ascl:1110.006
Dotter, A. et al. 2008, ApJS, 178, 89
Mauerhan, J. C. et al. 2013, MNRAS, 430, 1801
Sørensen, A. N. et al. 2004, XSH-TRE-DMK-2200-0007
Vernet, J. et al. 2011, A&A, 536, 105

Acknowledgements

We acknowledge the support of the SCIence OPerationS-musketeers and the Change Control Board committees.

Links

[1] X-shooter imaging mode manual: http://www.eso.org/sci/facilities/paranal/instruments/xshooter/doc.html
[2] AGCCD health monitoring plots: http://www.eso.org/observing/dfo/quality/XSHOOTER/reports/HEALTH/trend_report_BIAS_AGC_HC.html
[3] Analysis of the CCD linearity with detmon: http://www.eso.org/sci/software/pipelines/detmon/detmon-pipe-recipes.html

Phase 3 Status and Access to Science Data Products from ESO Public Surveys

Magda Arnaboldi[1]
Nausicaa Delmotte[1]
Stephan Geier[1]
Laura Mascetti[1]
Alberto Micol[1]
Jörg Retzlaff[1]
Martino Romaniello[1]

[1] ESO

By January 2014, the eleven currently ongoing ESO Public Surveys had successfully completed their initial submissions and publication of their science data products through the ESO Science Archive Facility. The submission and validation process for the science data products through the Phase 3 process is summarised. The science data products available in the archive and their usage by the astronomical community are presented in view of the legacy value of these projects.

Introduction

The policies to manage the ESO Public Survey projects cover the delivery of data products for ingestion and publication via the Science Archive Facility (SAF). An overview of the wavelength and area coverage of the nine ESO imaging surveys on the VISTA telescope and the VLT Survey Telescope (VST) was presented in Arnaboldi et al. (2007). Summaries of the progress of the nine imaging and two spectroscopic Public Surveys are presented in the special section of *The Messenger* 154, except for the Variables in the *Via Láctea* (VVV) survey presented in Hempel et al. (2014). Additional allocation of telescope time to Public Surveys is conditional on the submission of science data products via Phase 3 and their successful publication through the SAF.

Phase 3 concludes the process started with the submission of the letters of intent, followed by Phase 1 (proposal preparation and submission) and the preparation and submission of observing blocks (OBs) for observations in service mode, i.e., Phase 2. Phase 3 is a partnership between the principal investigators (PIs) of the Public Survey and ESO and is based on the definition of a science data product standard, thereby guaranteeing uniformity in terms of data format and characterisation across the entire archive. As a result of Phase 3 the community can access and download the data products from the SAF and is able to carry out independent science projects in addition to those targeted by the survey teams (c.f., Arnaboldi et al., 2011).

From data upload to archive publication

When the PI, or their co-investigator(s) (Co-Is), uploads the data products to the dedicated Phase 3 ftp staging area and closes a release, checks are made and a valid status signals that the data are formally compliant with the ESO science data products standards. This step certifies that the files are standard FITS, i.e., were not corrupted during transfer, that the mandatory keywords are present, the provenance keywords are correctly mapped to products already archived in the SAF, or within the current upload, and the associations with the ancillary files are correct and complete. Being formally compliant with the standard is a necessary condition for publication via the SAF, but it does not guarantee that the data content is consistently documented to the required level of detail that would allow further scientific analysis independent of the survey team. The process that brings the formal compliance to published science data products via the SAF is the content validation of a Phase 3 submission.

The content validation of a Phase 3 submission by an ESO Public Survey team is carried out by the Archive Science Group (ASG). The release description is the starting point to assess whether the submitted data are consistent with the associated data documentation in terms of quantity (i.e., number of files), science quality and types of products, i.e., OB level products (those on the level of a single OB, such as pawprints, source lists or 1D spectra) or high-level products (such as deep stacks, aperture-matched, band-merged source lists and catalogues). ASG members make use of *ad hoc* scripts to check the values of the mandatory keywords, and the consistency of interconnected keywords. For example total exposure time values are checked against the Julian dates and the consistency of the NCOMBINE keyword for number of combined images and spectra is checked against the number of provenance (PROV) keywords given in the header. The content validation also includes spot checks for corrupted data.

For high-level data products, e.g., deep stacked images and catalogues, extensive tests are carried out to ensure the overall consistency of the science content in the archive. For the high level products, the PROV keywords are essential to ensure consistency within the hierarchy of products, from OB level products (pawprints and source lists) already published through the SAF, or delivered in the same data release, to the deep stacked images and catalogues. An additional test for catalogues covers statistics on the distribution of the values of the records in the different catalogue columns to check for outliers that may prevent the ingestion into the database, which supports the query interface of the ESO Catalogue Facility. ASG members also check for consistency of the Unified Content Descriptor (UCD) identifiers, the uniqueness of the name identifier for source records and presence of the primary source tag. For 1D spectra, specific tests are carried out on the FITS tabular format to ensure that the wavelength solution is monotonic. Further details can be found in the Phase 3 user guide[1].

In Figure 1 we plot the time to publication for the second VISTA submission (#2), VST submission #1 and the spectroscopic surveys submission #1. In this figure, $T = 0$ refers to the start of content validation by ASG and it accounts for both ASG and the PI/Co-I interventions. In Figure 2 we report the number of ASG content validation reports prepared for the survey submissions prior to publication of the data products in the archive.

The figures of merit shown in Figures 1 and 2 illustrate that the partnership of the survey teams and ESO is essential in order to achieve publication within two/three months from closing a Phase 3 submission. The leadership role of the PIs of the surveys is a cornerstone of the policies for Public Surveys, and follows from the agreement signed by the ESO Director General prior to the allocation of

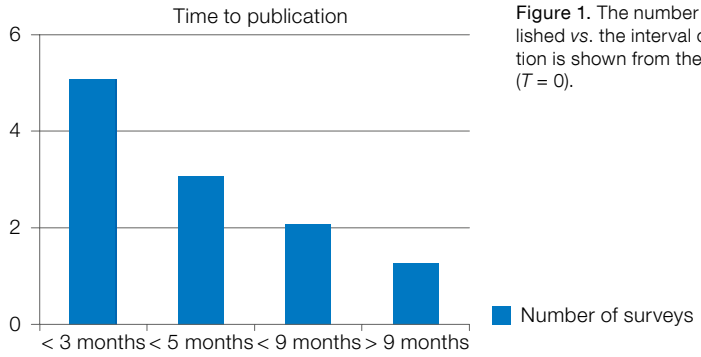

Figure 1. The number of survey releases published *vs.* the interval of time (months) to publication is shown from the start of content validation (T = 0).

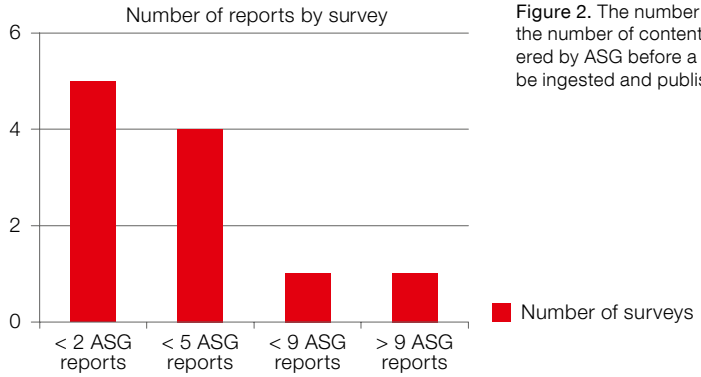

Figure 2. The number of surveys plotted against the number of content validation reports delivered by ASG before a Phase 3 submission can be ingested and published in the archive.

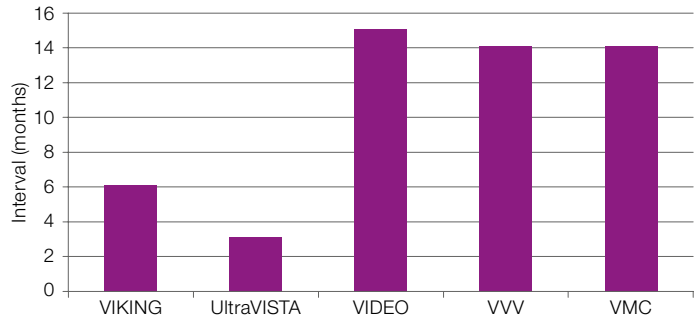

Figure 3. Interval between ingestion of catalogue products and archive publication is shown for the first catalogue submission.

telescope time to a survey project. Hence ESO assists the survey teams to define and package their data products in a manner consistent with the SAF and Virtual Observatory standards, enabling them to be integrated into the SAF.

Once the teams have ascended the learning curve on the science quality of the products, their data format and metadata, provenance information and content, another major delay can occur whenever there is a lack of consistency among the quantity and quality of delivered products, or the content of the uploaded Phase 3 submission is unclear, i.e., there are inconsistencies between the release description and uploaded files.

Content validation of catalogue products

Most catalogue products that were uploaded during the first catalogue submission did not fulfil the scientific quality required by the Phase 3 standard, primarily with respect to the qualifying attribute of the uniqueness of the source identifier. This issue is relevant for all surveys, except the UltraVISTA survey, for those sources in the region of overlap among tiles. Following discussion with the survey teams and the Public Survey Panel in October 2012, a strategy was identified so that catalogues now include an additional column which lists the primary source tag. Since catalogues are clearly the highest level science products from imaging surveys, it was necessary that ESO and the survey teams work together towards the common goal of achieving the required uniqueness of sources in the catalogue records. In Figure 3 we show the time from submission to ingestion for the catalogue products.

Dissemination of the catalogues from the ESO Public Surveys is further supported by an agreement between ESO and the Centre de Données astronomiques de Strasbourg (CDS). Only those catalogues from the Public Surveys that have been validated and published via the SAF are curated and published at CDS (in addition to those published in the refereed journal *Astronomy & Astrophysics*).

Current published science data products assets

The core deliverables of data products from the Public Surveys to the SAF are:

- Astrometrically and photometrically calibrated, co-added, re-gridded tiles, along with their respective confidence maps, in all of the project-relevant filters.
- Source lists for each tile based on individual, co-added bands. The single band catalogues will be ingested and accessible from the SAF as FITS files.
- 1D wavelength-calibrated, and flux-calibrated or continuum-normalised, spectra, including the 1D sky spectrum used for subtraction of the object spectrum, and an error map.
- Catalogues containing a list of parameters of individual objects across all of the observed filter bands. Their precise content will depend on the scientific goals and exploitation possibilities of each Public Survey.

The content of the Phase 3 submissions, completed during 2013, for the VST and VISTA Public Surveys (Tables 1 and 2 respectively) and for the spectroscopic Public Surveys are described.

ESO Public Survey data submissions

In 2011 Phase 3 operations began with the first submission of ESO Public Survey data products from five of the six VISTA Public Surveys (VISTA submission #1). A total of 5.5 TB of compressed imaging data including single-band source lists were submitted and published in the SAF. VISTA submission #2 (see Table 2) is a subsequent data release following VISTA submission #1. It included logical dependencies among archived and newly submitted data, which are mapped in the database that supports the Phase 3 workflow and the Phase 3 query interfaces of the SAF. This functionality of the Phase 3 infrastructure was fully tested and deployed to support archive operations during this process. It ensures that science data products can be searched and downloaded conjointly across all active data releases.

VISTA survey PIs were invited to deliver high-level catalogue data products before the reference date of 1 October 2012. The primary deliverables are aperture-matched multi-band catalogues, which were provided by five of the six VISTA surveys. The Ultra-VISTA band-merged catalogue of the COSMOS field is based on the previously released deep stacked images. The VIDEO team delivered the multi-band catalogue based on the deep stacked data of the VIDEO-XMM3 field. In order to support variability studies, the VVV and VISTA Magellanic Clouds (VMC) survey teams delivered the requested multi-epoch photometric data (light curves) and catalogues of variable objects.

The first submission of the VST Public Surveys took place in 2012 leading to the publication of 4.4 TB of imaging data covering over 2700 square degrees in the *u,g,r* and *i* bands, including *z* and Hα bands according to each survey (Table 1).

The first submissions of data from the spectroscopic Public Surveys, Gaia–ESO and Public ESO Spectroscopic Survey of Transient Objects (PESSTO), took place in 2013. They include as primary deliverables the 1D wavelength-calibrated spectra from those observations, which were completed before the reference date 15 December 2012. As ancillary products, the PESSTO team further delivered 2D spectral frames and associated images.

Table 1. Content of the VST submission #1. All data products based on observations completed before the reference date of 15 September 2012 on a tile-by-tile basis.

Survey	Deliverable 1 — tiles & confidence maps	Deliverable 2 — single band source list for each tile
V-ATLAS	*u,g,r,i,z* (2341 deg^2)	*u,g,r,i,z*
KiDS	*u,g,r,i* (56 deg^2)	*u,g,r,i*
VPHAS+	*u,g,r,i*,Hα (375 deg^2)	*u,g,r,i*,Hα

Table 2. Content of the VISTA submission #2. All data products based on observations completed before the reference date of 1 July 2012 on a tile-by-tile basis.

Survey	Deliverable 1 — tiles & confidence maps	Deliverable 2 — single-band source list for each tile	Deliverable 3 — co-added deep stacked tile
UltraVISTA	*Y,J,H,Ks*,NB118	Single bands for each stack (1.5 & 0.74 deg^2)	*Y,J,H,Ks*,NB118
VHS	*Y,J,H,Ks* (3800 deg^2)		–
VIDEO	*Z,Y,J,H,Ks* (9 deg^2)		Deep stacks for XMM field
VVV	*Z,Y,J,H,Ks* (564 deg^2)		–
VIKING	*Z,Y,J,H,Ks* (235 deg^2)		–
VMC	*Y,J,Ks* (3.5 deg^2)		–

Table 3. Summary of VISTA and VST Public Survey products in the ESO SAF. The quoted sky coverage in column 2 is the total geometric area covered by the image products, which normally differs from the nominal survey area.

Survey	Bands	Sky coverage[1] (sq. deg.)	Data volume (GB)	Sky coverage of raw data at Oct. 2013 (sq. deg.)
VHS	*YJHKs*	4210	8511	8260
VIKING	*ZYJHKs*	235	288	700
VVV	*ZYJHKs*	564	2877	562
VMC	*YJKs*	3.6	26	105
Ultra-VISTA	*YJHKs*	1.8	86	1.8
VIDEO	*YJHKs*	9.0	70	10.2
ATLAS	*ugriz*	2341	3015	2410
VPHAS+	*ugri*,Hα	375	747	600
KIDS	*ugri*	56	701	360

Table 4. Summary of the Gaia–ESO and PESSTO Public Survey products in the ESO SAF (status at 15 April 2014).

Survey	1D spectra	Total number of files	Data volume (GB)
Gaia–ESO	Spectra and weight maps	5654	1.3
PESSTO	Spectra, weight maps and images	4991	18

The complete sky coverage of the science data products from the Phase 3 submissions of the ESO Public Surveys is shown in Figure 7 of Arnaboldi et al. (2013).

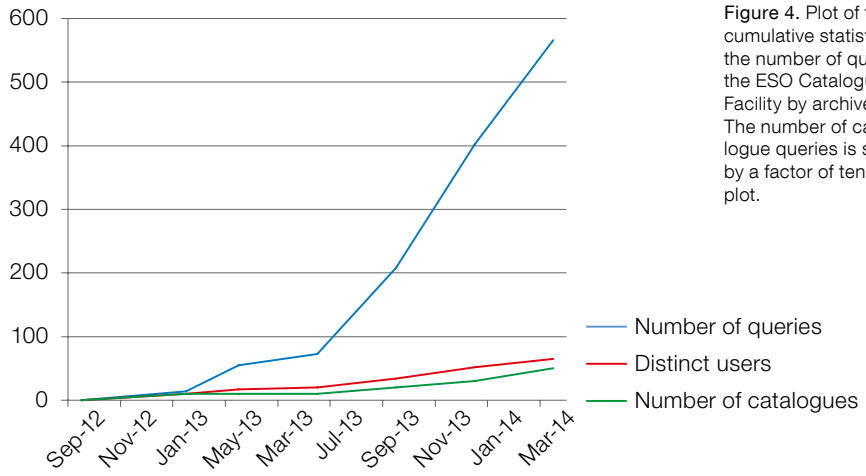

Figure 4. Plot of the cumulative statistics of the number of queries of the ESO Catalogue Facility by archive users. The number of catalogue queries is scaled by a factor of ten in this plot.

Publication of science data products from the ESO Public Surveys

The year 2013 was a very important one for Phase 3 activities, as all eleven ESO Public Surveys submitted and published their data products via the SAF. The milestones for Phase 3 were the second VISTA submission for images and source lists, and the first submission for catalogues. The first data release of the VST surveys was announced in September 2013. The spectroscopic Public Surveys completed the publication of their data products in January 2014. Thus far, a total volume of 16 TB of data products — images, weight maps, source lists, 1D spectra and catalogues – is now available and fully searchable via dedicated query interfaces[2]. In Table 3 we provide an overview of the data volume, wavelength and sky coverage of the data releases from the imaging surveys. In Table 4 we provide a summary of the submission by the Public Spectroscopic Surveys. Further information and detailed descriptions of the data releases from the ESO Public Surveys are available[3].

Public Survey data are published through the ESO Archive interfaces conjointly with other products, such as the stream of UVES echelle data that result from in-house generation of science data products. All Phase 3 data products comply with the established standard for ESO science data products[4], thereby guaranteeing uniformity in terms of data format and characterisation across the entire ESO archive.

In Figure 4 we show the cumulative statistics of the number of queries carried out by archive users at the Catalogue Facility since September 2012. The increase in the cumulative curves signals a "critical mass" effect: as more catalogues become available, more users are interested in the catalogue products available from all the Public Surveys. The current results from the publication of science data products from ESO Public Surveys show that we are moving in the right direction towards making these products available to the community.

In general, the delivered OB-level products cover smaller areas than those for which the raw data are available, as shown by comparing the areas covered by the science products (Column 3 of Table 3) and the areas covered by the raw products from successfully executed OBs (Column 5 of Table 3). The comparison between science data products and delivered raw data also shows that we are only at the beginning of this endeavour: more science data products will become available in the future Phase 3 calls for submission and in the course of the Public Survey observations.

A new cycle of Phase 3 calls is taking place in 2014. It will comprise the VISTA submission #3, VST submission #2 and submission #2 for the spectroscopic surveys. The VST submission #2 and spectroscopy survey #2 will also entail the delivery of high-level products, e.g., catalogues.

Refereed publications from Public Survey data products

Merit parameters for the Public Surveys are the number of refereed publications by the survey teams and archive users, and the cumulative download of data products from the SAF. There are now 135 refereed publications from the survey teams; a significant increase on the number of refereed publications (up 100 %) since October 2013. There are also 15 refereed papers from archive users who are not members of the survey teams, such as the analysis of data products from the VVV survey by Wegg & Gerhard (2013).

The statistics on archive downloads shown here, either by volume or number of files, does not include download by operational accounts of the ESO User Portal. We define as operational accounts those associated with PIs and Co-Is of the survey teams that are delegated for the Phase 3 data upload, and those of ESO users who have functional duties related with Phase 3 and the SAF.

The parameters on the data download by the community also demonstrate a strongly increasing interest. The cumulative downloads from the SAF since December 2011 amount to more than 10.5 TB of data products and ~ 50 000 files. In Figures 5a and 5b these numbers are differentiated by survey project and in Figure 6 by data product type. From the cumulative trend plots shown in Figures 5a and 5b, it is obvious that the community is most eager to access data from the VVV, UltraVISTA, KiDS (with the largest volume downloaded) and Gaia–ESO surveys. The largest data volume downloaded for products is for the source lists, followed by tile images and 1D spectra; see Figure 6. Since we believe catalogues to represent very valuable archival assets, since they are the highest level products for surveys, we are working hard to ingest the remaining VVV and VISTA Hemisphere Survey (VHS) catalogues so that the community can benefit even more from the joint efforts of ESO and the survey teams. Figure 7 shows the download of 1D spectral products.

We can also map the number of distinct archive users and the number of requests

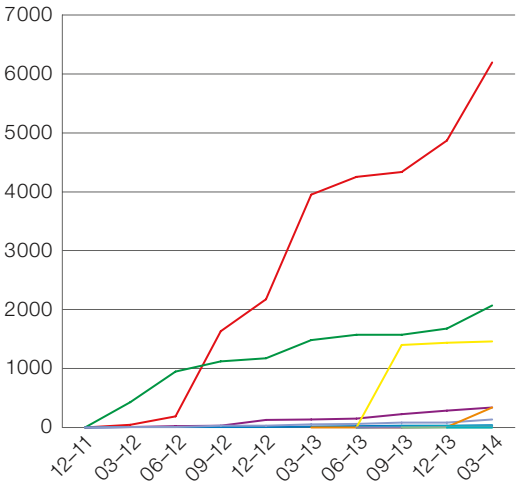

Figure 5a. Data volume downloaded (GB) for the ESO Public Surveys.

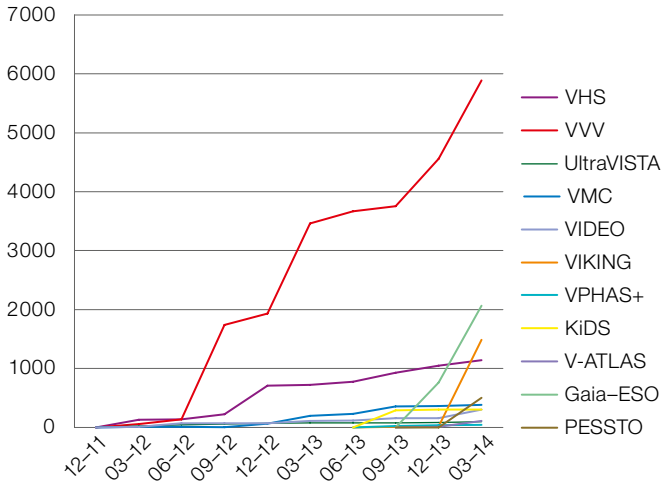

Figure 5b. Number of files downloaded for the ESO Public Surveys.

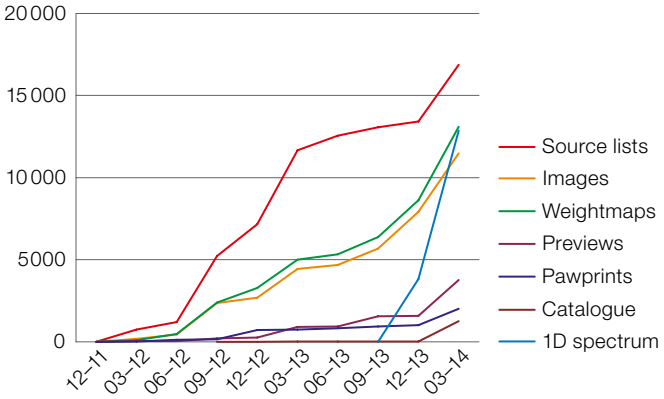

Figure 6. Number of files downloaded from the SAF for the different data product types. For catalogues, the number of files refers to a whole catalogue download. This figure of merit is complementary to the number of queries shown in Figure 4, in the sense that queries for catalogue records may not require the full download of a catalogue FITS file.

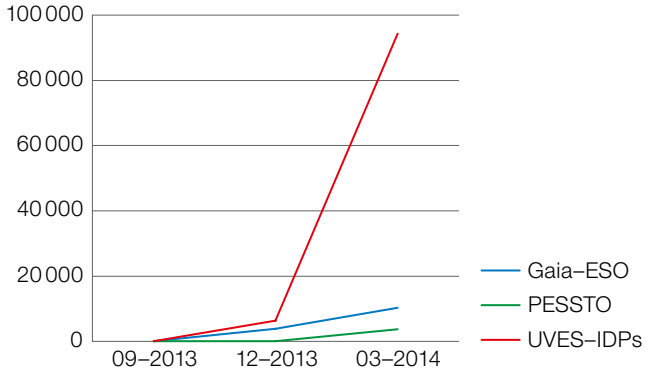

Figure 7. Download of 1D spectral products, including the UVES echelle science data products and the Gaia–ESO and PESSTO Public Survey products. The strong increment in the first quarter of 2014 is also associated with the download of all the available UVES data products by a single user.

per user. Again these statistics are carried out for users who are not associated with operational accounts. The access to data products in the SAF was performed by 517 distinct users, with about 50% having executed at least two requests resulting in a successful download of data products.

Concluding remarks

By monitoring the access and download of data products from the SAF we are witnessing a "critical mass" effect caused by the successful publication of homogeneous science data products across the Public Surveys. We note that since October 2013 and the completion of the first Phase 3 submission cycle from all the eleven Public Survey projects, the download of science data products (number of files and volume) from the SAF has doubled. There is also a "threshold" effect in the interest/awareness of the astronomical community: the dedicated section in the December 2013 issue of the *The Messenger* on Public Surveys triggered interest and an increased download of science data products from the SAF. There is evidently a strong scientific community interest in the study of the Milky Way (beyond the science goals of the Public Survey teams) as shown/triggered by the increased download of VVV products after the ESO Release on the intrinsic peanut shape of the Milky Way Bulge (Release 1339) and by the synergies created between the ESA Gaia mission and the Gaia–ESO spectroscopic survey.

Synergies are also present between products from different surveys. Since Public Survey data are published through the ESO archive interfaces conjointly with other science data products, such as the stream of UVES echelle spectra

(uniform in terms of data format and characterisation across the archive), archive users can exploit the links between products. The statistics indicate that the VISTA Kilo-degree Infrared Galaxy (VIKING) survey download increased after publication of catalogues and KiDS (Kilo-Degree Survey) images; UltraVISTA download increased after catalogue and second release of high level data products; and the publication of UVES echelle data products, which showed in six months a cumulative download of one fifth of all science data products downloaded in terms of number of files (Figure 7), also increased the visibility of 1D spectral products from the Public Surveys.

It is clear that the community involved in the science carried out with the ESO Public Survey projects is expanding: further to the nearly three hundred astronomers involved in the eleven Public Survey teams as PIs and Co-Is, there is now a community of archive users which is similar in size, or even larger, and is accessing these data for their own independent science.

Acknowledgements

The Archive Science Group would like to thank all the Public Survey teams for their hard work and their support in making the ESO Public Survey projects a success.

References

Arnaboldi, M. et al. 2007, The Messenger, 127, 28
Arnaboldi, M. et al. 2011, The Messenger, 144, 17
Arnaboldi, M. et al. 2013, The Messenger, 154, 18
Wegg, C. & Gerhard, O. 2013, MNRAS, 435, 187

Links

[1] Phase 3 User Guide: http://www.eso.org/sci/observing/phase3/p3userguide.pdf
[2] Phase 3 generic query interface: http://archive.eso.org/wdb/wdb/adp/phase3_main/form
[3] Descriptions of the data releases from the ESO Public Surveys: http://www.eso.org/sci/observing/phase3/data_releases.html
[4] Science Data Products standard: http://www.eso.org/sci/observing/phase3/p3sdpstd.pdf

ESO/G. Brammer

A fish-eye lens view of the Paranal Observatory, showing the four Unit Telescopes (UTs) and four Auxiliary Telescopes. The laser guide star emerges from the dome of UT4 (Yepun). The Large and Small Magellanic Clouds can be seen at the top of the image and the Galactic Plane near the horizon.

ALMA (ESO/NAOJ/NRAO)/NASA/ESA/F. Combes

Composite Hubble Space Telescope (HST) image and map of CO(3-2) emission taken with ALMA of the nearby (10 Mpc) Seyfert 2 galaxy NGC 1433. The dim blue background image is from HST combining BVI filters, the orange and red coloured structures highlight the CO emission intensity. See Release eso1344 for more details.

An Advanced Scattered Moonlight Model

Amy Jones[1]
Stefan Noll[1]
Wolfgang Kausch[1,2]
Cezary Szyszka[1]
Stefan Kimeswenger[3,1]

[1] Astro and Particle Physics, Leopold Franzens Universität Innsbruck, Austria
[2] Department of Astrophysics, University of Vienna, Austria
[3] Instituto de Astronomía, Universidad Católica del Norte, Antofagasta, Chile

Correcting and predicting the flux coming from the background sky is a crucial aspect of observational astronomy. We have developed a sky background model for this purpose, and it is the most complete and universal sky model that we know of to date. The largest natural source of light at night in the optical is the Moon, and it is a major contributor to the astronomical sky background. An improved spectroscopic scattered moonlight model, which is applicable from 0.3 to 2.5 µm has been developed and studied with a set of FORS1 spectra and a dedicated X-shooter dataset. To our knowledge, this is the first spectroscopic model extending into the infrared and it has been tested for many lunar phases and geometries of the Moon and target observations.

Introduction

The current trend in astronomy is to build larger and larger telescopes, for example the future European Extremely Large Telescope (E-ELT). The operating costs for running these large telescopes are high and careful planning of observations is crucial since telescope time is expensive and always in demand. Thus, more accurate predictions and estimations of the noise coming from the sky background are needed to better understand how long an exposure is necessary for a given observation to reach a desired signal-to-noise ratio. The brightest natural source of light in the night sky in the optical, is the Moon (when it is above the horizon). Even in the near-infrared (NIR), there is some flux from the Moon that should be considered.

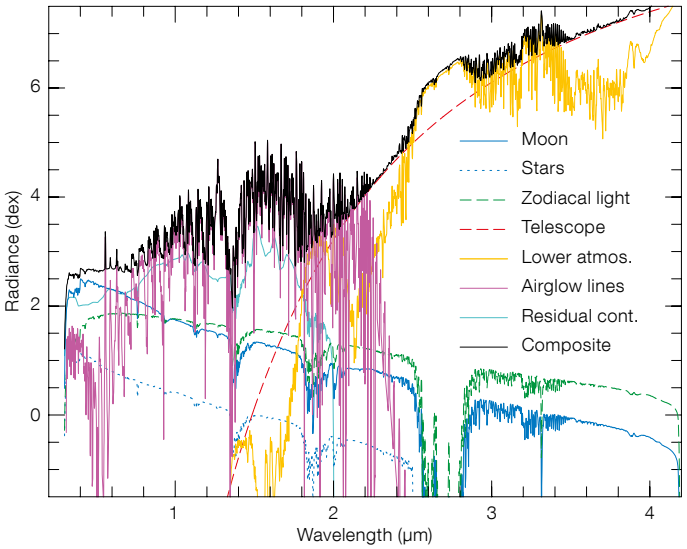

Figure 1. An example of the output from the sky background model of Noll et al. (2012). The output of the sky background model includes an emission spectrum (shown here) and a transmission spectrum. The various components of the sky background model are also shown.

As part of the Austrian contribution to ESO, the University of Innsbruck in-kind group developed a spectroscopic sky background model from 0.3 to 30 µm for the Very Large Telescope (VLT) and the nearby future site of the E-ELT, for the ESO Exposure Time Calculator (ETC). The model is described in Noll et al. (2012). An example of an output emission spectrum from our sky background model is shown in Figure 1, and the model is available[1]. Part of this sky background model is an advanced, spectroscopic scattered moonlight model, verified from 0.3 to 2.1 µm. It provides a spectrum of the scattered moonlight, visible at the observer, depending on the atmospheric conditions, the altitude of, and the angular distance between the target and Moon, and the lunar phase and distance.

The long-standing scattered moonlight model used by ESO for the ETC was due to Walker (1987). It provides a table of the magnitudes for five photometric bands of the night sky at five different moon phases. This model is limited when it comes to producing a scattered moonlight spectrum which is accurate enough for current and future telescope operations.

Another, widely used scattered moonlight model was developed by Krisciunas & Schaefer (1991). It again only uses a photometric model based on 33 observations in the *V*-band taken at Mauna Kea (2800 metres above sea level). This empirical fit was separated into various specific functions, such as initial intensity from the Moon, Rayleigh and Mie scattering. It is simple, convenient, and easy to use with an accuracy between 8 and 23 %, when not near full Moon and for *V*-band data from Mauna Kea. In a previous paper (Noll et al., 2012), we presented a spectroscopic extension of the Krisciunas & Schaefer (1991) model, which was originally used in our sky background model. It was optimised for Cerro Paranal and covered the optical regime. Several scaling factors for the different functions were introduced to better fit data from Cerro Paranal.

We have improved the scattered moonlight model and it has evolved beyond the initial ESO ETC application. In the optical, the model was calibrated and investigated with 141 spectra and has an overall uncertainty of $\sigma \lesssim 0.2$ mag. With some dedicated X-shooter observations, we have verified the model in the optical and extended it to the NIR. It has been split into physically based modules which are given by either physical models or the best current fits. The present version is optimised for Cerro Paranal, but can be modified for any location with information about its atmospheric properties. Since our scattered moonlight model produces a spectrum, it can be used for finding spectral features and trends as well as photometric magnitudes.

We will first present the scattered moonlight model in the optical, then the model from the ultraviolet (UV) to the NIR.

Scattered moonlight model in the optical

Scattered moonlight is most influential in the optical. The scattered moonlight model was originally developed, tested, and calibrated in the optical regime with a FOcal Reducer/low dispersion Spectrograph (FORS1) dataset from Patat (2008). We used 141 spectra which had moonlight present and decent weather conditions. For a full description of the model, the data and analysis, see Jones et al. (2013).

The moonlight model is divided into several modules. The first module is the Solar spectrum from Colina et al. (1996) which is the initial source of the scattered moonlight. Then the light is reflected off the lunar surface and for this we use the empirical fit from Kieffer & Stone (2005), which depends on several lunar parameters. This fit was done using narrowband photometry, so we interpolated it as a function of wavelength. We also needed to extrapolate it to a new moon phase. Next the reflected light is scattered and absorbed in the Earth's atmosphere before reaching the telescope.

We have designed fully 3D single and double scattering calculations with an approximation to higher orders. For the scattering we use the Rayleigh approximation for the molecules and Mie scattering for the aerosols. Rayleigh scattering can be well parametrised and the molecules in the atmosphere are fairly stable. On the other hand, Mie scattering can be complicated and the aerosols can vary on timescales of hours. In the optical, an empirical fit was derived from Patat et al. (2011). We decomposed this fit into reasonable aerosol size distributions for a remote continental area, like Cerro Paranal, from Warneck & Williams (2012), by scaling the column density of the various components. Then we used the scaled distributions to produce the Mie phase function (Grainger et al. 2004; Bohren & Huffman 1983).

Altogether we had developed a scattered moonlight model, which is spectroscopic and tested from 0.4 to 0.9 μm. It depends on the altitude of, and the angular distance between the Moon and target, lunar phase and distance and the atmospheric conditions.

Results for the optical scattered moonlight model

We found that the sky background model with the new scattered moonlight model fitted the FORS1 observations well, with an uncertainty of $\lesssim$ 0.2 mag. Figure 2 shows an example of observed data with the scattered moonlight and sky background model overlaid. The model is able to reproduce the observed radiance spectra.

In Figure 3, we show the mean and uncertainty, σ, of the difference between the sky background model and the FORS1 observations. Also shown are the mean and σ for the nights with and without moonlight. The uncertainty increases towards redder wavelengths where the sky emission lines are prominent.

The scattered moonlight model performs better than the previous extrapolated version of Krisciunas & Schaefer (1991), as shown in Figure 4. For this analysis, we took the sky observations and subtracted the other background components using the sky background model. Then we compared these spectra containing only observed scattered moonlight with the scattered moonlight model. The error bars include the errors associated with the other components in the sky background model. This analysis was done for both the new advanced scattered moonlight model and the previous one based on Krisciunas & Schaefer (1991), labelled in the Figure as KS91. The error bars for the new model are consistently smaller, and the mean for all the spectra is closer to zero. For the mean of new scattered moonlight model minus the FORS1 observations to be at zero, we needed to multiply the model by 1.2. We suspect that the uncertainty in the flux calibration of the FORS1 data could significantly contribute to this global scaling factor.

Scattered moonlight model from UV to NIR

We have now extended and verified our scattered moonlight model. With dedicated observations from X-shooter (Vernet et al., 2011), we were able to test the model from 0.3 to 2.1 μm. With the data in the NIR and observations at multiple distances from the Moon, we can better investigate the aerosol scattering and constrain the Mie scattering used in the model.

We have a unique dataset taken with X-shooter for the purpose of verifying and extending our scattered moonlight model (Proposal ID: 491.L-0659) to the NIR. These data include observations of plain sky taken at three different lunar phases (runs a, b, and c) and at six different angular distances (7, 13, 20, 45, 90, 110 degrees) from the Moon. Additionally, the same standard star was observed at two different airmasses for each lunar phase run.

For the analysis we selected certain wavelength ranges, hereafter called inclusion regions. These regions are parts of the spectrum that should be free of sky emission lines and absorption features. The number of pixels per arm are 850, 850, and 653 for the UVB, VIS, and NIR X-shooter

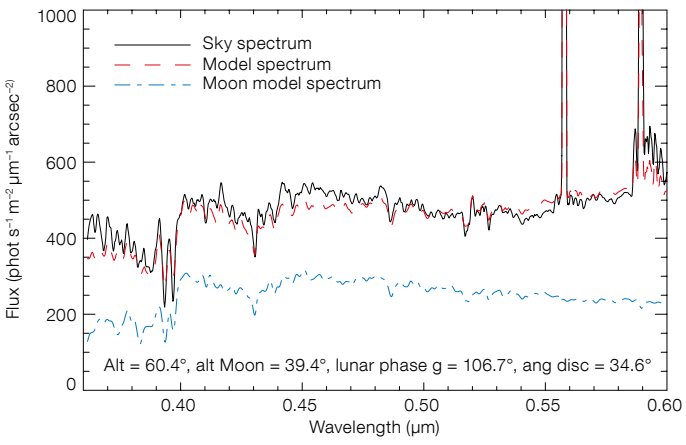

Figure 2. An example of the quality of the sky background model. The observed sky spectrum is shown in black with the full sky background model in red. The scattered moonlight portion of the model is in blue. The model fits the observed spectrum fairly well. This observation was done with moderate amount of moonlight, which comprises roughly half of the overall sky background flux.

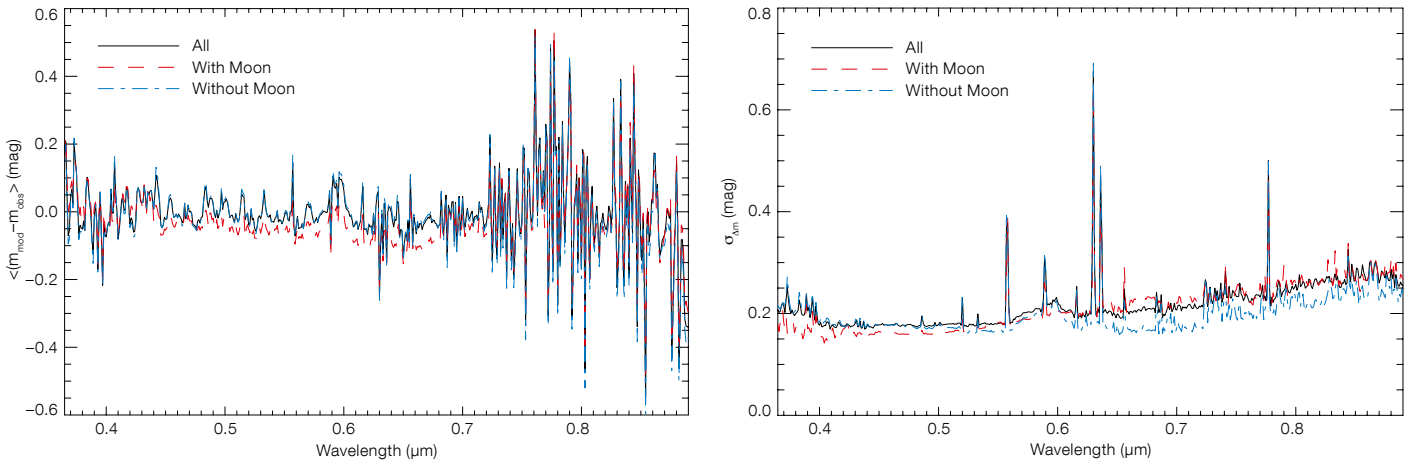

Figure 3. Mean (left) and σ (right) of the difference between the observed FORS1 and modelled spectra for the full sky background of all the spectra, those with moonlight, and only those without moonlight. See text for more details.

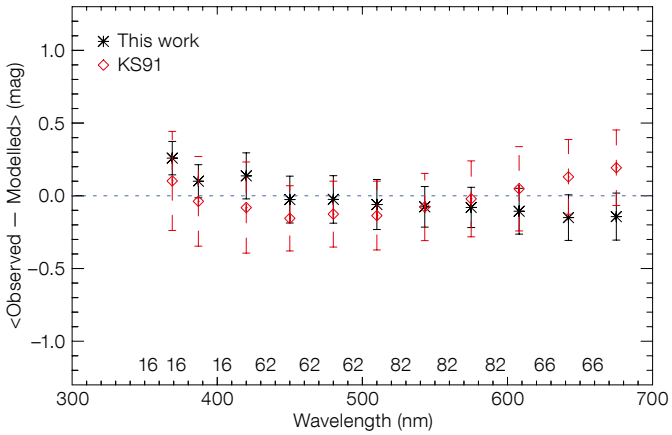

Figure 4. Means and uncertainties for the scattered moonlight model versus observed data at several 4 nm wide continuum bands. The *y*-axis is the average of the observed minus modelled fluxes for data with good weather conditions and a significant amount of moonlight. Over-plotted is the same analysis with the previous model from Noll et al. (2012), based on Krisciunas & Schaefer (1991), and labelled as KS91. The numbers below each point are the number of spectra considered. See the text for more details.

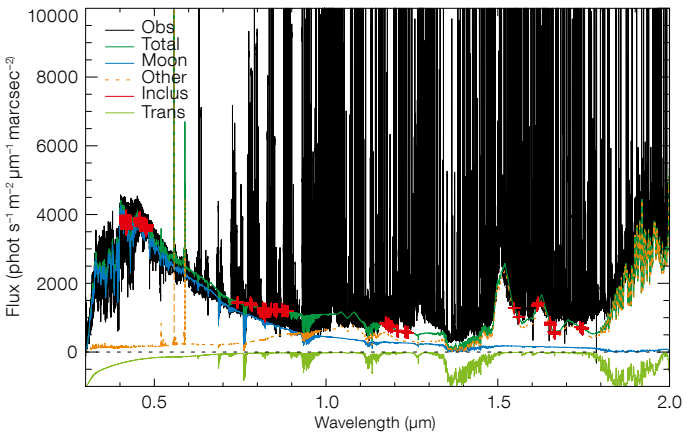

Figure 5. An example spectrum for the scattered moonlight extinction curve determination. The observed spectrum (black) is from run b with offset 45°. Overlaid is an example total sky background model (green) with the sky lines removed for clarity and the inclusion regions for the analysis (pink +). The scattered moonlight model (blue) and the other model components (orange dotted), except the sky lines, are also shown. Below the dotted black line is the transmission curve (light green).

arms, respectively and are non-consecutive. In Figure 5, we show the observed spectrum from run b at 45 degrees; overlaid are the sky background model (without sky emission lines for clarity), the scattered moonlight model, other components (except the sky emission lines) of the sky background model, the inclusion regions and the transmission spectrum.

For the aerosol extinction curve, in the optical, we used a decomposition of the empirical fit found in Patat et al. (2011). With the X-shooter data, we can take a different approach. We use the remote continental tropospheric and stratospheric aerosol size distributions (Warneck & Williams, 2012), and produce a grid of different scalings of the column density for each aerosol type. Then we used these parameters to produce the Mie phase function using an IDL code based on Bohren & Huffman (1983) and Grainger et al. (2004). Each aerosol distribution is approximated as a lognormal distribution described by *n* the number density of particles, *R* the mean radius of the particles, and a parameter *s* which determines the spread in radii of the particles. The default parameters for the various aerosols are listed in Table 1.

Type	n (cm^{-3})	R (10^{-1} μm)	log s (10^{-1})
Trop nucleation	3.20×10^{3}	0.10	1.61
Trop accumulation	2.90×10^{3}	0.58	2.17
Trop coarse	3.00×10^{-1}	9.00	3.80
Stratospheric	4.49×10^{0}	2.17	2.48
Added coarse	1.00×10^{0}	10.0	1.00

Table 1. Aerosol modes.
Note: the values used for Mie scattering of remote continental aerosols are from Warneck & Williams (2012), except for the added coarse mode (see text for details).

The grid is logarithmically spaced, varying the column density for each aerosol type, except for the tropospheric nucleation mode which is negligible and left at 100 %. The column density is directly related to the number density *n*, where we assumed a convenient effective aerosol layer width of 1 km. We also linearly varied the atmospheric refractive index, *N*.

The amount of aerosols can vary each night (e.g., Buton et al. 2013), and so far the full analysis has been done for the one night of run b (23 July 2013). We also performed a similar analysis with the aerosol grid for the spectrophotometric standard star observations taken that night. More details will be given in a future publication (Jones et al, in prep.).

When the sky observation was at close angular distances to the Moon, in particular the 7 and 13 degree offsets, we noticed a significant amount of extra observed flux compared with the modelled flux. We speculate that this could be caused either by some direct moonlight entering the detector or some additional tropospheric coarse mode which would increase the Mie forward scattering. Since we have no control over the first scenario, we explored the likelihood of the second. We added an additional aerosol size distribution for a particle with R = 1μm and log s = 0.1, which is optimal for increasing the flux at small angular distances. We also varied the column density of this new mode in the same way as the others (see Table 1).

Results of UV to NIR scattered moonlight model

After analysing the X-shooter observations with the scattered moonlight model for the various aerosol parameters, we have found the model with the highest likelihood. As shown in Figure 6 our model with the highest likelihood matches the data well. Also shown for comparison is the model which is the least likely from our grid. This model, with different amounts of aerosols, does not fit the observations, especially at smaller angular distances. The two spectra with the largest angular distances (90 and 110 degrees) are not very sensitive to the choice of aerosols. The model here

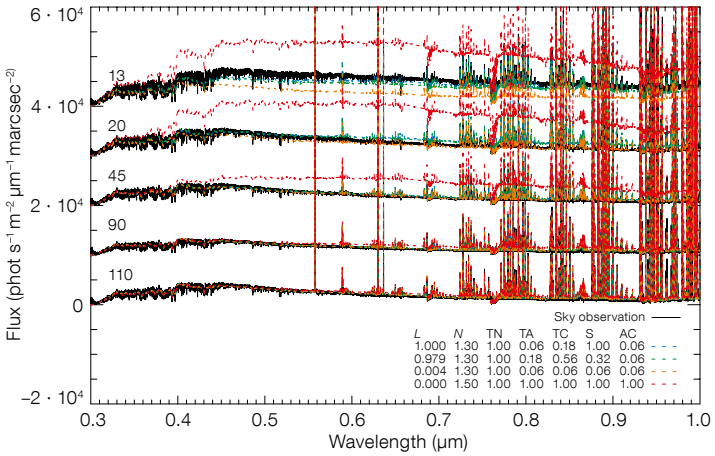

Figure 6. Four examples of how well the sky background model fits the observations. The observations at the five different angular distances to the moon (13, 20, 45, 90, and 110°) are shown, offset in flux for clarity. Overlaid for each are the most and least likely models. The overall likelihood, *L*, the refractive index *N*, and the fractions of column density (n × 1 km) for tropospheric nucleation TN, accumulation TA, coarse TC, stratospheric S, and added coarse mode AC for the different observations are shown in the legend.

reproduces the data, which leads credence to the other parts (non-aerosol scattering) of the model being accurate. By adding in the additional coarse mode, we were not able to successfully reproduce the extra flux seen at 7 degrees (not shown in Figure). Additionally, the spectrum at 13 degrees seems to behave differently than the other spectra analysed. The possibility of having extra flux coming from direct moonlight entering the dome and hitting the detector cannot be excluded. We would like to caution others about observations close to the Moon. Even in the *J*-band, some extra flux is detected.

Prospects

From the UV to the NIR, our scattered moonlight model seems to fit the observed data well. With the X-shooter data we can better constrain the aerosol scattering. The optical depth of aerosols τ_{aer} for the night of run b is quite a bit lower than the one empirically found by Patat et al. (2011). We deduce that the variation in the amount of aerosols can be large. We plan to extend our study of using the sky background model and archival X-shooter data to investigate the fluctuations in the amount of aerosols present at Cerro Paranal.

Overall, our improved scattered moonlight can well represent the observations. It has now been verified in the optical with FORS1 data and from the UV to NIR with X-shooter data. In addition, we have tested the model for many different lunar phases and at a range of distances between the Moon and target observation. The remaining main source of uncertainty is with the atmospheric conditions.

Acknowledgements

This study is carried out in the framework of the Austrian ESO in-kind project funded by BM:wf under contracts BMWF-10.490/0009-II/10/2009 and BMWF-10.490/0008-II/3/2011, and by the Austrian Science Fund (FWF), Project P26130.

References

Bohren, C. F. & Huffman, D. R. 1983, *Absorption and scattering of light by small particles*, (New York: Wiley VCH)
Buton, C. et al. 2013, A&A, 549, A8
Colina, L. et al. 1996, AJ, 112, 307
Grainger, R. G. et al. 2004, Appl. Opt., 43, 5386
Jones, A. et al. 2013, A&A, 560, A91
Kieffer, H. H. & Stone, T. C. 2005, AJ, 129, 2887
Krisciunas, K. & Schaefer, B. E. 1991, PASP, 103, 1033
Noll, S. et al. 2012, A&A, 543, A92
Patat, F. 2008, A&A, 481, 575
Patat, F. et al. 2011, A&A, 527, A91
Vernet, J. et al. 2011, A&A, 536, A105
Walker, A. 1987, NOAO Newsletter, 10, 16
Warneck, P. & Williams, J. 2012, *The Atmospheric Chemist's Companion*, Springer

Links

[1] ESO Exposure Time Calculator sky model: http://www.eso.org/observing/etc/skycalc/skycalc.htm

A PIONIER View on Mass-transferring Red Giants

Henri M. J. Boffin[1]
Nicolas Blind[2]
Michel Hillen[3]
Jean-Philippe Berger[1]
Alain Jorissen[4]
Jean-Baptiste Le Bouquin[5]

[1] ESO
[2] Max-Planck-Institut für extraterrestrische Physik, Garching, Germany
[3] Instituut voor Sterrenkunde, Katholiek Universitet Leuven, Belgium
[4] Institut d'Astronomie et d'Astrophysique, Université Libre de Bruxelles, Belgium
[5] UJF-Grenoble CNRS-INSU, Institut de Planétologie et d'Astrophysique de Grenoble, France

Symbiotic stars display the absorption lines of a cool red giant together with the emission lines of a nebula ionised by a hotter star, indicative of an active binary star system in which mass transfer is occurring. PIONIER at the VLT has been used to combine the light of four telescopes to study in unprecedented detail how mass is transferred in symbiotic stars. The results of a mini-survey of symbiotic stars with PIONIER are summarised and some tentative general results about the role of Roche lobe overflow are presented.

Symbiotic stars are a class of bright, variable red giant stars, which show a composite spectrum: on top of the typical absorption features of the cool star, there are strong hydrogen and helium emission lines, linked to the presence of a hot star and a nebula. It is now well established that such a "symbiosis" is linked to the fact that these stars are active binary systems, with orbital periods between a hundred days and several years. On account of the variable nature of these systems and their clear signs of accretion (many are often associated with novae or undergo outbursts of some sort), it is usually accepted that the red giant is losing mass that is partly transferred to the accreting companion — either a main sequence (MS) star or a white dwarf (WD). This picture was developed by Kenyon & Webbink (1984) and Mürset et al. (1991). Symbiotic stars are *de facto* the low- and intermediate-mass interacting binaries with the longest orbital periods and the largest component separations. They are thus excellent laboratories in which to study a large spectrum of very poorly understood physical processes, with wide-ranging applications (Mikolajewska, 2007). Symbiotic stars containing a white dwarf may also be progenitors of Type Ia supernovae.

The mass transfer process

One of the main questions related to symbiotic stars is how the mass transfer takes place: by stellar wind, through Roche lobe overflow (RLOF) or through some intermediate process? Red giants naturally lose mass through a stellar wind, with typical mass-loss rates of $10^{-8}\,M_{\odot}$ yr^{-1} on the first ascent of the red giant branch, and up to $10^{-6}\,M_{\odot}$ yr^{-1}, or more, on the asymptotic giant branch (AGB). The wind velocity is rather low, about 5–30 km s^{-1} in most cases, and part of this wind can thus be accreted by the companion. Moreover, the red giants in symbiotic systems are known to have stronger mass-loss rates than normal red giants. Although still not understood, this means that mass transfer can be even stronger.

Alternatively, if the system is a close enough binary, the red giant may fill its Roche lobe and start mass transfer through RLOF. However RLOF by a red giant with its huge convective envelope is quite problematic. Unless the mass ratio (initially greater than one, as it is the more massive star that evolves first into a giant) is smaller than some critical value (between about 1 and 1.5), the mass transfer will be dynamically unstable, leading to a common envelope (CE) phase, whose inescapable outcome is a very short period (a few days or less) binary system. Such a process is able to explain short period binaries such as cataclysmic variables or some central stars of planetary nebulae, but would not explain the long observed periods of symbiotic stars. Thus, it is generally assumed that for RLOF to take place, and be stable so as to avoid the CE, the giant primary star will first need to lose some mass by a stellar wind in order to bring the mass ratio down.

We now know about 200 symbiotic stars, but have orbital elements for only 40 systems or so. There are, however, also similar systems to symbiotic stars, i.e., binaries with a red giant primary but with lower mass loss or mass transfer. Until very recently, it was not possible to firmly establish whether the mass-loss process in symbiotic and related stars took place via a wind or through RLOF. Answering this question does require being able to compare the radii of the stars to the Roche lobe radius (which depends on the star separation and the mass ratio). However, determining the radius of the red giant in symbiotic systems is not straightforward, and there has always been some controversy surrounding these determinations.

During the last decade, clear evidence of ellipsoidal variations in the near-infrared light curves of many symbiotic systems has been presented, suggesting that the giants are filling their Roche lobes, or are at least very close to doing so. The radii estimated from the light curves, however, lead to a continually embarrassing problem: they are different from the radii derived from rotation velocities by a factor of two (Mikolajewska, 2007)! Several explanations have been proposed to account for this discrepancy, but the only way to answer it is by measuring the giant's radius for symbiotic stars directly.

Optical interferometry is currently the only available technique that can achieve this aim. Interferometry allows us to determine the size and distortion of the giant star, and in some cases the orbital parameters of the system, without any *a priori* estimate on their characteristics. This unique ability has already allowed us to study in unprecedented detail the interacting binary system SS Leporis, leading to a complete revision of the system (Blind et al., 2011).

Revisiting SS Lep

SS Leporis is composed of an evolved M giant and an A star in a 260-day orbit, and presents the most striking effect of mass transfer, known as the Algol paradox; that is, the M giant is less massive than the A star. The A star is unusually luminous and surrounded by an

expanding shell, certainly as the result of accretion. The observation of regular outbursts and of ultraviolet activity from the A star shell are further hints that mass transfer is currently ongoing. Additionally, a large circumbinary dust disc surrounds the binary system, implying that the mass transfer process is non-conservative.

We observed SS Lep during the commissioning of the PIONIER visitor instrument at the Very Large Telescope Interferometer (Le Bouquin et al., 2011). Since it combines four telescopes (in our case, the four 1.8-metre Auxiliary Telescopes), PIONIER provides six visibilities and four closure phases simultaneously, which allows reliable image reconstruction. We were able to detect the two components of SS Lep as they moved across their orbit (see Figure 1) and to measure the diameter of the red giant in the system (~ 2.2 milliarcseconds [mas]). By reconstructing the visual orbit and combining it with the previous spectroscopic one, it was possible to well constrain the parameters of the two stars.

The M giant is found to have a mass of 1.3 $M_{\odot}$, while the less evolved A star has a mass twice as large: thus a clear mass reversal must have taken place, with more than 0.7 $M_{\odot}$ having been transferred from one star to the other. Our results also indicate that the M giant only fills around 85 +/- 3 % of its Roche lobe, which means that the mass transfer in this system is most likely by a wind and not by RLOF. However, as the M giant is currently thought to be in the early-AGB phase where mass loss is still very small, it is difficult to understand how the star could have lost so much mass in a few million years (the time spent on the AGB until now), unless one invokes the companion-reinforced attrition process of Tout & Eggleton (1988), i.e. assuming that the tidal force of the companion dramatically increases the wind mass loss. Although this process allows, in principle, the current state of SS Lep to be explained without resorting to a Roche lobe overflow, the validity of this assumption still needs to be proved by a more detailed study.

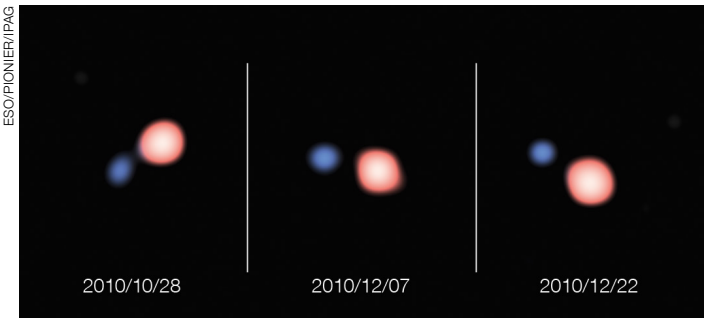

Figure 1. Image reconstruction of the PIONIER observations of SS Lep showing the orbital motion of the resolved M giant and the A star. The images are centred on the centre of mass. The distortion of the giant in the images is most certainly an artefact of the asymmetric point spread function. See Release eso1148 for more details.

The PIONIER mini-survey

It is not always possible to obtain as many data points as in the case of SS Lep (e.g., in most symbiotic systems, the companion would not have a detectable signature in the infrared) and thus to constrain the system to the same extent. However, there are several systems for which it is possible to determine, with great accuracy, the diameter of the mass-losing giant. Thus, when combined with previous data, the Roche lobe filling factor could already be constrained. Recently we observed several symbiotic and related stars with PIONIER, measuring their diameters – in the range 0.6–2.3 mas — and thereby assessing for the first time, in an independent way, the filling factor of the Roche lobe of the mass-losing giants (Boffin et al., 2014).

For the three stars with the shortest orbital periods (i.e., HD 352, FG Ser and HD 190658), we find that the giants are filling (or are close to filling) their Roche lobes, consistent with the fact that these objects present ellipsoidal variations in their light curves. In the case of the symbiotic star FG Ser, we find that the diameter is changing by 13% over the course of 41 days, while observations of HD 352 are indicative of an elongation at the level of 10 % (see Figure 2). Such deformations need, however, to be confirmed with more precise interferometric observations and compared with the outcome of light-curve modelling. The other three studied stars (V1261 Ori, ER Del, and AG Peg) have filling factors in the range 0.2–0.55, i.e., the star is well within its Roche lobe.

A possible dichotomy?

We here tentatively propose that the three systems which apparently fill their Roche lobes (HD 352, FG Ser and HD 190658) are those that contain a main sequence companion or a helium (He)

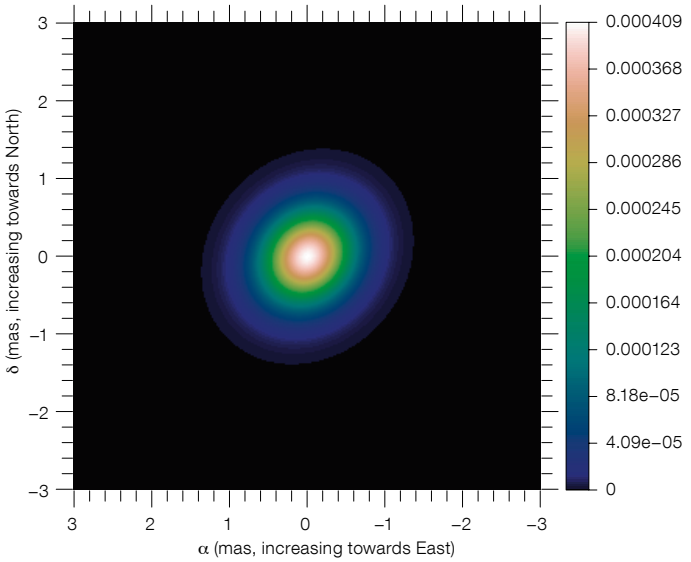

Figure 2. Model image of the elongated Gaussian that best fits the PIONIER visibilities for HD 352: the elongation ratio is 1.156 ± 0.026, the star is 1.38 × 1.6 mas in size, with the major axis position angle at 138 ± 4 degrees. Reproduced from Boffin et al. (2014).

Companion star	CO WD	He WD or MS
Red giant shows	*s*-process enhancement	No *s*-process enhancement
Rotation of giant	Non-synchronised	Synchronised
Eccentricity	$e > 0$	$e = 0$
Mass transfer	Wind accretion	RLOF

Table 1. A possible dichotomy among symbiotic stars?

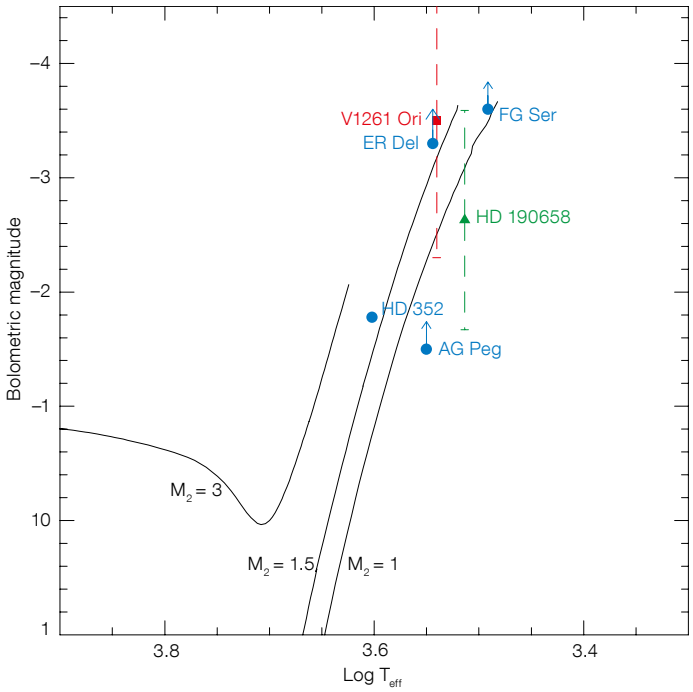

Figure 3. Hertzsprung–Russell diagram showing the positions of our target stars (full dots, in blue), together with Yonsei–Yale evolutionary tracks for solar abundance stars with initial masses of 1, 1.5, and 3 $M_{\odot}$. For FG Ser, ER Del, and AG Peg, we have only lower limits for the bolometric magnitude. The range for V1261 Ori is indicated with the red dashed line. Adapted from Boffin et al. (2014).

white dwarf (WD), and not a carbon/oxygen (CO) WD. It is, for example, very useful to compare the systems FG Ser and V1261 Ori. Despite the similarity of their orbital periods (P = 633.5^{d} and 638.2^{d}, respectively), and the not so different physical properties (*viz.*, temperature and luminosity of the red giant), the former has most likely a companion with too low a mass to allow for a CO WD, while the latter has a CO WD companion, given its pollution by *s*-process elements (Ake et al., 1991). We found that FG Ser is a nominal case of a synchronous giant filling its Roche lobe, while the red giant in V1261 Ori is filling only about 30 % of its Roche lobe and mass transfer occurs by a wind. The fact that in FG Ser the giant has a rotation synchronised with the orbital motion and a circular orbit (both properties expected for a Roche lobe filling system), while V1261 Ori is clearly not synchronised and still has a slightly eccentric orbit (e = 0.07), is another illustration of this possible dichotomy (see Table 1).

This conclusion on Roche lobe filling would provide some credit to the work of Kenyon & Webbink (1984) who concluded that, in order to explain the properties of symbiotic stars, one needed RLOF (or quasi-RLOF) in systems with main sequence companions, but wind mass-loss in systems with white dwarfs. SS Lep, which almost fills its Roche lobe, and which has a clear main sequence companion, also fits the picture. It is, however, still difficult to understand why, if Roche lobe overflow takes place in our three systems, it does not lead to a dynamic common envelope, as the mass ratio we determine for our Roche-lobe filling giants are often larger than 1.5. Clearly more theoretical work is needed along those lines.

Our detailed analysis of these stars also allows us to place the systems in a Hertzsprung–Russell diagram (Figure 3). The analysis has shown that red giants in symbiotic systems are rather normal and obey similar relations between colour, spectral type, temperature, luminosity and radius. Thus, the fact that they have larger mass-loss rates than single giants must be linked in some way to their binarity, adding credence to the companion-reinforced attrition process mechanism.

The observations presented here clearly reveal the power of interferometry for the study of interacting binary stars. The major limitation to our study is the rather imprecise knowledge of the distance of these objects. The Gaia survey, soon to begin, will be most useful in this respect.

References

Ake, T. B. et al. 1991, ApJ, 383, 842
Blind, N. et al. 2011, A&A, 536, A55
Boffin, H. M. J. et al. 2014, A&A, 564, A1
Kenyon, S. J. & Webbink, R. F. 1984, ApJ, 279, 252
Le Bouquin, J.-B. et al. 2011, A&A, 535, A67
Mikolajewska, J. 2007, Baltic Astronomy, 16, 1
Mürset, U. et al. 1991, A&A, 248, 458
Tout, C. A. & Eggleton, P. P. 1988, MNRAS, 231, 823
Verhoelst, T. et al. 2007, A&A, 470, L21

ALMA Resolves Turbulent, Rotating [C II] Emission in a Young Starburst Galaxy at $z = 4.8$

Carlos De Breuck[1]
Rebecca J. Williams[2]
Mark Swinbank[3]
Paola Caselli[4]
Kristen Coppin[5]
Timothy A. Davis[1]
Roberto Maiolino[2]
Tohru Nagao[6]
Ian Smail[3]
Fabian Walter[7]
Axel Weiß[8]
Martin A. Zwaan[1]

[1] ESO
[2] Cavendish Laboratory, University of Cambridge, United Kingdom
[3] Institute for Computational Cosmology, Durham University, United Kingdom
[4] School of Physics and Astronomy, University of Leeds, United Kingdom
[5] Centre for Astrophysics, Science & Technology Research Institute, University of Hertfordshire, Hatfield, United Kingdom
[6] Research Center for Space and Cosmic Evolution, Ehime University, Matsuyama, Japan
[7] Max-Planck-Institut für Astronomie, Heidelberg, Germany
[8] Max-Planck-Institut für Radioastronomie, Bonn, Germany

Over the last decade, the [C II] 158 µm line has emerged as one of the most powerful probes of the interstellar medium at high redshift. It is one of the brightest far-infrared lines, opening up the possibility to spatially and spectrally resolve the emission in high-redshift galaxies. ALMA has already demonstrated this during Cycle 0. Our ALMA [C II] kinematical study of the galaxy ALESS73.1 at $z = 4.8$, observed 1.2 Gyr after the Big Bang, shows evidence for turbulent, rotating emission in a galaxy that is still forming most of its stars.

In the local Universe, studies of the [C II] fine structure line (rest wavelength 158 µm) can only be performed from space, since the Earth's atmosphere is opaque at wavelengths around 160 µm. Since far-infrared space telescopes only have relatively small apertures, it remains difficult to spatially resolve [C II] emission in compact sources. Recent Herschel observations have begun to resolve [C II] at 0.1–1 kpc scales in nearby galaxies (Beirao et al., 2012; Parkin et al., 2013), but full dynamical studies are not yet possible. Ironically, observing [C II] becomes easier with redshift as the line shifts into increasingly better transmission windows of the Earth's atmosphere. However, to observe a line at such a short wavelength requires good atmospheric transparency and hence a dry site, like Chajnantor.

The Atacama Large Millimeter/submillimeter Array (ALMA) has already demonstrated its potential to study high-redshift galaxies in [C II] from Cycle 0 observations (e.g., Swinbank et al., 2012). We have now deepened such studies by observations of the dusty star-forming galaxy ALESS73.1 at $z = 4.8$ with ALMA Band 7. This source was first detected in the submillimetre (submm) with the Atacama Pathfinder EXperiment (APEX) telescope in the course of the Large APEX BOlometer CAmera (LABOCA) Extended Chandra Deep Field South (ECDFS) Sky Survey (LESS; Weiß et al., 2009). ALESS73.1 had been identified as an active galactic nucleus (AGN) from spectroscopy with VLT FORS (Faint Object Red Spectrograph) of this field (Vanzella et al., 2006). At the time of discovery, ALESS73.1 was the most distant submm-selected galaxy, and, as such, subject to an intensive follow-up campaign which includes: a CO(2-1) detection with the Australia Telescope Compact Array (Coppin et al., 2010); an initial [C II] detection with APEX (De Breuck et al., 2011); an ALMA [N II] detection (Nagao et al., 2013); and deep X-ray spectroscopy suggesting that the source hosts a Compton-thick AGN (Gilli et al., 2011; 2014).

ALMA observations of ALESS73.1

Our ALMA observations of ALESS73.1 (De Breuck et al., 2014) were performed in the extended Cycle 0 configuration, providing a spatial resolution of 0.5 arcseconds, or 3 kpc at this redshift. This ALMA spatial resolution approaches that of the Hubble Space Telescope (HST) in the optical/near-infrared. HST has also obtained deep observations of this galaxy as part of the Cosmic Assembly Near-infrared Deep Extragalactic Legacy Survey (CANDELS). HST's identification is spatially unresolved because it is dominated by the AGN, whose nature is revealed by the power-law emission from the restframe ultraviolet to near-infrared. In contrast, the far-infrared emission is dominated by strong star formation with rates of 1000 $M_\odot$ yr^{-1} (for comparison, the Galaxy forms stars at a rate of only a few $M_\odot$ yr^{1}).

In an independent ALMA Band 6 observation, Gilli et al. (2014) showed that the dust continuum emission is marginally spatially resolved at 0.3-arcsecond scales. This implies a compact host galaxy with a very high star formation density. The gas and dust associated with this vigorous starburst may even explain some of the high column density absorption seen in the X-ray spectrum (Gilli et al., 2014).

The high signal-to-noise provided by the ALMA observations allows the [C II] data-cube to be binned into 18 channels of 25 km s^{-1} width each (Figure 1), enabling the first detailed dynamical study of the [C II] line in such a high-redshift object. Interestingly, the [C II] emission is extended over 0.6 arcseconds and shows a pronounced velocity gradient, as is evident from Figure 2. This velocity field is consistent with a rotating disc with a radius of ~ 2 kpc, i.e., about twice as large as the dust continuum extension.

Our disc models (see Figure 2) constrain the dynamical mass to $3 \pm 2 \times 10^{10}\ M_\odot$. Combined with the observed H_2 mass of $1.6 \times 10^{10}\ M_\odot$ and the atomic gas of $5 \times 10^{9}\ M_\odot$ derived from the [C II] luminosity, the stellar mass is constrained to $< 3 \times 10^{10}\ M_\odot$. ALESS73.1 therefore has a very high specific star formation rate of > 80 Gyr^{-1}. This galaxy will thus double its stellar mass in ~ 12 Myr, and we are likely observing it during one of its first major star-forming episodes.

The spatially resolved kinematical study also allows us to check whether this rotating emission is stable against gravitational collapse. Figure 3 shows the intrinsic velocity dispersion (σ), which is only three times lower than the rotational velocity (V), i.e. $V/\sigma \sim 3$, suggesting that this is a dispersion-dominated disc. We confirmed this by deriving the Toomre Q

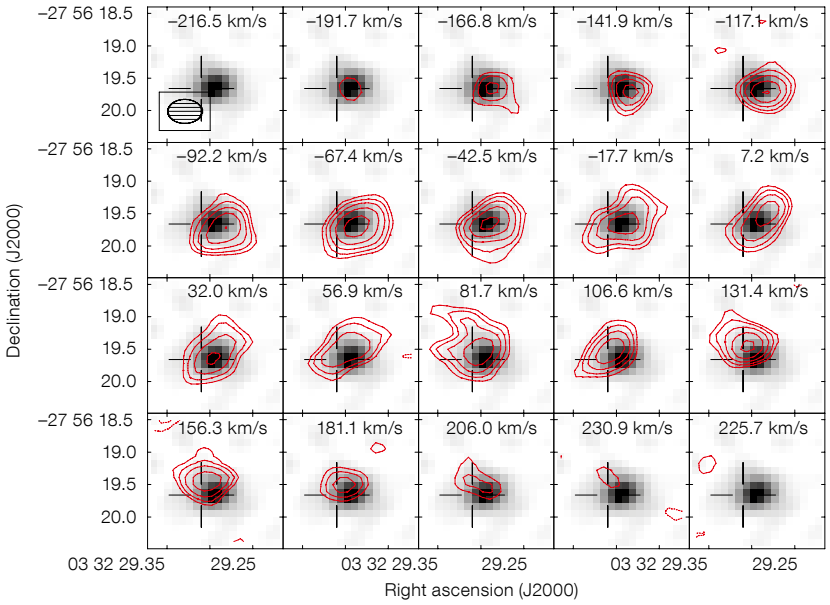

Figure 1. (Upper) ALMA channel maps (red contours) of [C II] overlaid on the line-free 326 GHz dust continuum image. The open cross marks the position of the AGN in the HST image of this source. Note that the dynamical centre coincides with the compact dust continuum source.

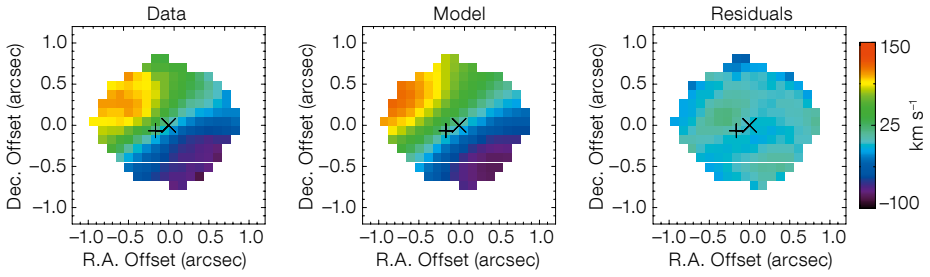

Figure 2. (Lower) The [C II] velocity field of ALESS73.1 is shown. The left panel presents the observed data, the central panel the best-fit rotating disc model and the right panel the residuals on this fit. The plus and cross mark the locations of the AGN and the [C II] peak, respectively (c.f., Figure 1). The observed motions of the [C II] emission are consistent with a rotating disc model.

parameter, and find it to be < 1 throughout the disc, indicating that the disc is unstable. This suggests that the [C II] line may be tracing the star-forming gas of this young galaxy.

Prospects

These [C II] observations show that ALMA can perform a dynamical analysis at an epoch when galaxies were undergoing their first major burst of star formation. Our Cycle 0 observations are still limited by spatial resolution (but not by signal-to-noise). The spatial resolution of the final ALMA array will improve on this by more than an order of magnitude. This improvement should open up new opportunities for kinematical studies of galaxies at wavelengths which can probe deep into the dust-obscured regions and at a resolution of ~ 100 pc, i.e., the size of their individual star-forming clouds.

References

Beirao, P. et al. 2012, ApJ, 751, 144
Coppin, K. et al. 2010, MNRAS, 407, L103
De Breuck, C. et al. 2011, A&A, 530, L8
De Breuck, C. et al. 2014, A&A, 565, A59
Gilli, R. et al. 2011, ApJ, 730, L28
Gilli, R. et al. 2014, A&A, 562, A67
Nagao, T. et al. 2012, A&A, 542, L34
Parkin, T. et al. 2012, ApJ, 766, 65
Swinbank, M. et al. 2012, The Messenger, 149, 40
Vanzella, E. et al. 2006, A&A, 454, 423
Weiß, A. et al. 2009, A&A, 707, 1201

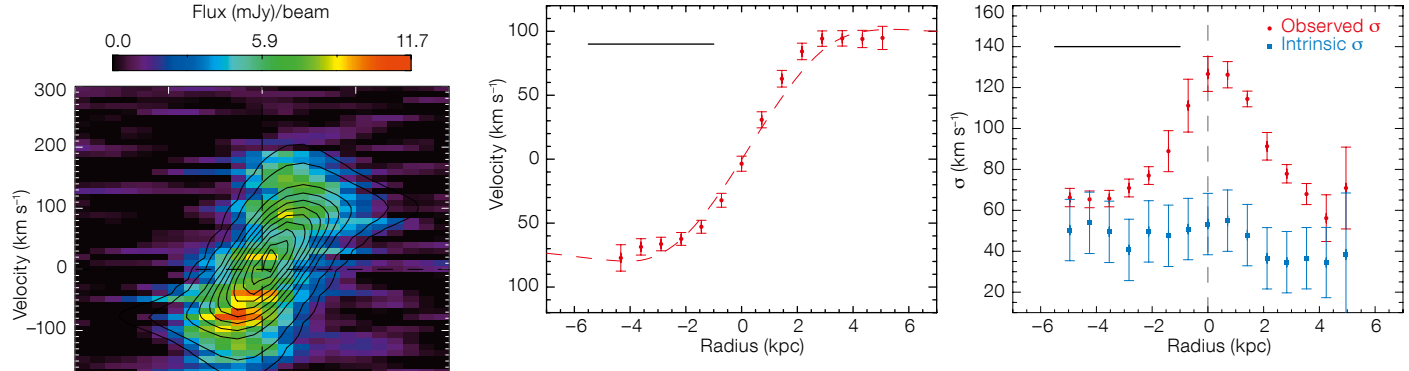

Figure 3. Left: Position–velocity diagram along the major axis of the disc model with our best fit rotating disc model overlaid as contours. Centre: Rotation curve extracted along the major axis with our best-fit model overplotted as a dashed line. Right: The variation in velocity dispersion as a function of radius in the disc. The low $V/\sigma \sim 3$ value shows this is a turbulent and dynamically unstable disc. The rise in dispersion towards the centre in the observed dispersion is an artefact resulting from the limited spatial resolution of the data. For reference, the synthesised beam size is shown as a horizontal black bar in the top left corner of the central and right panels.

Combining ALMA with HST and VLT to Find the Counterparts of Submillimetre Galaxies

Tommy Wiklind[1]
Christopher J. Conselice[2]
Tomas Dahlen[3]
Mark E. Dickinson[4]
Henry C. Ferguson[3]
Norman A. Grogin[3]
Yicheng Guo[5]
Anton M. Koekemoer[3]
Bahram Mobasher[6]
Alice Mortlock[2]
Adriano Fontana[7]
Romeel Davé[8,9,10]
Haojing Yan[11]
Viviana Acquaviva[12]
Matthew L. N. Ashby[13]
Guillermo Barro[5]
Karina I. Caputi[14]
Marco Castellano[7]
Avishai Dekel[15]
Jennifer L. Donley[16]
Giovanni G. Fazio[13]
Mauro Giavalisco[17]
Andrea Grazian[7]
Nimish P. Hathi[18]
Peter Kurczynski[19]
Yu Lu[20]
Elizabeth J. McGrath[21]
Duilia F. de Mello[22]
Michael Peth[23]
Mohammad Safarzadeh[23]
Mauro Stefanon[11]
Thomas Targett[24,25]

[1] ESO/Joint ALMA Observatory, Santiago, Chile
[2] Department of Physics and Astronomy, University of Nottingham, United Kingdom
[3] Space Telescope Science Institute, Baltimore, USA
[4] National Optical Observatory, Tucson, USA
[5] UCO/Lick Observatory, Department of Astronomy and Astrophysics, University of California, Santa Cruz, USA
[6] Department of Physics and Astronomy, University of California, Riverside, USA
[7] INAF–Osservatorio Astronomico di Roma, Monteporzio, Italy
[8] University of the Western Cape, Bellville, South Africa
[9] South African Astronomical Observatories, Cape Town, South Africa
[10] African Institute for Mathematical Sciences, Muizenberg, South Africa
[11] Department of Physics and Astronomy, University of Missouri, Columbia, USA
[12] Physics Department, CUNY New York City College of Technology, Brooklyn, USA
[13] Harvard-Smithsonian Center for Astrophysics, Cambridge, USA
[14] Kapteyn Astronomical Institute, University of Groningen, the Netherlands
[15] Center for Astrophysics and Planetary Science, Racah Institute of Physics, The Hebrew University, Jerusalem, Israel
[16] Los Alamos National Laboratory, USA
[17] Department of Physics and Astronomy, University of Massachusetts, Amherst, USA
[18] Aix Marseille Université, CNRS, Laboratoire d'Astrophysique de Marseille, France
[19] Department of Physics and Astronomy, Rutgers, The State University of New Jersey, Piscataway, USA
[20] Kavli Institute for Particle Astrophysics & Cosmology, Stanford, USA
[21] Department of Physics and Astronomy, Colby College, Waterville, USA
[22] Department of Physics and Astronomy, Catholic University of America, Washington, USA
[23] Department of Physics and Astronomy, Johns Hopkins University, Baltimore, USA
[24] Institute for Astronomy, University of Edinburgh, Royal Observatory, Edinburgh, United Kingdom
[25] Department of Physics and Astronomy, Sonoma State University, Rohnert Park, USA

The identification of optical/near-infrared counterparts to submillimetre galaxies (SMGs) has been one of the most enduring obstacles in learning more about the nature of these massively star-forming systems, including their true redshift distribution. Various techniques have been partially successful but it is only by imaging the submillimetre (submm) emission at the same angular resolution as the optical images that counterparts can be securely assigned. With ALMA it is now possible to image the redshifted dust emission from these objects with a minimum investment of observing time. The results of an analysis of the properties of the counterparts of ten submm galaxies that fall within the CANDELS coverage of the GOODS-S field is presented. All ten SMGs show homogeneous properties in their dust and gas content, but only eight show (surprisingly) homogeneous properties in terms of the stellar mass and characteristic age of the stellar population. The two deviating counterparts are discussed.

From the very beginning, the formidable angular resolution of the Hubble Space Telescope (HST) was a benchmark used in the planning for the Atacama Large Millimeter/Submillimeter Array (ALMA). With the same angular resolution at submillimetre (submm) wavelengths as in the optical, it is possible to study the cold Universe on the same scales as with HST and to make a detailed multi-wavelength comparison of the cold and hot components of astrophysical objects. This quest for high angular resolution was a driver pushing the ALMA array to both shorter wavelengths and to accommodate longer baselines. In the end, the angular resolution of ALMA will surpass that of HST, although it will take some more testing and verification of ALMA's performance before this becomes a standard observing mode.

The ability to combine the input from different telescopes to allow multi-wavelength coverage with comparable angular resolution, stretching from optical/ultraviolet (UV) through millimetre wavelengths, enables us to better understand the physical processes governing a range of astrophysical phenomena. There are, however, cases where the mere identification of optical counterparts to radio-detected sources, viewed at similar angular resolution, is a big achievement. One such class of objects is the elusive submm galaxies initially detected through their continuum emission at submm wavelengths. This emission originates as redshifted thermal emission from dust grains heated by UV photons, and probes the presence of young and massive stars and/or the presence of a dust-embedded active galactic nucleus (AGN).

Submm galaxies and the quest for optical counterparts

The possibility of detecting redshifted far-infrared (FIR) emission at submm wave-

lengths was discussed in a seminal paper by Andrew Blain and Malcolm Longair (Blain & Longair, 1993). The first bolometer array with a wavelength coverage and sensitivity to detect this high-redshift FIR emission was SCUBA (Submm Common User Bolometer Array), which was used on the 15-metre single-dish James Clerk Maxwell Telescope (JCMT) from 1997 until 2005. Some of the first projects pursued with SCUBA were to search for redshifted FIR emission towards the Hubble Deep Field (HDF) North and toward lensing clusters (Hughes et al., 1998; Smail et al., 1997). Several submm sources were detected, but identifying the optical counterparts proved to be very difficult due to the poor angular resolution achieved with the JCMT/SCUBA combination, resulting in a positional accuracy of ~ 15 arcseconds.

During the following decade several methods were employed to pinpoint the optical counterparts of SMGs and/or to estimate their redshift distribution. By pushing radio continuum observations to a sensitivity level where massive star formation is the main contributor to the continuum emission, and using radio interferometers to achieve sub-arcsecond angular resolution, it was possible to identify the counterparts of some SMGs and thereby obtain optical spectroscopic observations (Chapman et al., 2003; Arextaga et al., 2007). This method, however, can only account for a subset of all SMGs. A significant fraction of SMGs remained undetected even in the deepest radio continuum observations, possibly due to being at high redshift where the radio continuum falls below the detection limit, and some galaxies do not reveal optical emission so no spectroscopy can be done. An illustrative example of an elusive SMG is the brightest submm source in the HDF North (Hughes et al., 1998). Despite a large observational effort, no optical or near-infrared (NIR) counterpart has yet been identified. The redshift was only recently determined using rotational CO emission lines, and found to be z ~ 5.2 (Walter et al., 2012).

Several other methods have been used to find the counterparts of SMGs, most notably association via near-infrared and far-infrared emission (e.g., Targett et al. [2013] and references therein). However, these methods, while partially successful, have the common thread that they are indirect methods and thus prone to potential biases and misidentifications. Despite this, our knowledge of the properties of the submm galaxy counterparts has grown, albeit slowly and at a huge cost in telescope time.

It is really only through the use of submm interferometry, targeting the same emission as seen with bolometers, that the positional accuracy of the FIR emission can be determined with enough accuracy to allow a direct association of the optical counterpart, thus eliminating the potential for misidentifications and biases. This approach was pioneered with the SMA (SubMillimeter Array), IRAM's (Institut de Radioastronomie Millimetrique) Plateau de Bure and CARMA (Combined Array for Research in Millimeterwave Astronomy) telescopes. This approach, however, has been a time-consuming exercise, requiring up to eight hours of observing time per source. Hence, only a limited number of counterparts have been identified using this method. This is where ALMA, with its unprecedented sensitivity and high angular resolution, is a true game changer.

First results on SMGs with ALMA

During the very first cycle of ALMA Early Science (Cycle 0), one project (2011.0.00294.S) used the 16 available antennas to observe dust continuum emission at 870 µm towards 126 submm galaxies in the Extended Chandra Deep Field South (ECDFS). These submm galaxies were first identified using the Large Array Bolometer CAmera (LABOCA) bolometer on the Atacama Pathfinder EXplorer (APEX) telescope (Weiss et al., 2009). The ALMA observations and the results have been described by Swinbank et al. (2012) and in Hodge et al. (2013).

In short, with only ~ 2 minutes of observing time per source, both the sensitivity and the angular resolution were substantially improved compared to previous observations. The ALMA data was obtained in a compact configuration, resulting in a typical angular resolution of 1.6 by 1.1 arcseconds. The positional accuracy of the centre of the emission is, in most cases, 0.2–0.3 arcseconds (Hodge et al., 2013). Several instances of multiple submm sources within a single LABOCA "footprint" were found, and quite often, the submm emission was found to be offset from the centre of the LABOCA position (see Figure 1 in Swinbank et al., 2012).

A note on naming and the designation of the SMGs: the submm sources detected in the ECDFS with APEX/LABOCA are designated LESS (LABOCA ECDF Submillimeter Survey) followed by a number. The sources observed with ALMA are designated as ALMA-LESS # or ALESS #. The correct International Astronomical Union designation for these sources is, for instance, LESS J033219.0-275219. Here we will refer to the sources as LESS #, and use ALESS # when specifically addressing the submm emission observed with ALMA.

Combining ALMA with HST and VLT

In Wiklind et al. (2014) we used the results presented in Hodge et al. (2013) to identify optical/NIR counterparts to the ALESS sources within the Great Observatories Origins Deep Survey South (GOODS-S) field. The counterparts were analysed in terms of their physical properties, morphology and environment using the data amassed within the Cosmic Assembly Near-infrared Deep Extragalactic Legacy Survey (CANDELS) project.

The GOODS-S field is located within the ECDFS and is one of five fields observed in the CANDELS project. The CANDELS data (Grogin et al., 2011; Koekemoer et al., 2011) provides very deep near-infrared imaging using the Wide-Field Camera 3 (WFC3) installed on HST in 2009. Deep *K*-band data was provided through the VLT Hawk-I instrument and the HAWK-I Ultra Deep Survey and GOODS Survey (HUGS; Fontana et al., 2014). Overall, the CANDELS survey provides photometric data in 18 bands ranging from UV to mid-infrared. The data contains UV (VLT/VIMOS), optical (HST/ACS), and infrared (HST/WFC3, VLT/ISAAC, VLT/HAWK-I and Spitzer/IRAC) photometry (Ashby et al., 2013). A catalogue (Guo et al., 2013) was made based on source detection in the WFC3 F160W band. Photometry in bands other than WFC3 F160W is measured

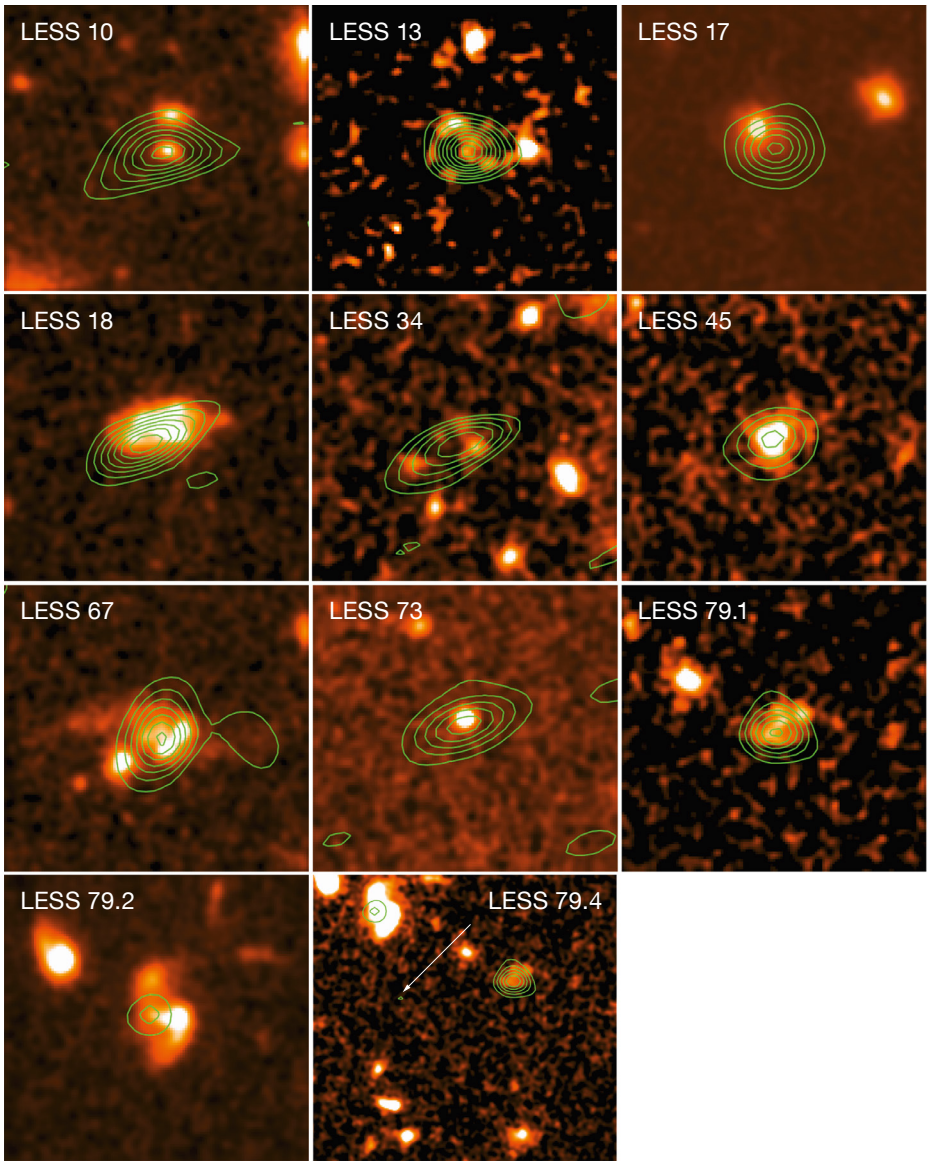

Figure 1. HST/WFC3 F160W images of the ten SMGs with identified counterparts in the CANDELS coverage of the GOODS-S field. Each image is ~ 7 by 7 arcseconds and has been smoothed to enhance the faint NIR emission. Contours show the ALMA 870 μm continuum emission, with contours starting at 0.1 mJy/beam and in steps of 0.1 mJy. The last image shows ALESS 79.4 (Hodge et al., 2013), which is much fainter than any of the other submm sources and has no identified counterpart.

using point spread function matching. Photometry of lower resolution images is done using the TFIT template-fitting method (see Guo et al. [2013] and references therein). The CANDELS survey also includes Spitzer/MIPS 24 μm data (Magnelli et al., 2011).

The *H*-band selected catalogue contains 34 930 sources with the representative 50 % completeness reaching 25.9, 26.6 and 28.1 AB mags in the F160W band for three different regions. The sources were extracted using SExtractor. Thirteen of the 126 LESS sources are located within the GOODS-South field as defined by the CANDELS coverage. ALMA observed nine of these. Hodge et al. (2013) reported multiple submm emission regions for three of the nine LESS sources within the WFC3/F160W area, for a total of 14 submm emission sources. Due to low signal-to-noise we retained only one of these multiple regions as a true individual SMG. Therefore the total number of individual SMG sources analysed was ten.

Identifying the counterparts

We identified the optical/NIR counterparts to the ALESS sources by matching the coordinates of the submm sources seen with ALMA (Hodge et al., 2013) with galaxies in the CANDELS WFC3 F160W selected catalogue (Guo et al., 2013). Given ALMA's positional accuracy of 0.2–0.3 arcseconds, combined with the 0.06-arcsecond pixel scale of the HST data, ensures that we can securely connect the SMGs with their nearest optical/NIR counterparts. There are, however, two caveats. The central location of the submm emission may not coincide with the centre of optical/near-infrared emission due to strong dust extinction. This effect has been seen in other submm galaxies and is exacerbated with increasing redshift, as shorter wavelength emission is shifted into a given optical/NIR filter. We must therefore allow for coordinate offsets of the order of 0.5 arcseconds, or ~ 4.5 kpc at z ~ 2. The second caveat is the possible, although improbable, coincidence of a background SMG with a foreground galaxy. While this is unlikely for the small sample discussed here, the fact that the initial LABOCA survey is luminosity limited creates a bias towards sources that may be gravitationally magnified by a foreground object.

The WFC3 counterparts to the ALESS sources are shown in Figure 1 together with contours of the submm emission observed with ALMA. From the figure it is clear that in most cases the position of the submm and NIR emission agrees quite well. There are, however, cases where the submm emission is offset from the NIR counterpart by up to 0.6 arcseconds, sometimes because the counterpart is part of a gravitationally interacting system (LESS 13, 67 and 79.2). Nevertheless, all of the submm sources were found to have a counterpart within 0.6 arcseconds of the centre of the submm emission with the exception of LESS 79.4 (Hodge et al., 2103). This submm source is faint and may be a spurious detection; it was not analysed in Wiklind et al. (2104).

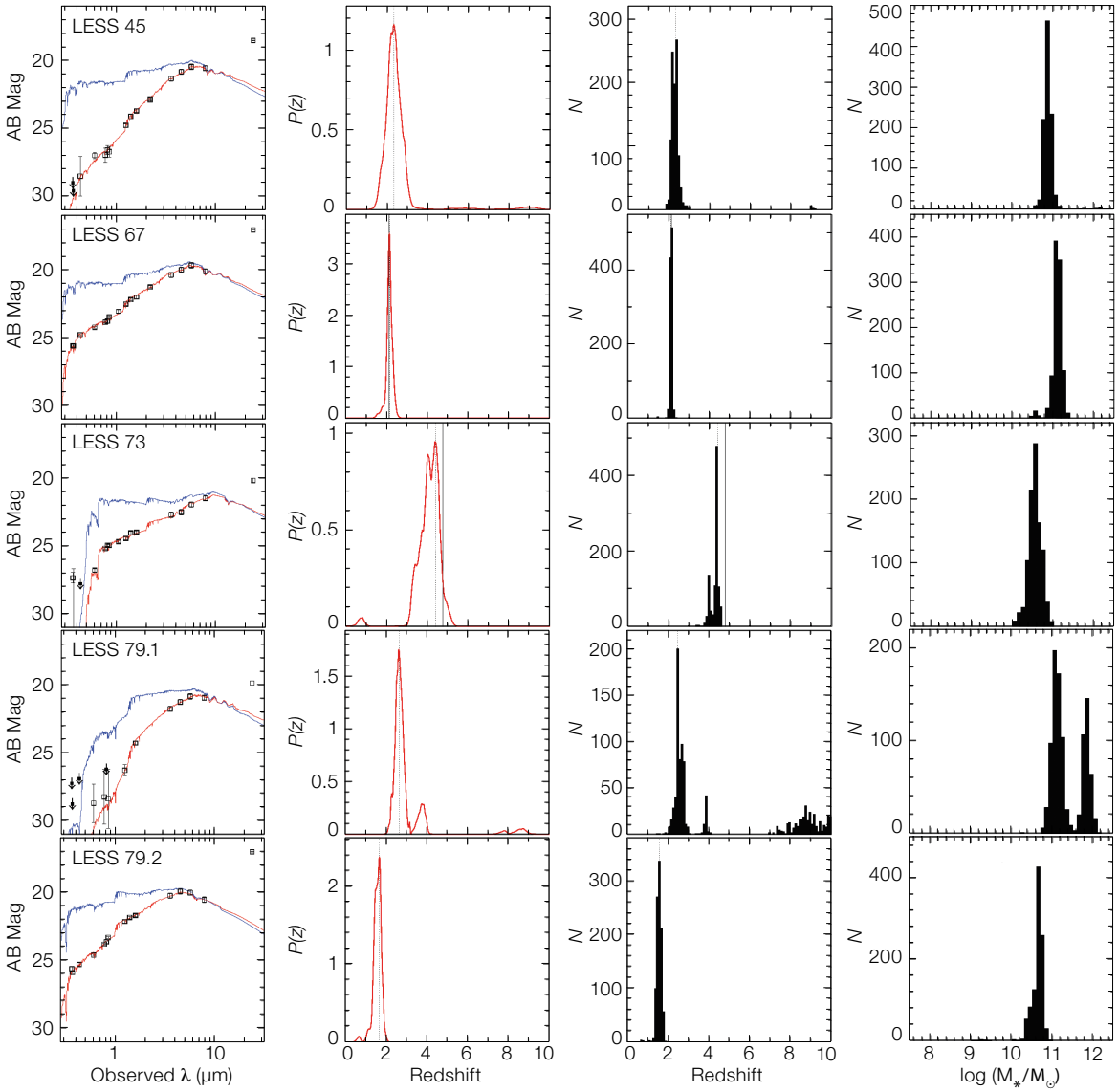

Figure 2. Results from the SED fitting of the UV through NIR photometry of the counterparts of the submm galaxies. The first column shows the actual SED, with the red line corresponding to the fit including dust obscuration and the blue line the corresponding SED corrected for dust extinction. The second and third columns show the probability distribution, *P(z)*, of the photometric redshift and the result from Monte Carlo simulations, respectively. The fourth column shows the simulation results for the stellar mass of the counterparts.

Physical properties of the counterparts

With the counterparts identified, parameters, such as photometric redshift, stellar mass, characteristic age of the stellar population, extinction and metallicity were derived by fitting spectral energy distributions (SEDs) using the stellar population synthesis models of Bruzual & Charlot (2003) and the CANDELS data. For each counterpart we explored a large parameter space for redshift, stellar age, dust extinction and star formation history. The star formation history was parameterised as a delayed-τ model, which allows for an initial increase in the star formation rate, up to an age $t = \tau$, followed by a declining star formation rate. This form of the star formation history is superior to the simple exponentially declining star formation rate (cf., Lee et al., 2010). The SED-fitting algorithm and the star formation rate parameterisation are described in Wiklind et al (2014).

The stability of the SED fits with respect to photometric uncertainties was explored using Monte Carlo simulations, where the photometric values were allowed to vary stochastically within their nominal errors. For each galaxy the result gives an estimate of the confidence of the various solutions with respect to the photometric values and uncertainties. For each solution of a photometric redshift, we also constructed a probability distribution *P(z)* representing the uncertainty of the photometric redshift associated with the fitting of a single set of photometric values. Combining the *P(z)* distributions from the Monte Carlo simulations gives a probability distribution that also takes the stability of the solutions into consideration. Examples of the results from the Monte Carlo simulations as well as the probability distributions for the photometric redshifts and stellar masses are shown in Figure 2.

The Bruzual & Charlot (2003) models only include stellar components and are not

designed to model an AGN contribution to the SED. Since a substantial fraction of SMGs are known to contain an AGN (e.g., Donley et al., 2010), the SED-fitting results could be biased by the UV contribution of the AGN. This would be handled by the SED fit as a young stellar component and/or as having less extinction than actually is the case. However, this bias does not appear to be present in the SED-fitting results for the LESS sources, even though almost 50 % of them are designated as containing an AGN based on X-ray, radio and infrared signatures. In fact, the stellar populations of the SMGs are characterised by relatively evolved stars, with characteristic ages ranging from a few hundred Myr to 1–2 Gyr, as well as containing a significant amount of dust extinction. The photometric redshifts range from z = 1.6 to z = 4.7. At least two of the SMGs are located at z > 4, while the average redshift for the remaining eight SMGs is ~ 2.0.

The stellar mass is estimated from the SED fit. This method has been shown to give robust mass estimates when compared with galaxies from semi-analytical models, where the mass of the stellar component is known (Lee et al., 2010). The stellar masses of the SMG counterparts are remarkably uniform, with two glaring exceptions. For eight of the SMGs the average stellar mass is $1 \times 10^{11}\ M_{\odot}$ with a surprisingly small dispersion, see Figure 3. The two remaining sources (LESS 10 and LESS 34) stand out with stellar masses almost two orders of magnitude smaller.

The most likely explanation of the two discrepant sources is that the submm emission originates from a background source not visible in the optical/NIR. Inspection of Figure 1 shows that this could very well be the case for LESS 34, where the submm emission is offset from the designated counterpart. For LESS 10, however, the submm emission and the counterpart are very well aligned and it is more difficult to consider this as a misaligned fore- or background source. Nevertheless, it is even less plausible that these two SMGs are in a different stage of evolution. In the case of LESS 34, the estimated stellar mass is actually smaller than the dust mass derived from the optically thin submm emission. This is clearly a contradiction and can be resolved if the submm emission originates in a background source, invisible in the optical/NIR images.

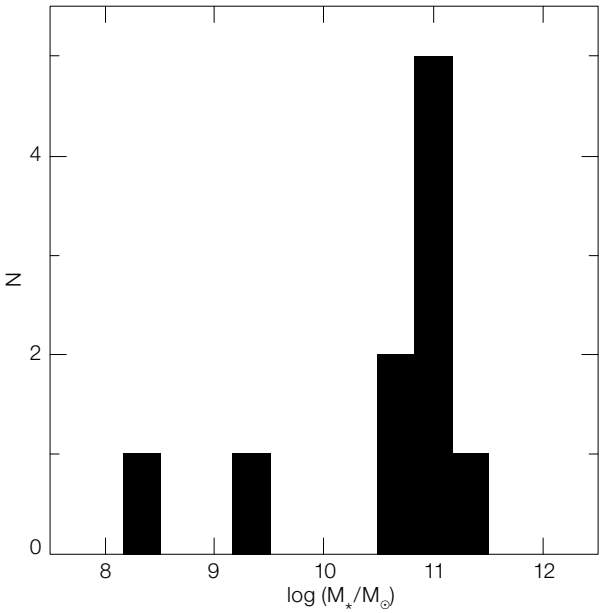

Figure 3. The distribution of stellar masses for the ten submm galaxies in the CANDELS GOODS-S coverage. The two low-mass galaxies are LESS 10 and LESS 34. In the case of LESS 34 ($\log(M_{*}/M_{\odot})$ ~ 8.4), the stellar mass is less than the estimated dust mass, which is clearly unphysical.

Morphology of the counterparts

We measured the morphology of the SMG counterparts through both visual inspection of the HST images and by using non-parametric parameters (so called CAS — concentration, asymmetry and clumpiness). For this analysis we used the HST/WFC3 F160W images, in most cases corresponding to a restframe wavelength of ~ 5000 Å. The CAS parameters represent a non-parametric method for measuring the forms and structures of galaxies in resolved CCD images (for further details see Conselice et al., 2003). We also derive the Gini and M_{20} coefficients for the SMGs. The Gini parameter is a statistical tool originally used to determine the distribution of wealth within a population, with higher values indicating a very unequal distribution. The M_{20} parameter is similar to the concentration parameter (C) in that it gives a value that indicates if light is concentrated within an image; it is, however, calculated slightly differently from the C and Gini coefficients (e.g., Lotz et al., 2008).

From visual inspection, we designated an SMG counterpart as a merger if it shows signs of gravitational interaction and has tidal tails. If the counterpart has one or more neighbours within 30 kpc and $\Delta z \pm 0.1$, but without signs of interaction, we designate it as a neighbour. In the absence of any interaction and neighbour within 30 kpc, the SMG is designated as isolated. Of the ten SMG counterparts, only three show clear signs of being part of a merger system. This is in contrast to local ultraluminous infrared galaxies (ULIRGs), which are almost always part of merging systems.

In order to assess whether the asymmetry values of the SMGs are different from non-SMG galaxies of similar mass and at the same redshift, we constructed a control sample for each SMG, consisting of galaxies with stellar mass within ± 0.2 dex of that of the SMG and $\Delta z \pm 0.2$ of the photometric redshift of the SMG in question. The control galaxies were drawn from the same CANDELS GOODS-S F160W selected catalogue as the SMG counterparts. Comparing the asymmetry parameter values for the galaxies in the control samples with the SMGs shows that the three SMGs with the highest asymmetry parameter (LESS 34, 67 and 79.2) have values that are higher than 98 % of their respective control sample. The LESS 67 and LESS 79.2 counterparts show clear signs of merging, while LESS 34 is one of the sources with abnormally low stellar mass,

possibly because the counterpart is a foreground system.

We also did a Monte Carlo simulation where we compared the average asymmetry parameter of our SMGs with that of a randomised sample of galaxies and randomly selected ten galaxies, each appropriate to the control samples. The average asymmetry value of these ten galaxies was derived and compared with the average value of the SMGs. Repeating this procedure 1000 times, we find that in 99 % of the Monte Carlo realisations, the average asymmetry of the SMG counterparts is higher than the average asymmetry value of the control sample.

These results suggest that the SMGs are intrinsically more asymmetric than the typical galaxies at the same redshift and mass range. The small fraction of mergers among the SMG counterparts suggests that the high asymmetry is due to intrinsic clumpiness and/or patchy dust distribution (an example of a patchy dust distribution is shown in Figure 4) rather than being caused by gravitational interaction.

Gas and dust properties

For redshifts low enough that the observed submm emission samples the Rayleigh–Jeans part of the dust SED, the emission is optically thin. For typical dust SEDs, this is the case as long as $z < 4$. In the optically thin case, the luminosity of the submm emission is a measure of the total dust mass. Adopting dust properties from a sample of local galaxies, we used the ALMA submm fluxes and our photometric redshift estimates to derive dust masses for the ALESS sources. The average dust mass is $(4.0 \pm 1.3) \times 10^8\ M_{\odot}$. As mentioned above, the dust mass of LESS 34 exceeds the estimated stellar mass, which is an argument for the SMG being a background source. It is also possible to empirically derive a conversion factor between the 870 μm luminosity and the gas mass (Scoville et al., 2014). This leads to very similar values of the dust mass as derived by simply assuming that the dust properties of the high-z SMGs are similar to local galaxies.

Overall, the gas and dust properties of the SMGs are remarkably homogeneous, with a small dispersion. This is similar to the results obtained for the stellar masses, with the exception for the two deviating sources LESS 10 and LESS 34. The fact that these two sources appear to have normal SMG properties but deviate in the properties of their assigned counterparts further strengthens the suspicion that their true counterparts are background sources that remain undetected.

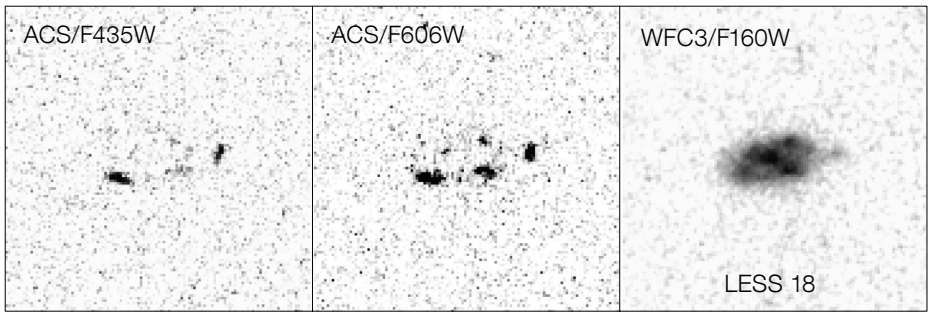

Figure 4. Detail of one of the sources, LESS 18, showing how it breaks up into several clumps at short wavelengths. The UV clumps do not appear to suffer from large extinction, while the central part of the galaxy only shows up at longer wavelengths, perhaps resulting from patchy dust obscuration.

Conclusions

The sensitivity and high angular resolution provided by ALMA are clearly illustrated by the first SMG observations in Cycle 0, and it promises a bright future for this type of study. The optical/NIR counterparts of the ten SMGs within the CANDELS GOODS-S field show that, in contrast to local ULIRGs, there are only a few cases of ongoing mergers and most appear to be isolated systems. Furthermore, the SMGS clearly have a "history" as portrayed by their evolved stellar populations. While the redshift range of the SMGs discussed here ranges from $z = 1.65$ to $z = 4.76$, the overall stellar masses and dust masses are remarkably homogeneous, with the exception of two sources LESS 10 and LESS 34.

If the discrepant properties of LESS 10 and LESS 34 can be explained by the submm emission from a background source, while the designated counterpart is in the foreground, then it shows that even with the improved capability provided by ALMA, there are still cases where the identification of the optical/NIR counterpart of an SMG remains elusive. This situation is similar to the very first SMG detected in the Hubble Deep Field, HDF850.1, for which no optical/NIR counterpart has yet been identified despite a tremendous observational effort; the redshift is now known from molecular emission lines (Walter et al., 2012). A similar technique can be used on the SMGs observed with ALMA and will be the ultimate arbiter of whether the submm emission is associated with the designated optical/NIR counterparts or not.

References

Ashby, M. L. N. et al. 2013, ApJ, 769, 80
Aretxaga, I. et al. 2007, MNRAS, 379, 1571
Blain, A. W. & Longair, M. S. 1993, MNRAS, 264, 509
Bruzual, G. & Charlot, S. 2003, MNRAS, 344, 1000
Chapman, S. C. et al. 2003, Nature, 422, 695
Conselice, C. J. et al. 2003, ApJS, 147, 1
Donley, J. L. et al. 2010, ApJ, 719, 1393
Fontana, A. et al. 2014, The Messenger, 155, 42
Grogin, N. A. et al. 2011, ApJS, 197, 35
Guo, Y. G. et al. 2013, ApJS, 207, 24
Hodge, J. A. et al. 2013, ApJ, 768, 91
Hughes, D. H. et al. 1998, Nature, 394, 241
Koekemoer, A. M. et al. 2011, ApJS, 197, 36
Lee, S.-K. et al. 2010, ApJ, 725, 1644
Lotz, J. M. et al. 2008, ApJ, 672, 177
Magnelli, B. et al. 2011, A&A, 528, 35
Scoville, N. Z. et al. 2014, ApJ, 783, 84
Smail, I. et al. 1997, ApJ, 490, L5
Swinbank, M. et al. 2012, The Messenger, 149, 40
Targett, T. A. et al. 2013, MNRAS, 432, 2012
Walter, F. et al. 2012, Nature, 486, 233
Weiss, A. et al. 2009, ApJ, 707, 1201
Wiklind, T. et al. 2014, ApJ, 785, 111

Two recent workshops both took place in the large auditorium (seating capacity 236) in the new ESO Headquarters extension building. Upper: the participants at a coffee break of the E-ELT Workshop on Exoplanets (see Spyromilio & Liske, p. 51). Lower: participants at the 3D2014 workshop (see Lehnert et al., p. 53) pictured in front of the new building.

Report on the Workshop

Metal Production and Distribution in a Hierarchical Universe

held at Observatoire de Paris Meudon, France, 21–25 October 2013

Ivo Saviane[1]
Piercarlo Bonifacio[2]
Monique Spite[2]
Lorenzo Monaco[1]

[1] ESO
[2] Observatoire de Paris, Meudon, France

The workshop aimed at taking a global view of the evolution of metal abundances from the Big Bang to the present day, considering both observations and simulations. Abundance studies in stars and galaxies, and the variety of interstellar and intergalactic media, were covered. A summary of the workshop topics in order of decreasing redshift is presented, with considerable attention given to abundance studies of the Milky Way.

Almost a hundred researchers convened to discuss how metal abundances across cosmic time can help us to understand the evolution of the Universe and its main structures. The conference was hosted in the beautiful Pavillon Bellevue palace owned by the Centre national de la recherche scientifique (CNRS) and located in Meudon. As the title of the conference suggests, it tried to bridge often-separated research topics, in the hope of obtaining a global view of abundance studies, and of fostering cross-field collaborations. To reach these goals, the review talks were ordered to follow the metallicity evolution of the Universe from the very beginning to the present day, and to show how this evolution can be understood using the latest computer simulations and theories. In addition, contributed talks and posters enriched the programme with an exciting diversity of topics.

Two highlights of the conference were also the conference dinner in the grandiose Cassini Hall at the Paris Observatory, and an organ concert by Dominique Proust in Meudon-Bellevue Church. The dinner was preceded by a guided tour of the Observatory and the vista of the Paris landscape, and the concert was accompanied by a visual show of images related to music and astronomy.

Figure 1. The participants on the steps outside the Espace Isadora Duncan, Pavillon Bellevue where the workshop was held.

It would be impossible, in this limited space, to give a full account of the whole programme, so we extract the highlights to give an idea of the range of topics that were covered. More details can be gathered from the conference proceedings that will be published in the Memorie della Società Astronomica Italiana, and we hope that the fruits of the five-day discussion will appear in the literature in the coming months.

Introductory talks

The conference started with a talk by Anatoly Klypin updating the audience on the latest Lambda Cold Dark Matter (ΛCDM) simulations of the evolution of the Universe. The talk underlined one of the recurrent themes of the conference, i.e., that modelling gas processes and star formation feedback is exceedingly difficult, so critical constraints to theory must be placed by measuring abundances at all redshifts and for different cosmic structures. After primordial nucleosynthesis, chemical elements are produced in stars (either quiescent or explosive) so a review of stellar nucleosynthesis was given by Paolo Ventura. He recalled how stars of different mass pollute the interstellar medium (ISM) with different elements, and at different times. In the rest of this article, summaries of invited and contributed talks are arranged in order of decreasing redshift. Table 1 provides an overview chronology of events and observational data together with the abundances (where measured) at particular epochs.

$z = \infty$

Naturally, the first measurements are those of elements produced in the initial ~ 15 min in the life of the Universe, during Big Bang nucleosynthesis (BBN): D, ^{3}He, ^{4}He and ^{7}Li. Yuri Izotov and Ryan Cooke presented their most recent estimates: from absorption spectra of damped Lyman-α absorbers, for deuterium $(D/H)_p = 2.53 \pm 0.04 \times 10^{-5}$ (Cooke et al., 2014); extrapolating from abundances measured from emission spectra of H II regions in metal-poor galaxies, the helium mass fraction $Y_p = 0.254 \pm 0.003$ (Izotov et al., 2013); and from spectra of very metal-poor stars the upper limit on the lithium abundance is $A(^7\mathrm{Li}) \equiv 12 + \log(^7\mathrm{Li/H}) = 2.2$ (Asplund et al., 2006; Sbordone et al., 2010). Gary Steigman then pointed out that when inserted in the models, the abundances of D and ^{4}He can constrain the baryon-to-photon ratio (η_{10} or $\Omega_B h^2$) and the number of equivalent neutrinos (ΔN_ν) to be added to the three standard ones.

Time since Big Bang	Redshift z	Event	Abundance
~ 1 to ~ 10^3 sec	> 150 × 10^6	BBN	Observed: $(D/H)_p$ = 2.53 ± 0.04 × 10^{-5}; Y_p = 0.254 ± 0.003; Predicted: $A(^7Li)$ = 2.7
After 0.1 Myr	~ 2000	Cosmic Microwave Background (CMB)	
~ 0.2–0.1 Gyr	~ 20–30	First star formation (SF)	When $H_2 \lesssim 10^{-4} \Rightarrow$ SF starts; pollution depends on mass function (pair instability SNe or not) and stellar rotation
		Most metal-poor MW stars	SMSS J031300.36-670839.3 has [Fe/H] < –7.1 (Keller+14); two populations of very metal poor stars (in terms of C abundance) (Norris+13; Spite+13)
0.2 < t < 0.48 Gyr	20 > z >10	Dwarf galaxies in Ricotti's simulations (progenitors of ultra-faint dwarfs?)	Mass density function (MDF) peaked at [Fe/H] ~ –1
0.27 < t < 0.48 Gyr	15 > z > 10	Pop III galaxies in low-density regions; candidates at 6.3 < z < 8.8 behind lensing clusters	
~ 0.4 Gyr	~ 11	Lensed galaxy of 10^8–10^9 $M_\odot$ (Coe+13);first galaxy candidates, Large Magellanic Cloud (LMC) mass or larger (Oesch+13)	
t > 0.48 Gyr	< 10	Reionisation completed	
0.71 Gyr	7.51	Furthest galaxy redshift confirmed by Ly-α (Finkelstein+13)	
0.97 Gyr	5.9	GRB 130606A (Chornock+13)	[Si/H] ≤ –1.7 and [S/H] ≤ –0.5
t < 1.2 Gyr	> 5	High density clumps ("discs") from DLA measurements	Enrichment by SN II from Pop II stars and prompt SN I
1.2 Gyr	5.0	GRB 111008A (Sparre+14)	log N(H I)/cm^{-2} = 22.30 ± 0.06; [M/H] ≈ –1.7 ± 0.1 for S, Cr, Fe, Ni
1.3 Gyr	4.7	GRB 100219A (Thoene+13)	[S/H] = –1.1 ± 0.2
~ 2.19 Gyr	~ 3	IGM measurements from Ly-α forest	[C/H] ~ –3.5
~ 2.19 Gyr	~ 3	Galaxy halo measurements from Lyman limit systems	[M/H] from pristine to ~ +0.7
1.2 → 12.38 Gyr	5 → 0.1	Average "disc" metallicity from DLA measurements	[M/H] = –0.22; z ~ 0.65; [α/Fe] ~ +0.3
1.8 Gyr	3.5	SF galaxies in Maiolino+08	[M/H] ~ –0.5 for galaxies of ~ 10^{10} $M_\odot$
3.34 Gyr	2	MZR from H II regions (Cullen+14); highest-mass galaxies (3 × 10^{10} $M_\odot$)	[O/H] ~ –0.5
3.34 Gyr	2	First detected galaxy clusters	
	1.49	Negative metallicity gradient for lensed galaxy (Yuan+11); "inside-out" formation?	–0.16 dex kpc^{-1}
4.6 Gyr	1.4	End of Milky Way (MW) thick Disc formation, began at 1.2 Gyr (Haywood+13)	
7.7 Gyr	< 0.65	Galaxies with 9.8 < log $M_\star/M_\odot$ < 11.5 start to evolve as closed boxes (Rodrigues)	

Table 1. Chronology of main events discussed in the article. The conversion from redshift to time was done using CosmicCalc[1], assuming H_0 = 71, Ω_M = 0.270, Ω_{vac} = 0.730.

20 ≤ z ≤ 30

In his review, Volker Bromm recalled that the first stars form at redshifts z ≈ 20–30 (≈ 0.2 – 0.1 Gyr after the Big Bang) inside ~ 10^5–10^6 $M_\odot$ mini-haloes. The subsequent evolution of both metallicity and cosmic structures depends on whether the mass function of these Population III (Pop III) stars is limited to a few tens of solar masses, or it can reach ~ 140–260 $M_\odot$. In the latter case there will be pair-instability supernovae (SNe) together with core-collapse SNe, which will inject more metals, and will delay the reassembly of gas into long-surviving systems. At the current early stage, simulations cannot fully constrain the Pop III mass function, so observations must come to the rescue. Searches for surviving metal-free, Pop III, low-mass stars are ongoing, and their outcome will certainly lead to revisions of the current scenario.

Three such surveys were illustrated by Elisabetta Caffau, Heather Jacobson, and Katia Cunha. The first survey starts with the Sloan Digital Sky Survey (SDSS) Data Release 9 (DR9) spectra and identifies main sequence turn-off stars with metallicities [Fe/H] < –3 to be followed up with the UVES or X-shooter spectrographs at the Very Large Telescope (VLT). The second survey uses the multi-band photometry of SkyMapper to search for candidate extremely metal-poor stars, which are then confirmed with low- and high-resolution spectroscopy obtained with Magellan, Keck, and VLT. Heather gave us a preview of SMSS J031300.36-670839.3 (Keller et al., 2014) which has a record-breaking [Fe/H] < –7.1, and an abundance pattern consistent with gas enriched by a single 60 $M_\odot$ star that exploded as a low-energy supernova. While not explicitly targeted to metal-poor stars, the SDSS3 APO Galactic Evolution Experiment (APOGEE) survey, described by Katia Cunha, is an example of one of the many ongoing or planned large-scale surveys of Milky Way stellar abundances.

9 ≤ z ≤ 11

While the first star formation episode is beyond the reach of current facilities, galaxy candidates at ever-increasing redshifts are being found. Rychard Bouwens

updated us on the most recent results of these searches, which are typically carried out with the Hubble Space Telescope (HST). For example, Oesch et al. (2013) using Wide Field Camera 3 near-infrared data and the Lyman-break technique found seven $z \sim 9$ galaxy candidates, and one each at $z \sim 10$ and $z \sim 11$. The data show the early and fast assembly of galaxies, for example based on the ultraviolet (UV) luminosity density contributed by star-forming systems, which increased by two orders of magnitude in ~ 1.5 Gyr, between redshifts 10 and 3. With current facilities primordial galaxies smaller than 10^8–10^9 $M_\odot$ in stellar mass are below detection, but they are predicted by Massimo Ricotti through simulations; interestingly, if evolved to the present-day Universe, his objects would have properties comparable to the faintest dwarf spheroidal galaxies in the Local Group.

9 ≤ z ≤ 15

Chemically pristine galaxies in haloes with mass $M \sim 10^8$ $M_\odot$ may form at $z < 20$ in relatively underdense regions of the Universe. Stiavelli & Trenti (2010) expect that such galaxies in the range $10 \lesssim z \lesssim 15$ could be found if magnified by lensing clusters, so Claes-Erik Rydberg went out to check whether this is true. By fitting Pop III model spectral energy distributions (SEDs) to multiband photometry from the CLASH (Cluster Lensing And Supernova survey with Hubble) survey, he found candidate Pop III galaxies with redshifts between 6.3 and 8.8, lensed by four galaxy clusters.

5 ≤ z ≤ 6

In order to find galaxies for which metallicity can be measured, lower redshifts must be considered. The first galaxies to be encountered along this route are gamma-ray burst (GRB) host galaxies, as explained by Martin Sparre. A fraction of GRBs have host galaxies that give rise to damped Lyman-α absorption, which permits the measurement of their metallicity, currently up to redshifts of almost 6. Martin presented his X-shooter spectroscopy of the optical afterglow of GRB 111008A at $z = 5.0$, which yielded an H I-content of log N(H I)/cm^{-2} = 22.30 ± 0.06 and a metallicity [M/H] ≈ –1.7 ± 0.1 for several elements (S, Cr, Fe, Ni).

2 ≤ z ≤ 5

A review of intergalactic medium (IGM) metallicities in regions of different density was given by Michele Fumagalli who showed us that below $z \sim 5$, IGM pollution is already widespread. In the IGM, measured carbon abundances are [C/H] ~ –3.5 at z ~ 3, and they increase by a factor of ~ 2–3 from $z \sim 4.3$ to $z \sim 2.4$. Considerable substructure is observed in the IGM, so Michele formulated the hypothesis that a significant fraction of the metals seen in the IGM escaped from galaxies as clumps that subsequently mixed with the surrounding hydrogen. In galaxy haloes, a large metallicity spread is observed, from pristine to super-Solar values, while in higher density systems, damped Lyman-α absorbers (DLAs), the average metallicity depends on redshift and reaches about 1/10 Solar at $z = 0.1$. Interestingly, DLAs are found to be α-element enhanced with a median [α/Fe] ~ +0.3. The [M/H] and [α/Fe] distributions in $z > 2$ DLAs with [M/H] $\lesssim$ –1 agree with those observed for stars in the Galactic Halo.

More insight into IGM enrichment processes was offered by the presentations of Michael Rauch and Evan Scannapieco. Michael has an ongoing investigation of high-redshift Lyα galactic haloes, where young stellar populations and signs of tidal and/or ram-pressure stripping were found. The release of metal-enriched gas during interactions, which increases with redshift, may provide a mechanism for enriching the IGM as widely as observed. These ideas are directly supported by the simulations presented by Evan Scannapieco. He finds that long-range outflows are excluded, also because, by $z \approx 2$, intergalactic enrichment appears to be concentrated around large galaxies and due primarily to metals from similarly-biased higher-redshift sources.

0 ≤ z ≤ 3

As we move down in redshift, metallicities for larger galaxy samples can be obtained, which show that a mass–metallicity relation (MZR) is in place already at z ~ 3.5 (Maiolino et al., 2008). A discussion of the MZR based on spectra of lensed galaxies was presented by Lisa Kewley. She showed some results from Yuan et al. (2013), highlighting how good signal-to-noise spectra of lensed galaxies can be used to estimate metallicities using the same methods applied for local galaxies. The redshift evolution of [O/H] can thus be better constrained. In addition it is possible to explore how the MZR extends to low-mass galaxies (down to 3×10^7 $M_\odot$).

z = 2

Metallicities for high-redshift galaxies are obtained with calibrations of emission line ratios versus metallicity obtained from local fiducial H II regions. However, earlier in cosmic history the physical conditions in H II regions might have been different, as postulated by Fergus Cullen. He finds that his MZR is offset by ~ 0.3 dex to lower values compared to that of Erb et al. (2006); for example his highest-mass galaxies (3×10^{10} $M_\odot$) have [O/H] ~ –0.5 instead of ~ –0.2. However the two datasets can be reconciled if the effect of a higher ionisation parameter is applied to the Erb et al. (2006) sample.

0 ≤ z ≤ 0.6

Throughout cosmic history, galaxies are shaped by interactions and gas exchanges with the environment, an aspect of galaxy evolution that is being investigated by the IMAGES survey. François Hammer examined mergers between gas-rich disc galaxies in the last 6 Gyr of cosmic history, and, thanks to spatially-resolved kinematics, morphologies and multi-band photometry, he discovered that 50 % of spiral progenitors were experiencing major mergers by z ~ 0.6. Therefore a high fraction of present-day discs are the end products of rebuilt discs. In the second presentation of IMAGES, Myriam Rodrigues investigated the role of gas exchanges in the life of intermediate mass ($9.8 < \log M_*/M_\odot < 11.5$) disc galaxies. She considered the run of gas fraction with redshift, and found that galaxies in her sample had evolved as closed

systems since $z \sim 0.6$; however literature data show that at higher redshifts ($z \sim 2$–3) exchanges with the environment become more and more important.

$z = 0+$

Byproducts of mergers are various types of debris, of which the most conspicuous are tidal dwarf galaxies (TDGs), which were reviewed by Pierre-Alain Duc. The first step in understanding TDG role in IGM pollution would be a census: if they were found to be very numerous, it would mean that they manage to keep their material, despite the lack of dark matter, and therefore they would play a minor role in the enrichment of the intergalactic medium. One step toward this census was illustrated by Sarah Sweet, who searched for TDGs in "Choir" galaxy groups identified in the H I Parkes All Sky Survey (HIPASS) survey: 16 % of dwarfs were identified as strong TDG candidates based on their position in the luminosity–metallicity plane.

$z = 0$

At the end of the cosmic chemical evolution outlined so far are the objects that we observe in the local Universe. Clusters of galaxies and the intracluster medium (ICM) were discussed by Hans Boehringer. He showed that clues to the origin of the ICM can be obtained by studying the relative abundances of C and N that come primarily from winds of asymptotic giant branch (AGB) stars, of O and Mg that come primarily from core-collapse supernovae, and of Fe and Ni that are primary products of SN Ia. Hans recalled that this research field is in its infancy, so future missions like ASTRO-H should bring much progress. Later, Evgenii Vasiliev warned us that, based on his new ionisation models, current metallicities of the circumgalactic medium based on O VI might be over-estimated by factors of 2 to 3.

Abundances in the Milky Way

Several sessions of the conference were dedicated to reviewing abundance determinations for the Milky Way and associated structures. To summarise this broad section, we can start from the Solar Neighbourhood. Because the Solar System is immersed in the Galactic Disc, our observations suffer from extinction caused by gas and dust confined to the disc itself. Therefore a proper interpretation of the observations needs to take into account the ISM distribution around the Sun. The status of such knowledge was the subject of a very interesting talk by Rosine Lallement, who presented her latest maps of gas geometry within 2.5 kpc.

Milky Way Disc

Thomas Bensby started with a review of abundances of stars in different Galactic subsystems, especially the thin/thick Disc and the Bulge. By collecting abundances for distant stars, Thomas has found that the ratio of thick-to-thin Disc stars changes with distance in a way that shows that the thick Disc is more centrally concentrated than the thin Disc.

New results on the chemical evolution of the Disc were also presented, based on the large set of spectra collected by the HARPS Guaranteed Time Observing programme (Adibekyan et al., 2012). Sara Bertran de Lis confirmed the α-element enhancement of thick Disc stars with O abundances, and Garik Israelian found that thick and thin Disc populations are different also when looking at [Cu/Fe], [Y/Fe] and [Ba/Fe] abundance ratios. Afterwards, after a general introduction to the principles of galactic chemical evolution by Nicolas Prantzos, Misha Haywood presented evidence (based on Si abundances from the same HARPS database) that the thick Disc formed between 12.5 and 9 Gyr ago from large amounts of gas, and evolved as a closed-box model.

Success in reproducing the [Fe/H] and [O/Fe] distribution functions of the Milky Way Disc was also achieved by Rob Yates with his semi-analytic model of galaxy formation, which simultaneously reproduces the chemical properties of local elliptical galaxies and the mass-metallicity relation of local star-forming galaxies. Other simulations were presented by Noelia Jimenez who discussed how in her implementation, the "single degenerate" scenario for SN Ia is able to reproduce, amongst others, the [α/Fe] ratios for bulge-dominated galaxies.

Milky Way Bulge

In her review, Melissa Ness used results from the Abundances and Radial velocity Galactic Origins Survey (ARGOS) to show that, while the majority of stars in the Bulge belong to a boxy/peanut shape, which is a signature of formation from the Disc, there remains a metal-poor population which is not part of the boxy/peanut, whose origin is still unclear (either a classical bulge or a thick disc). Support for a secular formation of the Bulge was given by Paola di Matteo with her dissipationless, N-body simulations, and Davide Massari illustrated how Terzan 5 could be a pristine fragment based on its large metallicity spread matching that of the Bulge itself.

Galactic globular clusters

While the formation epoch of the Bulge might be debated, there is no question that globular clusters (GCs) are survivors from the first phases of galactic evolution, so they provide essential clues on the formation of the Galaxy. Alessio Mucciarelli illustrated how advances in spectroscopic facilities have revealed clusters with extended star formation histories, which could be possible remnants of dwarf galaxies being disrupted by the Milky Way. Javier Alonso Garcia then showed how, in many cases, Strömgren photometry can help uncover multiple stellar populations in a faster way. Loredana Lovisi showed that C and O depletion (measured with the FLAMES spectrograph) for some blue-straggler stars in 47 Tucanae, M30 and ω Centauri points to a mass transfer origin for these stars.

When coupled with accurate ages, GC metallicities can offer good insight into the formation of the Milky Way, as shown by Ryan Leaman: he found that GCs define two age–metallicity relations (AMR), and that clusters belonging to the more metal-poor AMR should have been generated in hosts with stellar masses $\sim 10^7$–$10^8\ M_\odot$. Studies like Ryan's benefit from homogeneous metallicity data-

bases, which is why efforts like the one illustrated by Bruno Dias are important. He is trying to obtain Fe and Mg abundances using low-resolution spectroscopy, in order to expand the homogeneous metallicity sample. In the future this will enable the same method to be used to collect abundances for large samples of stars inside Galactic satellites.

Milky Way Halo + dwarf galaxies

Andreea Font recalled the lines of evidence that support the dual nature of the Halo, when they are compared to simulations: for instance the break in luminosity profile that separates the de Vaucouleurs profile of the *in situ* component from the power-law profile of the accreted component. Giuseppina Battaglia then expanded the view on dwarf galaxies, both in general terms and as possible contributors to the accreted component of the Milky Way Halo. One of the interesting points touched on by Giuseppina is the discovery of very metal-poor stars in dwarf galaxies; the current record is set at [Fe/H] ≈ –4, but even lower metallicity stars may be discovered, thus offering another way to constrain the properties of Pop III stars.

One issue with the comparison of present-day dwarf galaxies with possible progenitors, is that many of them orbit around massive hosts, so when simulating their evolution, care must be taken to explore the effects of tidal forces. One such study, which was applied to Sextans, was illustrated by Pascale Jablonka, who could reproduce the observed chemical and structural properties of the galaxy by dedicated soft particle hydrodynamic simulations which include detailed modelling of the gas physics and star formation.

Acknowledgements

We should like to thank ESO and the Paris Observatory for financial support, and Paulina Jiron, Maria Eugenia Gomez, and Stephane Thomas for local support. Special thanks also go to the President of the Observatoire de Paris, Claude Catala, for permission to use the wonderful meridian hall of the Observatoire de Paris, designed by Gian Domenico Cassini, for the conference dinner.

References

Adibekyan, V. Z. et al. 2012, A&A, 545, 32
Asplund, M. et al. 2006, ApJ, 644, 229
Chornock, R. et al. 2013, ApJ, 774, 26
Coe, D. et al. 2013, ApJ, 762, 32
Cooke, R. et al. 2014, ApJ, 781, 31
Cullen, F. et al. 2014, MNRAS, 440, 2300
Erb, D. K. et al. 2006, ApJ, 644, 813
Finkelstein, S. L. et al. 2013, Nature, 502, 524
Haywood, M. et al. 2013, A&A, 560, A109
Izotov, Y. et al. 2013, A&A, 558, 57
Keller, S. C. et al. 2014, Nature, 506, 463
Maiolino, R. et al. 2008, A&A, 488, 463
Norris, J. E. et al. 2013, ApJ, 762, 28
Oesch, P. A. et al. 2013, ApJ, 786, 108
Sbordone, L. et al. 2010, A&A, 522, 26
Sparre, M. et al. 2014, ApJ, 785, 150
Spite, M. et al. 2013, A&A, 552A, 107
Stiavelli, M. & Trenti, M. 2010, ApJ, 716, 190
Thöne, C. C. et al. 2013, MNRAS, 428, 3590
Yuan, T.-T. et al. 2013, ApJ, 763, 9

Links

[1] Cosmology Calculator: http://www.astro.ucla.edu/~wright/CosmoCalc.html

---

Report on the Workshop

Exoplanet Observations with the E-ELT

held at ESO Headquarters, Garching, Germany, 3–6 February 2014

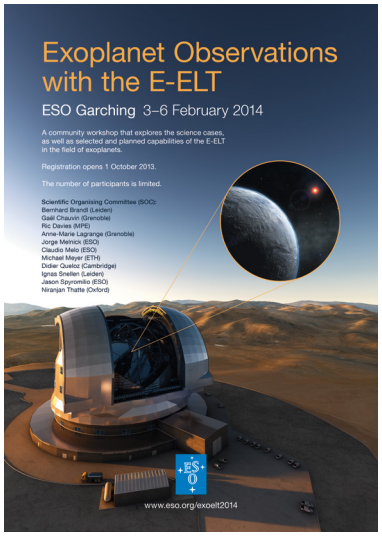

Jason Spyromilio[1]
Jochen Liske[1]

[1] ESO

A brief summary of the presentations and discussions at the workshop on exoplanet science with extremely large telescopes is sketched. A broad range of topics covering the lifecycle of planets and the instrumentation landscape were presented.

Over 140 participants from the Member States of ESO and beyond attended the first ExoELT2014 workshop. The programme included significant time for discussions (45 minutes at the end of each morning and afternoon session and a whole session on the last day). As a result the programme was short on presentations (typically five per session) and long on debate and conversation. This report does not aim to summarise in detail the entire workshop as all the presentations are available on the workshop website[1]. A wiki page, linked from the conference programme[2], will be set up where we hope to continue the discussion that started at the meeting.

In such a rapidly changing field as exoplanet science, it would be folly to try to establish any ground truths. The workshop took place just after the Gemini

Planet Imager (GPI) instrument had gone to sky with some brilliant observations of the disc and planet systems β Pic and HR 4796 (Currie et al., 2013; Galicher et al., 2014), and the European Space Agency (ESA) had not quite announced, but everyone seemed to know, the news about the Planetary Transits and Oscillations of stars (PLATO) mission. By the time this report is in press, it is likely that more exciting news of exoplanet endeavour will have been announced.

Discs and protoplanets

The topic of the evolution of discs and the initial conditions for forming protoplanets opened the meeting. Planets are expected to form from the debris of protoplanetary discs. The ongoing and forthcoming observations with the Atacama Large Millimeter/submillimeter Array (ALMA) of these objects are likely to revolutionise our understanding of the field. Leonardo Testi opened the scientific part of the meeting with an overview, posing a number of questions related to: the grain growth process that is necessary to form rocky cores; the co-evolution of the gas and dust; and the dissipation of the disc.

The combination of ALMA and thermal infrared observations is necessary to examine the different regions of protoplanetary discs. Jonathan Marshall provided a nice validation of this, showing how Herschel observations help us to understand debris discs. Maria Rosa Zapatero Osorio's presentation on free-floating giant planets showed how they help to extend the Hertzsprung–Russell (HR) diagram and provide us with a substellar mass function as the number of detected objects increases. The discussion brought to the fore the need for *L*-band imaging to detect planets in the disc gaps. While the sensitivity of the James Webb Space Telescope (JWST) will be difficult to surpass, the angular resolution of the European Extremely Large Telescope (E-ELT) in the *L*-band does provide a powerful tool to probe the discs.

Surveys for exoplanets

The morning session on the second day focussed on the direct detection surveys. Christophe Lovis reviewed the field. With multiple surveys in various stages (e.g., HARPS very advanced, KEPLER finishing, GPI and VLT SPHERE starting, ESA Gaia starting, etc.) much, if not all, of the parameter space for discovery is being actively probed. The E-ELT is to focus on spectrophotometry during eclipse or transit, high-resolution spectroscopy and high-contrast imaging/spectroscopy.

Beth Biller reviewed the statistics of the populations of exoplanets from different surveys and provided constraints on the numbers of planets per star. The question of stellar noise and whether it was better to observe in the near-infrared was addressed by Andreas Quirrenbach, and we can expect to have data from the CARMENES spectrograph at Calar Alto soon. The MICADO camera on the E-ELT as a powerful direct detector of exoplanets, when augmented by a coronograph, was presented by Anthony Boccaletti.

Part of the discussion focussed on whether the E-ELT would be used for surveys to detect planets, what the objectives of such surveys would be and how would they be complemented by existing instrumentation. With the first light of the E-ELT planned for 2024, Raffaele Gratton provided an overview of the overlaps, both temporal and in terms of capabilities, of the wide gamut of missions dedicated to this field over the coming two decades. An interesting question of whether we would be focussing on young stars, providing us with better contrast capabilities and easier access to the habitable zone, was a recurring theme of the workshop.

Exoplanet transits

Transit spectroscopy was the main theme of the next session with an overview presented by Mercedes Lopez-Morales. This is also a very exciting and rapidly evolving field, with the recent detection using the CRIRES spectrograph of the orbital motion of HD 209458b through the CO lines being an ESO highlight (Snellen et al., 2014). The combination of data from multiple telescopes and broad wavelength coverage is providing direct constraints on the composition of the atmospheres of transiting planets with a number of detections of clouds or haze (featureless spectra). Enric Palle reminded the audience just how hard it is to do millimagnitude photometry, but also how crucial a very big telescope (in this case the 10.4-metre Gran Telescopio Canarias [GTC]) is for collecting the photons needed.

Xavier Bonfils provided a detailed explanation of all the challenges involved in precision differential spectroscopy (fibre bundle filling factors, slit *vs*. fibre precision, centring accuracy, etc.). The observations and techniques for mapping of clouds in exoplanetary atmospheres were discussed by Brice-Olivier Demory, with tantalising ideas about expanding the parameter space through polarimetry. Matteo Brogi presented the exciting results from the CRIRES observations of CO, resolving the planet motion. Transit spectroscopy with the E-ELT is gearing up to become one of the most exciting areas where the power of the telescope will be of great benefit.

Direct imaging and spectroscopy

Markus Janson took us to the planets that we can see. He reviewed the resolved imaging and spectroscopy results and discussed the hot/cold start scenarios for planet formation and the disruption of disc structures due to the presence of planets. The field of high-contrast imaging and spectroscopy is extremely active, and Sasha Hinkley brought this very much to the fore in his talk on lessons learnt from a variety of systems, and in particular the Palomar project 1640 on the sky measurements of the suppression of speckle noise and the importance of spectral resolution.

In addition to the aforementioned GPI data from Gemini, Keck adaptive optics imaging results at very small angular separation were also shown. Much of this work is being done at contrast ratios of $<$ a few 10^5 and angular separations of a significant fraction of an arcsecond. The E-ELT, by virtue of its smaller diffraction limit, should be able to push the inner working angle to lower values and

will need coronographic capabilities built into the instruments. Astrometric observations to constrain the orbits of larger, sub-stellar sized companions, and by extension the formation history of these systems, were presented by Christian Ginski.

Bernhard Brandl and Niranjan Thatte presented the capabilities of the E-ELT instruments METIS and HARMONI, respectively, and Markus Kasper showed the path that we will need to follow to reach the Planetary Camera Spectrograph instrument. Together with the presentations on MICADO (see above) and the discussions on the usage of multi-object instrumentation and high resolution spectroscopy, the totality of the instrument roadmap was extensively discussed at the workshop.

The last session at the workshop with presentations focused on the search for habitable planets. David Charbonneau gave the invited review and reminded the audience of the advances the field had made in the last year alone. A sobering thought when planning for instrumentation to go to sky in a decade from now! Ignas Snellen gave a taste of where the combination of high-resolution spectroscopy techniques with high-contrast imaging would lead us. Jay Farihi reminded us that what is left behind after planet formation will eventually fall back onto the star and can be detected by spectroscopy. Thus the meeting moved from the birth of the planets to the death of the material that made them.

Acknowledgements

The Scientific Organising Committee consisted of Bernhard Brandl, Gaël Chauvin, Ric Davies, Anne-Marie Lagrange, Michael Meyer, Jorge Melnick, Claudio Melo, Didier Queloz, Ignas Snellen, Jason Spyromilio and Niranjan Thatte. The meeting would not have been so successful without the efforts of the Local Organising Committee: Jochen Liske, Samantha Milligan, Neale Gibson and Katia Montironi.

References

Currie, T. et al. 2013, ApJ, 776, 15
Galicher, R. et al. 2014, A&A, 565, 4
Snellen, I. et al. 2014, Nature, 509, 63

Links

[1] ExoELT2014 workshop website: http://www.eso.org/sci/meetings/2014/exoelt2014.html
[2] ExoELT2014 workshop programme: http://www.eso.org/sci/meetings/2014/exoelt2014/program.html

---

Report on the ESO/RadioNet Workshop

3D2014: Gas and Stars in Galaxies: A Multi-wavelength 3D Perspective

held at ESO Headquarters, Garching, Germany, 10–14 March 2014

Matt Lehnert[1]
Carlos De Breuck[2]
Harald Kuntschner[2]
Martin A. Zwaan[2]

[1] Institut d'Astrophysique de Paris, France
[2] ESO

This is the second ESO workshop devoted to the topic of 3D spectroscopy of galaxies; the last one took place in 2008. An overview of the workshop themes is presented and a discussion of the progress and open questions that have been resolved by new facilities and theoretical modelling since the last workshop.

With our current knowledge of both the standard model of particle physics and cosmology, combined with the successes of Lambda Cold Dark Matter (ΛCDM) cosmology, we now have a scientifically robust model of galaxy formation and evolution that can be tested with observations. The goal of this workshop was to gauge our progress in understanding the baryonic physics involved in galaxy formation and evolution, as it is the foundation for our ability to test the growth of galaxies and structures in the ΛCDM model. The workshop builds on the previous ESO 3D workshop, held in 2008 with the same title (see Lehnert et al. [2008] for a report). In our summary we have tried to be comprehensive, but not all contributions could be mentioned. There will be no published proceedings, but most of the presentations can be consulted via the workshop website[1].

Our ability to quantitatively test the ΛCDM model relies on our ability to exploit technology — using fast computers for large high-dynamic-range simulations, with advanced data visualisation techniques (contributions by Fluke, Ott, van der Hulst and Koribalski), robust and efficient algorithms, sensitive detectors and efficient instruments, and building large aperture space and ground-based telescopes (summarised in talks by Bershady, Braun and Emsellem). The meeting six years ago took place during, what was in many ways, the infancy of 3D technology, especially in the optical and near-infrared and in visualisation techniques. Also in the radio, the world is now a richer place with the advent of focal plane arrays for single-dish telescopes and phased array feeds on interferometers coming online soon. The capabilities of the Atacama Large Millimeter/submillimeter Array (ALMA) with its wide frequency coverage, both overall and in single observations, the increasing bandwidth of instruments like the Plateau de Bure interferometer and the broad wavelength coverage of current optical/near-infrared instruments, such as the *K*-band Multi-Object Spectrograph (KMOS) and the Multi-Unit Spectroscopic Explorer (MUSE) recently commissioned

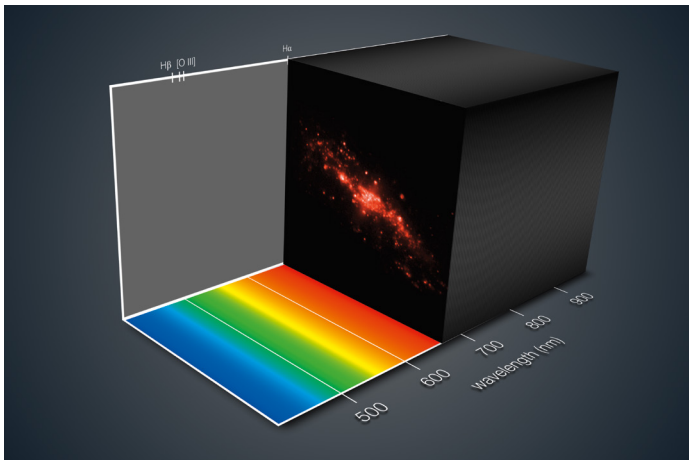

Figure 1. Visualisation of a MUSE datacube of the polar ring galaxy NGC 4650A. The galaxy image is a slice of the cube on the Hα emission line. More details available in release eso1407.

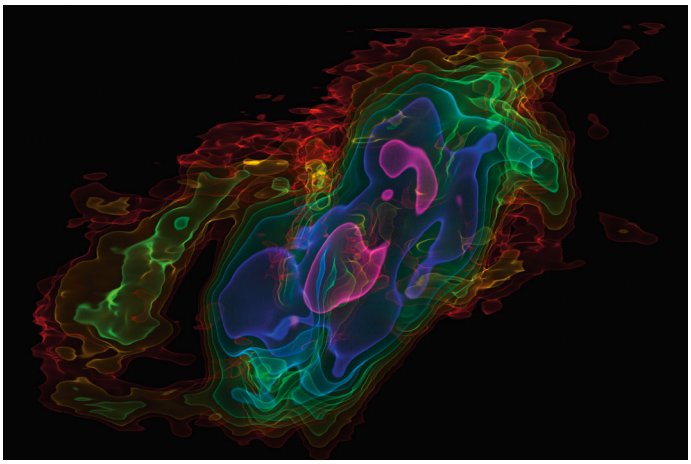

Figure 2. 3D visualisation of ALMA observation of cold CO gas in the nearby starburst galaxy NGC 253. The vertical axis shows velocity, the horizontal axis the position across the central region of NGC 253 and colours the intensity of the CO emission (pink strongest and red weakest). See release eso1334 for more details.

on the Very Large Telescope (VLT), means that the term 3D spectroscopy will soon become an anachronism — no longer a distinction, but the norm.

Moreover, these new instruments, as well as giving new life to older facilities, are leading to a convergence of multi-wavelength studies, especially blind spectroscopic surveys and studies of nearby galaxies and galaxy clusters. The instantaneous field of view of ALMA and MUSE, or the region sampled by KMOS in its mapping mode, are all approximately the same: multi-wavelength 3D observations are becoming well-matched.

In this meeting, the focus was on the *science exploitation* of telescopes and instruments, studying problems at the dawn of the era of ALMA, and on the science from H I absorption and emission line surveys and the potential of the Square Kilometre Array (SKA) and its precursors (talk by Braun). In particular, we hosted mini-workshops on the characteristics of and data analysis for ALMA, KMOS and MUSE, led by experts for each of these instruments (respectively Laing, Sharples and Bacon). While the future is now for ALMA, we had glimpses of the potential of both KMOS and MUSE to lead to real breakthroughs in our understanding of ΛCDM and galaxy formation and evolution. This conference gave the community a chance to learn about these phenomenal new instruments and facilities. Figures 1 and 2 show visualisations of MUSE and ALMA 3D data.

But, of course, we are not limited to those facilities only, as there is a huge variety of available and future facilities on the ground and in space in the ultraviolet, optical, and near-infrared using old and new technology (Bershady). These facilities allow us to study old problems in new ways and, because of their significantly increased efficiency or opening of new domains in wavelength, to dream of solving long-standing astrophysical questions that will undoubtedly lead us to propose new, but better framed and more significant, questions about the Universe in which we live.

The mysteries of local galaxies

While the idea that early-type galaxies always means a pressure-supported system with no recent star formation, and no significant gas content, was outmoded even before the last meeting, the full analysis of the ATLAS^{3D}, Calar Alto Legacy Integral Field Area survey (CALIFA) and other datasets, continues to offer a surprisingly rich variety of observed phenomenology. Our modern view of early-type galaxies, that they are composed of two classes — slow rotators and fast rotators — was developed in talks by Cappellari and Lyubenova. Early-type galaxies can also contain gas, both H_2 and H I, with about a quarter displaying detectable CO emission. The morphology of the CO emission shows a disc in about half the cases with the rest spread approximately equally between rings and bars and mildly or strongly distorted morphologies (Bureau). Almost half of the early-type galaxies have detectable H I with masses of 5–5000 × 10^6 $M_\odot$ (Serra). The H I morphologies are often extended discs and rings, which can reach beyond the high surface brightness inner regions, and outer rings often appear to be related to ongoing star formation. Two suggestions for the source of the gas in early-type galaxies are mass return from the stellar population and of external origin.

Beyond the structural characteristics of early-type galaxies, there are a number of theoretical evolution and relational puzzles. Kormendy & Bender (2012) advocated a parallel sequence between early-type galaxies and spiral galaxies with the origin of this sequence as evolutionary, or, put simply, some early-type galaxies are faded spirals. The evidence to support this origin appears to be complicated (Lyubenova).

By comparing dynamical and photometric masses, there appears to be a systematic change in the initial mass function (IMF) as a function of total stellar mass, whereby the lower-mass galaxies require a bottom-heavy IMF (Cappellari). Obviously, this has profound implications for our understanding of the conditions under which early-type galaxies formed. Additionally, these IMF variations must have been in

place early, as the abundance pattern of early-type galaxies at roughly half the age of the Universe is consistent with passive evolution (Conroy). It will be very interesting indeed to determine the evolutionary state of the progenitors of early-type galaxies, especially their abundance ratios, at even greater lookback times.

Our understanding of the theoretical side of early-type galaxy formation and evolution is certainly richer, but perhaps not clearer than it was six years ago. It appears that there may be no unique evolutionary path to the end point of an early-type galaxy, but rather many (Naab). Historically, much attention has been paid to merger mass fractions leading to the range of properties in early-type galaxies. However, with larger samples of well-observed and characterised galaxies, it is clear that other factors play a role, perhaps even a major role, such as dissipation and orbital characteristics. One difficulty in modelling is to explain the existence of early-type galaxies with thin discs. Another may well be the passive nature of early-type galaxies out to half the age of the Universe. It is interesting that as samples of well-studied local and distant early-type galaxies grow in size, the theoretical challenges become greater.

Nearby disc galaxies appear to follow the textbook relationships between scale length and scale height for exponential discs (Verheijen, Martinsson). From studies of the kinematics and stellar populations of disc galaxies, it is becoming clear that there is a tight relation between the central velocity dispersion of the disc and the maximum in the rotation speed, implying that discs are sub-maximal. The dark matter appears to be distributed in a manner consistent with N-body simulations for concentrations of about 10–20 (Martinsson).

In addition to time-consuming techniques that take direct advantage of the dynamics of discs, it is also possible to use photometry coupled with molecular and H I observations (for gas content and velocity fields) to estimate the mass distributions of disc galaxies. A consistent problem with all techniques that rely on 1D rotation curves is how to deal with distortions in the velocity field induced by peculiar motions. Fitting all the 2D data simultaneously is possible, but a technique is required that allows for the transformation of observations into a density field. With such a technique, distortions are not a problem, but part of the solution in understanding the full matter distribution. Such inversion techniques look promising and may be a way to tackle large samples of galaxies over a wide range of masses with data already available (Chemin).

"Inside-out" evolution of galaxies, whereby the earliest stars to form are in the central regions with the outer disc growing at later times, is widely accepted. However, it is not clear whether this is a unique model and that inside-out could not be mimicked in some other way, such as by the superposition of two discs with differing ages and scale lengths (Haywood et al., 2013). The CALIFA survey may provide some insight into this problem as it appears that the metallicity of the gas follows that of the underlying stellar population and the gradients are negative, but relatively small. In addition, the mass-weighted age gradients are approximately flat, while the luminosity-weighted age gradients are relatively shallow but significant (Sanchez-Blazquez). It is not clear what the implications of inside-out galaxy formation are, but a careful study of the metallicity gradients and stellar populations of nearby galaxies may help to constrain how galaxies grow.

Star formation is the bridge that links the gas flows from the intergalactic medium to the build-up of the stellar populations in galaxies. It is no hyperbole to say that without understanding the details of star formation we cannot understand galaxy evolution (but see Hopkins). Critical to this understanding is to probe the detailed properties of molecular clouds and star formation in different environments. With the advent of ALMA and the increased capabilities of other facilities, it is now possible to study the molecular gas on small scales and high sensitivity in nearby disc galaxies, starbursts and mergers. The external surface pressure on molecular clouds appears to be important, as the internal and external thermal pressures are in equilibrium for nearby spiral galaxies — galaxies with roughly constant global gas depletion timescales (Meidt). The importance of streaming motions implies that, at least for quiescent nearby spiral galaxies, large-scale shear and turbulence, as well as stellar feedback, play a less important role in regulating the local star formation surface density.

The processes occurring in the centres of galaxies may differ, since other types of phenomena may play a role in regulating the properties of molecular clouds and star formation. Detailed studies of nearby galaxy nuclei find that the CO-to-H_2 conversion factor may be different to other environments (generally lower); this change suggests that barred and unbarred galaxies have similar nuclear gas contents and that star formation efficiency is higher in galaxies with bars or oval shaped bulges (Sandstrom). It appears likely that these trends are related to the higher excitation of the molecular gas in galaxy centres, both in its temperature and turbulence.

Galactic centres/supermassive black holes

Gillessen opened this session with an update on the observations of the gas cloud G2 passing by the Milky Way Galactic Centre (GC). Already, these observations rule out several models for the evolution of the gas as it orbits the GC. The rich variety of phenomenology exhibited by the GC can help us understand black holes in nearby galaxies: more specifically, the similarity of the GC nuclear stellar cluster to the clusters observed in other galaxies. Nuclear star clusters are detected in about half to three-quarters of all galaxies and have multiple generations of stars, masses typically $10^{6-7}\,M_{\odot}$, the highest stellar densities of any objects in the Universe and some harbour supermassive black holes (SMBHs; Neumayer). The difficulty in knowing how similar these distant nuclear star clusters are to the one in the Galaxy is the large area that must be mapped in near-infrared imaging spectroscopy to understand our nuclear star cluster in its totality. Feldmaier presented innovative long-slit spectroscopy with ISAAC and early data from KMOS to map out a large enough area to encompass the star cluster. This rich 3D dataset supports the idea that much of the nuclear cluster was accreted into the GC.

The accurate determination of black hole masses is important in understanding the relationship between black holes and galaxy centres. With the advent of regular observations with ALMA, and the high spatial resolution offered by other facilities such as the Combined Array for Research in Millimeter-wave Astronomy (CARMA), it is possible to make extremely high resolution molecular maps of nearby, and increasingly more distant, galactic nuclei. Since CO is dynamically cold, it makes an excellent dynamical tracer even in dispersion-dominated systems such as early-type galaxies and galactic bulges. With ALMA, this technique can be potentially extended to thousands of galaxies out to 100 Mpc (Davis).

Active galactic nuclei/starburst galaxies

While studies of relatively quiet SMBHs enable us to understand the relation between black holes and stellar populations, they only hint at how black holes themselves might grow and evolve. Direct observations of accreting black holes are necessary to understand how they are fuelled and grow and what the impact on their surroundings is. Central to understanding these phenomena is high-resolution 3D spectroscopy of the gas on circum-nuclear scales and, since the inflow and outflow of gas is a multi-phase phenomenon, a variety of wavelength regimes and diagnostic lines are required.

New facilities and observations of larger samples of active galaxies are now painting a comprehensive picture of how active galactic nuclei (AGN) are fuelled and how they regulate the growth of the SMBH. Tracing the gas down to 1–10 pc scales suggests that: inflow rates are sufficient to fuel the AGN and these inflows may be driven by the bar (Fathi); compared to similar inactive galaxies, Seyfert galaxies have a significant gas reservoir which requires inflows/accretion and near nuclear gas that has also led to additional star formation (Hicks); large statistical studies in the near-infrared and millimetre suggest that Seyfert galaxies exhibit both inflows (molecular) and outflows (molecular and ionised), which are in rough balance, with the ionised gas requiring ~ 0.5 % of the bolometric luminosity to be energised (Mueller-Sanchez).

New observations show cavities in the molecular gas through which the AGN is emptying the nuclear region of gas; these cavities are then replenished by infalling material driven by instabilities (Mueller-Sanchez). Outflows are observed in H I as well as in the molecular and ionised gas. While we have reasonably good ideas of the outflow rates in H I in some nearby radio galaxies (a few to 50 $M_{\odot}$ yr^{-1}), the details of how they are driven remain poorly understood. High-resolution radio observations of H I in absorption against bright radio emission suggest that specific interactions, on scales of about 0.5 kpc, with the head of the jet account for the H I absorption and kinematics (Mahoney).

On larger scales, the AGN can illuminate the large (10–100 kpc) scale haloes surrounding powerful AGN, which show a striking similarity with Lyα blobs (Overzier). Detailed studies of nearby starburst galaxies and AGN suggest that the gas is rapidly depleted by outflows (timescale ~ 10 Myr); there is a good correlation between star formation rate and outflow rate, with any contribution from AGN boosting the flow rates. These outflows only require ~ 1–10% of the bolometric luminosity and have a typical momentum output of about 10–20 times that of the bolometric momentum generated by the starburst and AGN (Cicone). Outflow velocities increase with both increasing star formation rate (SFR) and specific star formation rate (sSFR) with the highest outflow velocities being associated with galaxies with the largest deviations from the ridge line in the SFR-stellar mass plane (Maiolino). [O III] optical emission does not trace mass particularly well, so other tracers of outflows are obviously important to investigate.

There are a number of possible mechanisms through which star formation and the growth of SMBHs might be regulated. Massive stars inject energy and momentum into the interstellar medium and thus regulate the conditions in the ISM and hence star formation and accretion onto the SMBH. Recent modelling suggests that galaxy and black hole growth can be understood as a symbiosis of the many processes that compete with and enhance each other in regulating gas heating and cooling, and hence star formation and the accretion rate onto black holes (Hopkins). Black hole accretion in such a complex environment then becomes one of stochastically digesting gas at rapidly fluctuating rates (Bournaud). The interaction between various physical mechanisms through which stars and black holes influence their environments may imply that the exact details of how stars form is not determinant in galaxy evolution (Hopkins). If true, this is a radical conclusion to draw. Clearly, we have much more work to do to understand the complex gas physics exhibited by galaxies and how much material is blown out by outflows driven by young massive stars (e.g., Lilly, Bouché).

Distant galaxies and AGN

New facilities have allowed us to observe galaxies as they grow and evolve in much more detail (see Figure 3 for an example derived from KMOS 3D data). High-redshift galaxies are dominated by rotating discs that are highly turbulent (Förster-Schreiber) and the most massive ones appear particularly well-settled (Buitrago). These findings have a number of consequences, including explaining why discs are so clumpy and how star formation might be self-regulating (Bournaud, Förster-Schreiber). In addition, it appears that outflows in the warm ionised gas are quite common in these discs, with the outflow rates typically being one to a few times the star formation rate.

Well-selected samples observed with high-multiplex 3D spectrographs are important in understanding the properties of distant galaxies in a robust way. Narrowband surveys targeting Hα constitute one approach, as they are relatively insensitive to mass, but efficiently select star-forming galaxies over a wide range of redshifts. Following up such narrowband surveys with integral field spectroscopy suggests that the SFR-mass and Tully–Fisher relation does not change with environment: metallicity gradients are mostly negative or flat (also when including absorption lines in the haloes; Péroux). The gradients increase with sSFR, suggesting that funnelling of gas into galaxy centres plays an important role in enhancing relative galaxy growth rates (Sobral). The future is very bright for these types of studies with KMOS, allowing us to observe larger

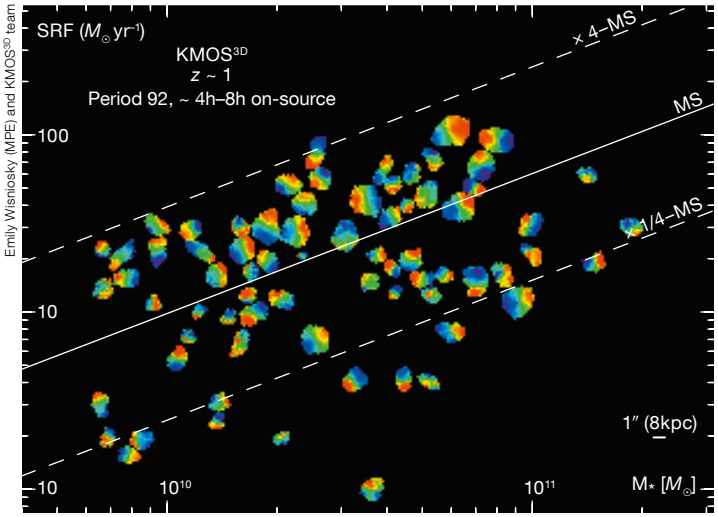

Figure 3. Hα velocity fields for the first 72 spatially-resolved sources at z ~ 1 observed as part of the KMOS^{3D} survey of > 600 mass-selected galaxies at $0.7 < z < 2.7$ (from Wisnioski et al., 2014, in prep.). Blue to red colours correspond to velocities that are blueshifted to redshifted relative to the systemic velocity of each galaxy. The galaxies are located according to their stellar mass (M_*) and star formation rate (SFR). The solid line indicates the locus, or main sequence (MS), of star-forming galaxies at $z = 1$, and the dashed lines show offsets by factors of 4 in SFR.

samples with a wider range of redshift and intrinsic properties.

Integral field observations of moderate-redshift galaxies suggest that many of the morphologies and kinematics are consistent with being produced by remnants of major mergers. For example, the tightness of the SFR–stellar-mass relation and the distribution of bulge-to-disc ratios are not in tension with such a picture. Major mergers could be a viable, or perhaps even the best, explanation for many of the properties of disc galaxies (Puech). By its very nature direct observations of gas accretion are challenging. However evidence is accumulating that perhaps some quasi-stellar object (QSO) absorption lines have properties consistent with those expected for cosmological accretion. There are possible signs of inflow in some sources, or at least there is material in the halo that has gravitational motion, and is likely a source of accreting gas (Bouché). But outflows are also probably very common and a source of the absorption line material (Péroux).

The combination of deep HST imaging data, especially in the near-infrared, and 3D spectroscopy in the near-infrared and millimetre enables a detailed look at the spatially resolved properties of distant galaxies, especially their clumpy structure and the relative growth of galaxy centres. Clumps have bluer colours, higher Hα equivalent widths, and higher specific star formation rates than the underlying discs, but do not seem to be a significant contributor to the global mass budget. It is particularly surprising that the clumps do not appear to be regions of mass enhancement as compared to the underlying disc (Wuyts). High resolution (~ 0.2 arcsecond) mapping with the Jansky Very Large Array (JVLA) of a distant, z ~ 4, submillimetre galaxy (SMG) shows a large massive rotating disc galaxy with a flat rotation curve. The molecular gas in this galaxy is clumpy and the properties suggest that the large 1 kpc scale clumps are self-gravitating and constitute about 50 % of the total molecular mass (Hodge). This differs markedly from the picture of the clumps detected in the restframe optical. At even higher redshift, $z = 4.76$, another SMG also exhibits a large extended disc (see De Breuck et al., p. 38).

The capabilities of ALMA and of other interferometers allow us to conduct surveys and types of observations that could only be imagined previously. Blind redshift surveys of individual sources, and even in wide (somewhat) blank fields, in both lines and continuum are now possible (Aravena, Ouchi, da Cunha, Decarli). These types of surveys break the stranglehold on both having to identify the source and determine its redshift from optical or near-infrared imaging and spectroscopy. We can now find sources that are not identified in any other way and their properties are surprising: they are at very high redshift, have particularly narrow emission lines and compact structures that suggest they are extremely gas-rich and dense (Ouchi). We are undoubtedly on the verge of a revolution in our understanding of distant galaxies by finally being able to select targets based on their dust emission and molecular gas content, instead of on the surface brightness of their stellar populations, and therefore robustly determining the evolution of the gas content of galaxies (Decarli).

While outflows driven by AGN are firmly established locally, at high redshift our observational census of the role in early galaxy evolution is still quite limited. ALMA allows for routine observations of distant z ~ 7 QSOs in [C II]. QSOs turn out to have a [C II] to infrared luminosity budget deficit similar to local powerful starbursts, but they also show diversity with hints for outflows in their kinematics and morphology (Venemans). In particular, J1148+5251 is driving an incredible outflow in the very early Universe, a mass-loss rate of thousands of $M_\odot$ yr^{-1} (Miaolino), and this outflow may be very extended (30 kpc; Cicone). Hopefully and eventually, it may be possible to observe both the infall onto the circum-nuclear region of distant AGN as well as their outflows. This would finally allow us to complete the feedback cycle in distant galaxies. As it stands now, we observe mostly one side of the gas ledger, the outflow.

Acknowledgements

We would like to thank the Local Organising Committee for the flawless organisation of this workshop: Timothy Davis, Claudia Lagos, Suzanne Ramsay, Joel Vernet, Dominika Wylezalek, and in particular Stella Chasiotis-Klingner and Christina Stoffer. We also acknowledge RadioNet3 for generous financial support.

References

Haywood, M. et al. 2013, A&A, 560, 109
Kormendy, J. & Bender, R. 2012, ApJS, 198, 2
Lehnert, M. et al. 2008, The Messenger, 133, 52

Links

[1] 3D2014 webpage: http://www.eso.org/sci/meetings/2014/3D2014/program.html

Report on the Workshop

Seven Years in Chile: The Accomplishments and Goals of Czech Astronomers at ESO

held at Prague, Czech Republic, 14–16 April 2014

Petr Kabáth[1]
Adéla Kawka[2]
Ernst Paunzen[3]
Stéphane Vennes[2]

[1] ESO*
[2] Astronomical Institute, Academy of Sciences of the Czech Republic
[3] Masaryk University, Brno, Czech Republic

The Czech Republic has been a member of ESO since 2007 and the workshop was held to mark this occasion. The primary aims of the workshop were to highlight the science done by Czech-affiliated astronomers who make use of ESO facilities and to encourage greater use of these facilities, particularly by the younger generation of astronomers in the Czech Republic.

Figure 1. The workshop participants at Villa Lanna, Prague.

Czech astronomy and ESO

Astronomical research in the Czech Republic covers many areas, including meteors and asteroids, the Sun, stars across the Hertzsprung–Russell diagram, Galactic structure as well as relativistic astrophysics. The majority of astronomers are affiliated with the Astronomical Institute of the Academy of Sciences and are based in Ondřejov and in Prague. Astronomical research is also conducted at Charles University in Prague, Masaryk University in Brno and the Silesian University in Opava. Finally, numerous public observatories and planetariums contribute to education outreach in the Czech Republic.

The Czech Republic became the 13th ESO Member State on 1 January 2007, an event that opened up many new opportunities for Czech astronomers. Currently, the Czech Republic contributes about 1% to the ESO budget. The return from this investment is potentially very high; ESO membership offers privileged access to many of the world's most advanced telescopes, the chance to contribute to instrument development and to take advantage of training and employment opportunities.

How can the Czech Republic effectively benefit from all these opportunities? How did ESO membership change Czech astronomy? Also, how can we help the Czech astronomical community to do better? We sought answers to these questions during this workshop.

The workshop

The workshop was structured in sessions based on observing techniques and instrumentation offered by ESO and covered the optical, infrared and submillimetre spectral ranges. The last day focussed on the next generation of astronomers, with an overview of the current state of Czech astronomy and a look to the future.

The first session was opened by Jan Palouš with an historical overview of ESO and the circumstances surrounding the accession of the Czech Republic. He was immediately followed by Johannes Anderson, former director of the Nordic Optical Telescope, who related the Danish experience with ESO and emphasised the need for a detailed plan to achieve higher objectives. A user's perspective was offered by Adéla Kawka while the head of the ESO Observing Programme Office, Ferdinando Patat, presented observing programme statistics and some advice on successful proposal writing. Miroslav Bárta reported on the Atacama Large Millimeter/submillimeter Array (ALMA) Regional Centre node in the Czech Republic and Soňa Ehlerová informed the meeting about ESO's public outreach effort.

The workshop proceeded with an overview of the instruments offered by ESO and the research conducted with these facilities. The Paranal Observatory overview was given by Petr Kabáth and the Atacama Pathfinder Experiment (APEX) by Palle Møller, while Stanislav Štefl talked about ALMA and the Very Large Telescope Interferometer (VLTI). In addition, Pavel Gábor and Petr Pravec introduced the Vatican Observatory and the 1.54-metre Danish telescope (La Silla), respectively, while offering collaboration opportunities.

The following presentations highlighted important results obtained with ESO facil-

* From 2015 at Astronomical Institute, Academy of Sciences of the Czech Republic

ities. Using the Fibre-fed Extended Range Optical Spectrograph (FEROS), Tereza Krejčová demonstrated that cool stars with closely orbiting planets exhibit stronger Ca II K emission than stars with more distant planets (Krejčová & Budaj, 2012) and Stéphane Vennes highlighted the effectiveness of the X-shooter spectrograph for abundance studies in white dwarf stars (Kawka & Vennes, 2012). Ernst Paunzen's contribution covered the Magellanic Survey with the Visible and Infrared Survey Telescope for Astronomy (VISTA) and how it is used to study peculiar and variable stars in the Magellanic Clouds.

Chemically peculiar stars were mentioned by several speakers: Martin Netopil shared his work on the origin of chemically peculiar stars; using FEROS spectra, Milan Prvák showed how to map the surface abundance pattern of the chemically peculiar star HD 114365. Next, Birgitta Nordström pointed out the complementary use of ESO facilities and other instruments in providing the ground work for a detailed analysis of ~ 15 000 Solar-type stars (Nordström et al., 2004). Michaela Kraus spoke about *K*-band spectroscopy and how it can be used to discriminate evolutionary stages of evolved massive stars (Oksala et al., 2013). Finally, Robert Klement explained how various types of observations may be used to constrain the disc structure of the B8Ve star Beta CMi.

In her contribution Ivana Orlitová handled integral field unit (IFU) spectroscopy with the VIsible Multi-Object Spectrograph (VIMOS), which was used to understand the origin of double-peaked [O III] lines in quasars. Using APEX, Pavel Jáchym showed that a large amount of cold molecular gas is present in the ram pressure stripped tail of ESO 137-001 (Jáchym et al., 2014). Another APEX study by Richard Wünsch revealed how two clouds in the Carina Flare supershell were observed in order to determine how they were formed (Wünsch et al., 2012). A comprehensive compilation of the results obtained with ESO by Czech affiliated astronomers is available at the Czech National Astronomical Committee (NAC) webpage[1], and the presentations are available at the workshop website[2].

Astronomy in the Czech Republic and the role of ESO

On the third and final day, the head of the ESO Office of Science in Garching, Eric Emsellem, discussed the opportunities available at ESO, including studentships, fellowships, as well as staff positions. Following this presentation, Lucie Jílková, a former ESO graduate student currently at Leiden, spoke about her experience in Chile. The ESO career session was followed by a panel discussion that encouraged students to get involved with ESO, either as guest observers supporting doctoral researchers, or as staff members. The panel was moderated by Jan Palouš and involved current and former staff at ESO. Two astronomers from the Czech Republic are currently employed at ESO and one Czech graduate student is supported by ESO's Director General Discretionary Fund; returning staff and students bring valuable experience to the Czech Republic and every effort must be made to foster future employment and studies at ESO.

The workshop concluded with a panel discussion led by Jiří Grygar concerning Czech astronomy and its future. The panel included representatives from Charles University, the Astronomical Institute of Academy of Sciences, Masaryk University, Brno, and the Czech NAC. Instructed by the experience of Danish astronomers in developing a national roadmap for research in astronomy, the Czech NAC was encouraged to prepare such a roadmap well ahead of any possible setbacks. This open discussion, involving astronomers in the Czech Republic and the commitment made to produce a roadmap, augurs well for the future.

The workshop presented ESO to the Czech astronomical community and, to a large extent, the Czech community to ESO. The relatively high number of participating students showed that ESO is important to the new generation of Czech astronomers. We hope that this workshop will contribute in encouraging further involvement with ESO. Finally, this workshop was the first in a series of planned events. Future events include a school on observing projects and university lectures about state-of-the-art instrumentation.

Acknowledgements

The workshop organisers would like to acknowledge the patronage of the Ministry of Education, Youth and Sport of the Czech Republic. Support from the Astronomical Institute (Academy of Sciences of the Czech Republic) and Masaryk University is acknowledged. Finally, ESO's generous support in material and travel grants for ESO personnel helped make this workshop possible.

We would also like to thank the personnel at Villa Lanna (Prague) for their assistance in ensuring a smooth and friendly event.

Tragically Stanislav Štefl, who was an ESO astronomer in Chile from 2004 and did much to foster relations between ESO and Czech astronomers, especially among the young generation, died in June of this year. An obituary follows this report.

References

Jáchym, P. et al. 2014, ApJ, submitted, arXiv:1403.2328
Kawka, A. & Vennes, S. 2012, A&A, 538, A13
Krejčová, T. & Budaj, J. 2012, A&A, 540, A82
Nordström, B. et al. 2004, A&A, 418, 989
Oksala, M. E. et al. 2013, A&A, 558, A17
Wünsch, R. et al. 2012, A&A, 539, A116

Links

[1] Czech NAC webpage: http://galaxy.asu.cas.cz
[2] Workshop webpage: http://astro.physics.muni.cz/cz-eso-2014

In Memoriam Stanislav Štefl

Dietrich Baade[1]

[1] ESO

On 11 June 2014, ALMA and ESO astronomer Stanislav (Stan) Štefl died in a car accident in Santiago. He was 58 years old.

Stan was born in Počátky (Czechoslovakia) and received his PhD from the Charles University in Prague in 1987. He then held a staff position at the Ondřejov Observatory. From 1991 to 1993, Stan worked at ESO Headquarters as a research associate and, from 2004 until 2012, he was a Very Large Telescope Interferometer (VLTI) support astronomer at Paranal Observatory. For the past year and a half, Stan had been on secondment to the Atacama Large Millimeter/submillimeter Array (ALMA), working in Santiago and at Chajnantor.

Stan's premier fields of research were the formation and evolution of rapidly rotating B-type stars that eject matter into a circumstellar disc. He was the first to notice and demonstrate that during the outbursts of Be stars their pulsational power spectrum changes. Stan initiated the integration of dynamic models of Be star discs with detailed radiative transfer calculations. He was chair of the International Astronomical Union Working Group on Active B Stars from 1999 to 2003. Throughout his career Stan kept expanding his observational expertise in an impressive way: from the ultraviolet work of his thesis to radio wavelengths, from photometry to spectro-interferometry, from photographic plates via electronic imagers to radio receivers.

Olivier Thizy

His modesty and fine Czech humour were Stan's personal trademarks. In the same unpretentious way, he served the ESO community as VLTI and ALMA support astronomer and on the organising committees of two ESO workshops and on many internal committees.

Stan was a passionate and skilled mountaineer: he climbed Aconcagua (but had to halt 200 metres below the summit on account of bad weather), Chimborazo, Kilimanjaro, and many more mountains in Chile and around the world. A few months ago, he also undertook a sailing expedition with friends to Antarctica.

Stan will be remembered as a hard-working and very cooperative colleague, as a passionate scientist, and as a man of rare human qualities. He, his wife Magdalena and their daughter Marketa were about to move to Ondřejov, where Stan was to lead the ALMA Regional Centre node, when his life ended so abruptly. Our thoughts are with them.

Fellows at ESO

Neale Gibson

It was quite late into my undergraduate degree that I considered pursuing astronomy as a career. As a child I remember staring at pictures in astronomy books, in particular being fascinated by the gas giants in the Solar System. Whilst astronomy may have inspired my interest in science, it was many years before I realised it was something you could actually do for a living!

I grew up in Carryduff, a small town near Belfast in the north of Ireland. Throughout

Neale Gibson

school, maths, science and art were my favourite subjects, but by the time I had to apply for university courses I hadn't settled on anything. All I knew was that I wanted to do something science related, and I ended up choosing a physics degree at the Queen's University of Belfast which allowed me to delay any serious career decisions to later in life. For the next few years I really enjoyed studying physics, but still had no idea what to do afterwards, other than something science related. In my final year of undergrad, I had the opportunity to specialise in astrophysics and undertook a project studying supernovae. It was only then that I realised that a career in astrophysics research was a realistic possibility, and doing a PhD in astronomy at Queen's was the perfect way to explore this and again avoid making any serious career decisions!

I began my PhD in the (then) small exoplanet group at Queen's working with Don Pollacco, trying to search for and characterise exoplanets using high precision transit light curves. This was an exciting field to be in – at this time (2006) there were only a handful of known transiting planets, none of them like anything in our Solar System. During my PhD I got my first taste of observing, spending two months living on the Canary Islands to be near the Roque de los Muchachos Observatory. We also built an instrument specifically for my project called RISE (Rapid Imager to Search for Exoplanets) on the Liverpool Telescope, giving me lots of valuable experience with observations and instrumentation. It was during these years that I decided that I wanted to continue in astronomy; making a living by learning new things and thinking about the Universe was just too good to be true.

My next step was taking a postdoc with Suzanne Aigrain and Frederic Pont, starting in Exeter and soon moving to Oxford. It was there that I started working on observations of exoplanet atmospheres, and three years later I was delighted to be accepted onto the ESO Fellowship programme in Garching. Aside from providing an exciting research environment, ESO Fellows get the opportunity to participate in observatory operations. I have joined the User Support Department at ESO where I support FORS2 (one of the older VLT instruments), and will also support SPHERE (the next generation exoplanet imager) in the near future.

Now about half way through my ESO Fellowship I continue to worry about how we can observe exoplanet atmospheres. Whilst exoplanets are relatively nearby compared to most objects of astrophysical research (although I have been called a cosmologist by Solar System folks), they are extremely difficult to study due to their faintness and the inconvenient fact that they're located right next to their very bright and noisy host stars. Development of observational and data analysis techniques has so far enabled us to peer at the atmospheres of hot Jupiters (gas giants orbiting their host stars much closer than Mercury orbits our Sun) although this remains challenging. With the next generation of ground- and space-based instrumentation like the James Webb Space Telescope and ESO's E-ELT we might just be able to peer into the atmospheres of terrestrial planets and even search for life beyond the Solar System. I have no idea where I will be after my ESO Fellowship, but I hope to play a part in this search.

Claudia Lagos

I started to think about astronomy as a real possibility for my career option when I was 16 years old. Before that it always seemed a bit of a dream, a fantasy. It was only when I was 16 that making life-long choices became reality. I always liked to think about space, about its scales, its geometry, its evolution. I think I was always a bit of a theorist though... My first approaches to astronomy were through cosmology books, where closed and open spaces were described, where they talked about the "seven samurai" and the Great Attractor. I always liked abstract thinking in that sense.

When the time came to make an actual decision about my university career I was seriously undecided between astronomy and philosophy; those were two areas that I felt really passionate about. Before that, I thought of doing engineering, since it's a more standard choice of career in Chile. What put me off that road was the comment of my literature teacher back then: "anyone can be an engineer but not everyone can be an astronomer... For astronomy you really need an abstract mind". So I decided to take up that challenge (although his statement was incorrect... engineering is as difficult!).

I may not be like many of the astronomers who write about themselves here, as I have to confess that I never liked staying up during all the night observing, nor suffering the cold (Oh yes! It really was cold in Santa Martina, the Observatory of Universidad Catolica in Chile). I enjoyed all my courses on astrophysics and other theoretical physics courses much more: general astrophysics, stellar and extragalactic astrophysics, mathematical methods in physics, etc... It was during my Bachelor degree that I started working on galaxy formation and simulations.

Both my Masters degree and my PhD were focussed on galaxy formation physics, albeit on very different aspects.

Claudia Lagos

The former was on active galactic nuclei, accretion onto black holes and spin development; while my PhD was focused on star formation, the interstellar medium and feedback from stars. All of these are challenging and very interesting topics. I really enjoy working in such a wide field as galaxy formation, where a large range of expertise is required.

I think I did a good job at convincing the Fellow selection committee in 2011 that a theorist at ESO was not oil on water, but instead a rather natural mixture. I joined ESO in October 2012 and I have greatly enjoyed my time here, where I'm intensively learning about observational astronomy. I perform my duties on ALMA, where I have discovered a passion for observing. I act as astronomer on duty, and I have also been involved in the ALMA Helpdesk and the creation of scheduling blocks. The ALMA Regional Centre at ESO have been great and patient at explaining to an inexperienced modeller how to do certain tasks and how ALMA works. I have another year left at ESO and I hope I can squeeze something out of every second of it and continue enjoying its great environment.

Personnel Movements

Arrivals (1 April–30 June 2014)

Europe	
Álvarez Méndez, Domingo (ES)	Detector Engineer
Arumugam, Vinodiran (MY)	Fellow
Gotschewski, Katrin (DE)	Administrative Assistant
Huber, Stefan (DE)	Integration Opto-mechanical Technician
Ivison, Robert Julian (GB)	Director for Science
Karabal, Muhammet Emin (TR)	Student
Steins, Steffi (DE)	HR Advisor

Chile	
Capocci, Robin (FR)	Safety Officer
Sanhueza, Sebastian (CL)	Mechanical Engineer
Tristram, Konrad (DE)	Operation Staff Astronomer
Zins, Gérard (FR)	Instrument Software Engineer

Departures (1 April–30 June 2014)

Europe	
Guieu, Sylvain (FR)	Fellow
Karban, Robert (AT)	Software Engineer

Chile	
Andersson Lundgren, Andreas (SE)	Deputy Program Manager
Aravena, Manuel (CL)	Fellow
Gitton, Philippe (FR)	System Engineer
Jager, Henderikus (NL)	System Integration Manager
Morel, Sébastien (FR)	System Engineer
Vuckovic, Maja (RS)	Fellow

ESO Fellowship Programme 2014/2015

The European Organisation for Astronomical Research in the Southern Hemisphere awards several postdoctoral Fellowships each year. The goal of these Fellowships is to offer outstanding early-career scientists the opportunity to further develop their independent research programmes in the exciting scientific environment of one of the world's foremost observatories.

ESO is the foremost intergovernmental astronomy organisation in Europe. Its approximately 110 staff astronomers, 40 Fellows and 50 PhD students conduct frontline research in fields ranging from exoplanets to cosmology, offering one of the most vibrant and stimulating scientific settings anywhere in the world.

Fellowships are available both at ESO's Headquarters in Garching near Munich, Germany, and at ESO's astronomy centre in Santiago, Chile.

The ESO Headquarters is situated in one of the most active research centres in Europe, boasting one of the highest concentrations of astronomers. ESO's offices are adjacent to the Max Planck Institutes for Astrophysics and for Extraterrestrial Physics and only a few kilometers away from the Observatory of Munich's Ludwig-Maximilian University. Additionally, ESO participates in the "Universe" Excellence Cluster at the Garching Campus, which explores the origin and structure of the Universe, and is also associated with the Computional Center for Particle and Astrophysics (C2PAP). Consequently, ESO Fellows in Garching have many opportunities to interact and collaborate with astronomers at neighbouring institutes.

In Chile, Fellows have the opportunity to collaborate with the rapidly growing Chilean astronomical community as well as with astronomers at other international observatories located in Chile. The advent of the new ALMA building next to ESO's Santiago offices and the arrival of many astronomers and Fellows working on the ALMA project have further enhanced the stimulating scientific environment available to ESO Chile Fellows.

The Fellowships in Garching start with an initial contract of one year followed by a two-year extension (3 years total). In addition to developing their independent research programmes, ESO Garching Fellows will be expected to engage in some functional work, for up to 25% of their time, related to, e.g., instrumentation, VLTI, ALMA, E-ELT, science operations support either in Garching or at one of ESO's observatories in Chile, or public outreach. This provides the Fellows with the opportunity to get involved with ESO projects or operations, and to gather valuable insights and experience not available in any other setting.

The Fellowships in Chile are granted for one year initially, with annual extensions for three additional years (4 years total). During the first three years, the Fellows are assigned to one of the science operations groups of Paranal, ALMA or APEX, where they will contribute to the operations at a level of 80 nights per year.

During the fourth year several options are provided. The Fellow may be hosted by a Chilean institution where she/he will be eligible to apply for time on all telescopes in Chile through competition for Chilean observing time. Alternatively, the Fellow may choose to spend the fourth year either at ESO's astronomy centre in Santiago, at the ESO Headquarters in Garching or at any astronomy/astrophysics institute in an ESO Member State. There are no functional duties during the fourth year, except in the case that this year is spent at ESO/Chile where Fellows have to carry out functional work at a level of 25% of their time.

The programme is open to applicants who will have achieved their PhD in astronomy, physics or a related discipline before 1 November 2015. Early-career scientists from all astrophysical fields are welcome to apply. Scientific excellence is the primary selection criterion for all Fellowships.

We offer an attractive remuneration package including a competitive salary and allowances (tax-free), comprehensive social benefits, and we provide financial support for relocating families.

If you are interested in enhancing your early career through an ESO Fellowship, then please apply by completing the web application form available at http://jobs.eso.org.

Please include the following documents in your application:
- a cover letter;
- a curriculum vitae with a list of publications;
- a proposed research plan (maximum of two pages);
- a brief outline of your technical/observational experience (maximum of one page);
- the names and contact details of three persons familiar with your scientific work and willing to provide a recommendation letter. Referees will be automatically invited to submit a recommendation letter. However, applicants are strongly advised to trigger these invitations (using the web application form) well in advance of the application deadline.

The closing date for applications is 15 October 2014. Review of the application documents, including the recommendation letters, will begin immediately. Incomplete or late applications will not be considered.

Candidates will be notified of the results of the selection process between December 2014 and February 2015. Fellowships will begin in the second half of 2015.

Further Information
For more information about the Fellowship programme and ESO's astronomical research activities, please see: http://www.eso.org/sci/activities/FeSt-overview/ESOfellowship.html.

For a list of current ESO Staff and Fellows, and their research interests, please see: http://www.eso.org/sci/activities/personnel.html.

Details of the Terms of Service for Fellows, including details of remuneration are available at: http://www.eso.org/public/employment/fellows.html.

For any additional questions please contact:
For Garching: Eric Emsellem, email: eemselle@eso.org.
For Chile: Claudio De Figueiredo Melo, email: cmelo@eso.org.

Although recruitment preference will be given to nationals of ESO Member States (members are: Austria, Belgium, Brazil, the Czech Republic, Denmark, Finland, France, Germany, Italy, the Netherlands, Portugal, Spain, Sweden, Switzerland and United Kingdom) no nationality is in principle excluded.

The post is equally open to suitably qualified female and male applicants.

ESO, the European Southern Observatory, is the foremost intergovernmental astronomy organisation in Europe. It is supported by 15 countries: Austria, Belgium, Brazil, the Czech Republic, Denmark, France, Finland, Germany, Italy, the Netherlands, Portugal, Spain, Sweden, Switzerland and the United Kingdom. ESO's programme is focused on the design, construction and operation of powerful ground-based observing facilities. ESO operates three observatories in Chile: at La Silla, at Paranal, site of the Very Large Telescope, and at Llano de Chajnantor. ESO is the European partner in the Atacama Large Millimeter/submillimeter Array (ALMA) under construction at Chajnantor. Currently ESO is engaged in the design of the European Extremely Large Telescope.

The Messenger is published, in hard-copy and electronic form, four times a year: in March, June, September and December. ESO produces and distributes a wide variety of media connected to its activities. For further information, including postal subscription to The Messenger, contact the ESO education and Public Outreach Department at the following address:

ESO Headquarters
Karl-Schwarzschild-Straße 2
85748 Garching bei München
Germany
Phone +49 89 320 06-0
information@eso.org

The Messenger:
Editor: Jeremy R. Walsh;
Design, Production: Jutta Boxheimer;
Layout, Typesetting: Mafalda Martins;
Graphics: Roberto Duque.
www.eso.org/messenger/

Printed by G. Peschke Druckerei GmbH,
Schatzbogen 35,
81829 München, Germany

ISSN 0722-6691

Contents

Front cover: The pair of galaxies NGC 1316 (lower, south) and NGC 1317 (upper, north). NGC 1316 is an early-type (S0) galaxy at a distance of about 21 Mpc and is the brightest member of the Fornax cluster. NGC 1316 contains the bright radio source Fornax A and has the largest number (4) of detected Type Ia supernovae in a single galaxy. The dust lanes and extended tidal tails display a history of interaction. NGC 1317 on the other hand is an apparently well-behaved barred spiral galaxy (type SAB) also in the Fornax cluster. See Release eso1411 for more information.